

# Advances in Unobtrusive Biomedical Sensing

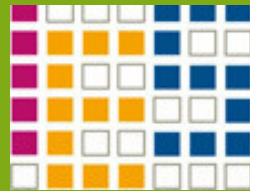
Danyal Iqbal

Prof. Dr. Mohamed Abd El Ghany Salem

Email: danyal.iqbal@stud.tu-darmstadt.de



TECHNISCHE  
UNIVERSITÄT  
DARMSTADT



width = 497.92325pt height = 480.5964pt



This work is dedicated to my good wife  
She always had an  
open ear for the challenges  
encountered in this work



## Abstract

Wireless technologies and advancements in sensor design seek to replace conventional health care systems with wearable health care systems. Wearable monitoring systems can transform patient care by providing continuous physiological data. Vital-sign monitoring systems have the potential to reduce health-care costs and improve chronic disease management. The wealth of data collected can aid in disease prevention and enhance the quality of life with better disease management. In this study, a wearable watch embedded with various bio-medical sensor is designed to monitor the vital signs of the subject. A mobile application is developed to save and display the data collected. The proposed vital signs monitoring system measures the Blood Pressure (BP), Photoplethysmogram (PPG), Electrocardiogram (ECG) and blood oxygen saturation in an unobtrusive wearable manner.

An ultra-low power, ultra portable, wearable integrated bio-medical device, Non Invasive Cuff Less Blood Pressure Monitor (NICBPM) is proposed to measure the Pulse Transit Time (PTT). The relationship between PTT and (BP) is investigated using linear and non linear regression models. Simultaneous reading obtained from an FDA approved, commercially available Blood Pressure monitor and the ECG and PPG signal from the NICBPM are used to calibrate the device for individual subjects during cardiopulmonary exercise test. The NICBPM can estimate sBP with 99% accuracy and 99% sensitivity.

A novel method for noninvasive measurement of blood glucose level is proposed. A range of ordinary hydrophilic daily disposable contact lenses were modified to sense the concentration of glucose in tears as a noninvasive technique for continuous physiological glucose monitoring. Our results suggest that the modified lenses were suitable for continuous ophthalmic sugar level monitoring in the range of 0.1 to 1000 micromolar. Since the blood sugar level is usually 5 to 10 fold higher, a calibration protocol for the modified lenses is proposed to track blood sugar. A design for integrating the finger-tip sized, ultra-compact spectrometer head in a wearable device is proposed. Since the proposed approach yielded promising results it has the potential of replacing invasive glucose monitoring techniques in the future .The proposed approach can be modified to detect biomarkers for a variety of diseases in the future. The integrated MEMS and image sensor technology can open up the world of molecular fingerprinting for biologist and doctors outside the lab environment.



# Contents

---

1	Introduction	7
1.1	Wearable Devices . . . . .	7
1.2	Motivation . . . . .	8
1.3	Goals . . . . .	9
1.4	Thesis Outline . . . . .	10
2	Background and Related Work	11
2.1	Photoplethysmogram Sensor . . . . .	11
2.1.1	SFH7050 . . . . .	12
2.1.2	PPG Analog Front End (AFE) . . . . .	13
2.2	Heart Rate Sensor . . . . .	13
2.3	Pulse Oximetry Sensor . . . . .	14
2.4	Electrocardiogram (ECG) . . . . .	15
2.5	Dehydration Sensor . . . . .	15
2.6	Oxygen Saturation . . . . .	16
2.7	Body Temperature . . . . .	17
2.8	Ultraviolet Exposure Sensor . . . . .	17
2.9	Ophthalmic Glucose Sensor . . . . .	17
2.10	Architecture Of the Monitoring System . . . . .	18
2.11	Cloud Connectivity . . . . .	19
2.12	Limitations Of The Existing System . . . . .	19
3	Non Invasive Cuff Less Blood Pressure Monitor (NICBPM)	21
3.1	Electrocardiogram (ECG) Sensor . . . . .	21
3.1.1	PR Interval . . . . .	21
3.1.2	QT Interval . . . . .	22
3.2	Circuit Design . . . . .	22
3.2.1	Analog Front End . . . . .	23
3.2.2	Communication . . . . .	23
3.2.3	Power . . . . .	23
3.2.4	User Interface . . . . .	23
3.3	Analog Front End (AFE) . . . . .	24
3.3.1	Extraction of the ECG signal . . . . .	24
3.3.2	Three electrode Configuration . . . . .	25
3.3.3	Two Electrode Configuration . . . . .	25
3.4	Requirements . . . . .	25
3.5	Design Choices . . . . .	26
3.6	Final Design . . . . .	29
3.6.1	Hardware . . . . .	30
3.6.2	Wearable Design . . . . .	31
3.6.3	Power Consumption . . . . .	32
3.7	Pulse Transit Time (PTT) . . . . .	32
3.7.1	Algorithm For PTT Calculation . . . . .	33
3.7.2	Pseudocode . . . . .	34
3.8	Calibration of BP sensor . . . . .	35
3.8.1	Data Analysis . . . . .	36
3.8.2	Statistical Analysis . . . . .	38
4	Noninvasive Ophthalmic Glucose Monitor	39

---

4.1	Challenges . . . . .	40
4.2	Principles of Non Invasive Ophthalmic Glucose . . . . .	40
4.2.1	Spectrophotometer . . . . .	41
4.2.2	The C12666MA Microspectrometer . . . . .	42
4.2.3	Molecular Absorbance Spectroscopy . . . . .	43
4.3	Boronic Acid Fluorophores . . . . .	44
4.3.1	Design of New Glucose Sensing Probes . . . . .	46
4.4	Materials and Methods . . . . .	46
<b>5</b>	<b>Results</b>	<b>49</b>
5.1	NICBPM . . . . .	49
5.1.1	Statistical Results . . . . .	50
5.1.2	Discussion and Future Work . . . . .	52
5.1.3	Conclusion . . . . .	54
5.2	Noninvasive Ophthalmic Glucose Monitor . . . . .	54
5.2.1	Wearable Design . . . . .	54
5.2.2	Ortho-BMQBA . . . . .	54
5.2.3	Ortho-BMQBA . . . . .	55
5.2.4	Discussion and Future Work . . . . .	55
5.2.5	Conclusion . . . . .	58
<b>6</b>	<b>Summary</b>	<b>59</b>
<hr/>		
List of Figures		62
<hr/>		
Acronyms		63
<hr/>		
<b>A</b>	<b>Schematics</b>	<b>65</b>
A.1	Schematic of Control Unit . . . . .	65
A.2	Schematic of ECG Analog Front End . . . . .	66
A.3	Schematic of C12666MA Analog Front End . . . . .	67
A.4	Schematic of PPG Analog Front End . . . . .	68
<hr/>		
Bibliography		69

# 1 Introduction

The design of wearable physiological measurement systems is attracting a lot of interests from researchers, due to the potential applications in medicine, sports and security. The size of elderly population and the prevalence of chronic disease is on the rise. Vital signs need to be monitored on a regular basis to prevent fatal disorders. At least 200,000 deaths from heart disease and strokes every year could be prevented by monitoring vital signals regularly as stated in [1] and [2]. Mobile health-care technology can enhance the quality of life for chronic disease patients and the elderly and collect valuable statistical data from healthy individuals. The data collected can be used to refine our understanding of various disease progressions and lifestyle choices. Furthermore, it has the potential to enable out-patient care and drastically reduce health care bills by preventing unnecessary hospitalizations and improving the odds of early disease detection.

The most critical parameter to a patient's health are mainly Heart Rate (HR), Body Temperature (T), Oxygen Saturation (SPO<sub>2</sub>) and Blood Pressure (BP). Any changes in the patient's vital signs need to be monitored closely. Conventional health care systems require the patient to be hospitalized for monitoring these parameters. This has an adverse effect on the accuracy of measurements [3], potency of the treatment and negatively impacts the patient's health and comfort. This is known as the white coat effect. Several wearable biomedical sensors, as shown in 1.1 have been developed to combat these problem.



Figure 1.1.: Popular Wearable Devices. Credit:elekslabs.com

## 1.1 Wearable Devices

Various portable vital signs monitoring systems have been designed in the past to combat these problems. However, these systems are often heavy, require extensive medical training to operate, consume a lot of energy, compromise on accuracy and comfort, and usually very expensive [4]. Technology has progressed very rapidly during the past years and recent developments in wireless technology and bio medical sensors enable us to design truly portable telemetry-home health care systems which can be worn by patients to collect their vital signal data and transmit them wirelessly to their remote health care professional. The evolution of unobtrusive sensing is shown in 1.3.

The miniaturization of sensors and minimal power consumption has lead to the development of wearable devices for biomedical sensing applications. Several types of wearable devices are being currently marketed as smart bands. These smart bands are ultra portable vital signs monitoring systems that require a smart phone to display and save the data or an LCD screen to display the result. One such smart band is shown in 1.4 Research is currently underway on several textile based wearable sensors as well. The miniaturization of sensors has allowed them to be easily integrated into clothing items. Some of the wearble textile sensors are shown in 1.2. Although textile based sensors are a very promising approach for remote monitoring of physiological data using [5] wearable devices and is being continuously

# Wearable Unit

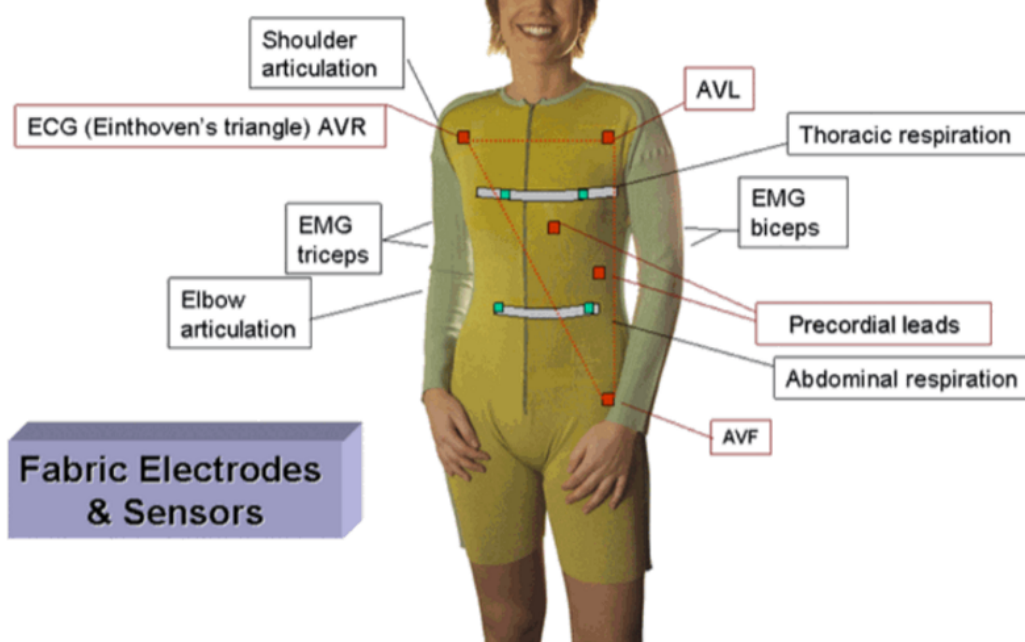


Figure 1.2.: E-Textile Monitoring Systems Credit:SmartX, Italy

researched at NASA for latest spacesuit designs, but the high manufacturing costs and the extreme conditions under which these sensors are developed at NASA make this approach unsuitable for our purposes.

## 1.2 Motivation

A wearable device to monitor the vital signals is essential to allow long term, continuous and unobstructed monitoring of physiologic information, such as PPG, HR, BP, ECG, T, UV and SpO<sub>2</sub>. An ultra low-power wearable design inspired from the recent popularity of smart watches and the commercial success of fitness bands and wearable biomedical devices could fill an important gap in this market segment driven by medical professionals and enthusiasts. The smart watch can measure these vital signal at any time and place. It is portable and measures all the vitals signals noninvasively. The patient can carry on with his daily activities while his measurements are being recorded and transmitted to his doctor. The low power design enables it to run on a standard 3.7 LiPo battery without the need for frequent recharging. The smart watch is cheap, durable, easy to use and can be used by anyone to monitor his vital signals.

The development of such technology is particularly interesting for small children and their parents and the elderly population. It can offer information that is otherwise inaccessible in clinical settings[6]. Since the existing smart band technology can already monitor HR, PPG, T, SpO<sub>2</sub>, count steps and track physical exercise reliably we strive to add new and better sensors in the current wearable sensing technology. We seek to minimize the power profile of the existing design to ensure longer battery times and to reduce the dimensions of the hardware so that these new sensors can be introduced to the wearable paradigm. With the integration of the biomedical sensors proposed in this study millions of hypertensive patients can monitor their BP with a cuff less BP monitor.

The population of diabetic adults is expected to reach 300 million by 2025 [7]. Conventional methods for the determination of the serum glucose concentration are invasive and require a blood sample which is obtained by puncturing a blood vessel. As noted by Badugu et al, millions of diabetics currently have no choice but to draw blood many times a day to determine their blood sugar levels[8]. Many technologies are being developed currently to combat this issue. However, the playing field is still wide open for a technology which can provide non-invasive and continuous physiological glucose monitoring[8] [9]. Various approaches such as near infrared spectroscopy (measurement of glucose through the skin by light waves)[10], transdermal measurement ( measurement of glucose by trying to pull glucose through the skin using electricity, electromagnetic waves or ultrasound), and measuring the rotation of polarized light due to the glucose in the aqueous humor etc, have attracted great attention from researchers in the past 30 years.

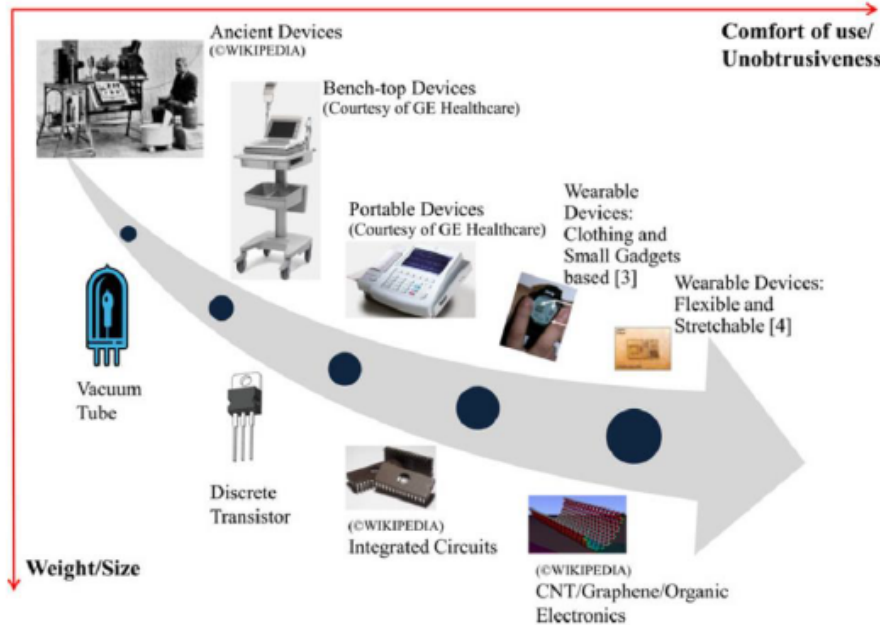


Figure 1.3.: Trends in unobtrusive sensing



Figure 1.4.: SmartBand Talk SWR30, Credit: Sonymobile.com

Despite conditional FDA approval and commercial launch of GlucoWatch in 2001, all these approaches have failed to deliver a viable alternative to invasive glucose measurement[11] and detection of hypoglycemia.

Tears are a rich source of biomarkers and the correlation of tear glucose and blood glucose has been studied by different methods [12]. In March 2015, Google has patented a miniature electrochemical sensor that is capable of detecting glucose concentration via an enzymatic reaction using an electrochemical cell (US Patent number US20150061837 ) [13].The patent can only be realized with considerable advances in current lenses manufacturing technology. This led to us to propose a new sensor based on the optical properties of fluorescent lenses to track ophthalmic glucose. The inspiration for an innovative new technique for monitoring ophthalmic glucose using disposable contact lenses and UV-VIS photo-spectrometer is drawn from the recent patent to track the blood glucose level continuously. The proposed technique offers a noninvasive, cheap, accurate and simple method to continuously monitor glucose level.

### 1.3 Goals

The aim of this thesis is to provide a low power, unobtrusive wearable and portable vital signs monitoring system . The system should overcome the challenges of designing reliable sensors, ensure reliable transmission of vital signs data and provide privacy and security for individuals. The device should easily connect to one's smart phone and provide means for continuous vital signal monitoring. The data can be uploaded to a server and can be accessed by the medical supervisor. The device should not limit the mobility of the user so that the user should be able to conduct his daily activities without hindrance while wearing this device, as shown in 1.5

A review of already implemented reliable sensors which conform to the wearable philosophy is conducted to draw inspiration for our work.

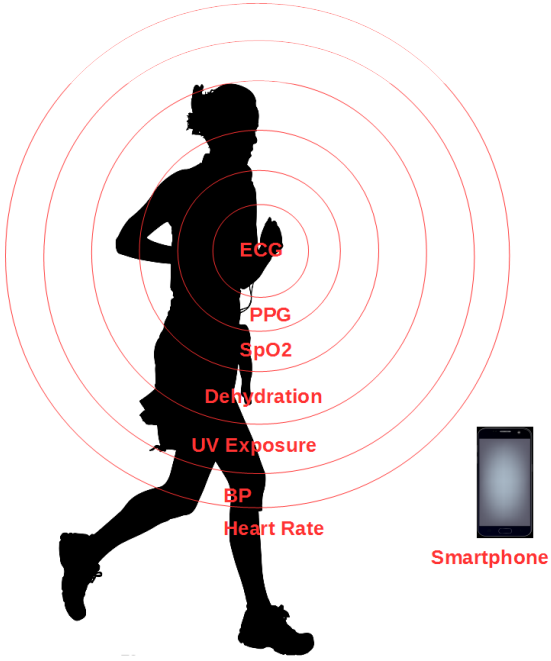


Figure 1.5.: Wearable Devices During Daily Activities

A cuff less method of measuring blood pressure through the measurement of PPG and ECG signals is to be proposed, designed, implemented and evaluated. The results obtained from this wearable design are compared with the results reported by other researchers. For the first time we propose a wearable design to monitor the pulse transit time. Statistical analysis and a comparison of the linear and the non linear regression model is reported for the first time on the same data set in human subjects from a low power ultra portable, minimalist wearable device.

A novel fluorescence dye based contact lens sensor is to be designed and implemented to detect extremely low concentrations of ophthalmic glucose in tears. The industrially optimized disposable plastic lens which has already has been assessed for safety and over the counter usage [8], is to be modified with a biocompatible glucose sensitive fluorescent dye. The sensitivity of the designed glucose probe is to be evaluated as a substitute for invasive methods.

#### 1.4 Thesis Outline

This thesis is organized as follows: Chapter 2 explores the background and related work in the domain of low power noninvasive biomedical sensors and the architecture of existing vital signs monitoring systems.

Chapter 3 discusses the design of an Analog Front End to measure the ECG signal and presents a signal processing algorithm to estimate BP from the ECG and PPG signal of a subject in a wearable manner.

Chapter 4 develops the basic concepts for the design of a new Ophthalmic Glucose sensor. An integrated MEMS based sensor is proposed as an Analog Front End to measure the concentration of glucose in human eye non invasively. Chapter 5 presents the results of the Non Invasive Cuff Less Blood Pressure Monitor (NICBPM) and the Non Invasive Glucose Monitor (NOGM). Chapter 5 also offers insight into possible avenues of future work. Finally a short summary is Chapter 6

## 2 Background and Related Work

A variety of wearable biomedical sensors have been developed by researchers. In this section a short review of some of the existing reliable biomedical sensors is presented. The proposed monitoring system consists of various sensors, an Atmel Atmega328P 8MHz microcontroller control unit and a HC-05 Bluetooth module. The Microcontroller is responsible for controlling all the sensors. The Microcontroller enables the sensors simultaneously and receives the output from each sensor. The sensor readings are converted to digital domain by an integrated ADC. The digital readings are sent to the smartphone via the HC-05 bluetooth module. In the low power operation mode, the sensors and the bluetooth module are powered on for only 30 seconds to collect and transmit the instantaneous reading. The proposed sensors are described in the next subsections:

### 2.1 Photoplethysmogram Sensor

Several low powered sensor have been developed in previous studies to measure the PPG signal of the user. These sensors are compact and can easily be integrated in wearable devices. The PPG signal is usually obtained from the fingertip but it can also be obtained from the wrist. The conceptual diagram of a conventional reflectance PPG sensor is shown in 2.1 Since, our design is inspired from a smartwatch we obtain the PPG signal from the wrist. The PPG signal obtained from the wrist is shown in the 2.2

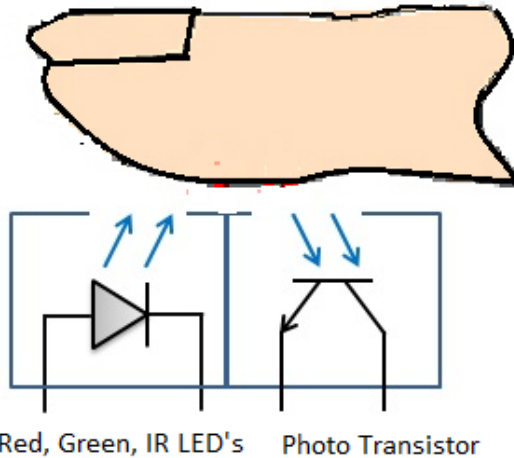


Figure 2.1.: Conventional reflectance Photoplethysmogram sensing from the Fingertip

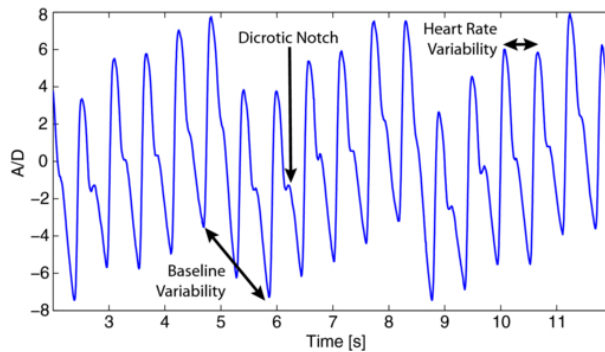


Figure 2.2.: Photoplethysmogram signal obtained from the wrist [14].

The readings from the PPG sensor can be used to measure the heart rate of the user and the inter-beat interval. The sensor comprises of a green LED and a photo detector to detect the intensity of light reflected from the skin. The changes in light absorption are plotted against time to obtain the PPG signal of the user. The PPG signal has become a useful diagnostic tool since its inception and is used by thousands of doctors every day to monitor the vital signals of critical care patient. In this study we use an SFH7050 reflective photoplethysmography sensor due to its small size, ultra low power consumption, adaptability, reliability and ease of use. This sensor forms the basis of many commercially available wearable biomedical devices. Some of the most important characteristics of the SFH 7050 are discussed in the next subsections.

---

### 2.1.1 SFH7050

---

The SFH 7050 is an integrated optoelectronic sensor, primarily designed and optimized for reflective pulse oximetry[15]. The large surface area of the sensor allows it to capture maximum light and provide a strong signal. The three integrated LED's serve as the light source for the sensor. A green LED at 535 nm, a red LED at 660 nm and an Infrared LED at 940 nm LED provide excitation sources in the visible light range as well the Infrared range [15] [16]. The heart rate can be measured using only the green LED, pulse oximetry measurements can be obtained by using the red and infrared LEDs or both [15].

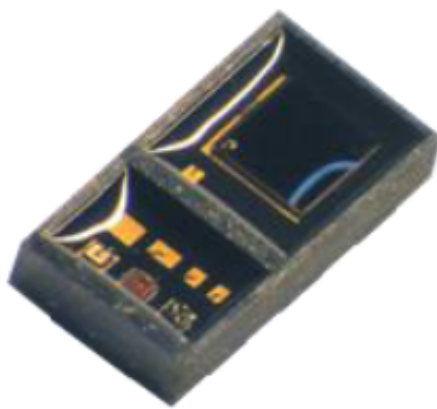


Figure 2.3.: SFH 7050 Sensor with integrated LEDs and photodiode [15].

The SFH 7050 operates in contact with human skin. Since, an air-gap between the skin and the sensors surface introduces noise in the PPG signal, the infrared LED can be used as a proximity sensor to ensure that the sensor is indeed in good contact with skin [15]. The measurement process can only be started when the sensor is close to the skin. An error message is displayed if the sensor is not in good contact with the skin.

The photodiode has a low dark current, which makes it suitable for low noise applications. The response of photodiode is highly linear which enables accurate SpO<sub>2</sub> measurements. The absorption spectrum of the human blood is shown in 2.4. Figure 2.4 is reproduced from the SFH7050 datasheet here to show the spectral response of the photodiode and normalized emission spectra of the LEDs [15]. It can be seen from the absorption spectrum that the 660 nm and 940 nm are suitable for pulse oximetry because they have opposite absorption levels for Haemoglobin and oxygenated Haemoglobin (Hb vs. HbO<sub>2</sub>). The 535 nm LED is suitable for heart rate monitoring. The current from photodiode is amplified and converted into a voltage with an external transimpedance amplifier[15]. The low capacitance and the fast response of the photodiode is excellent for short pulse operation to minimize power consumption [15].

The SFH 7050 is specifically designed for heart rate and pulse oximetry measurements, as shown in 2.3. It is compatible with each of the three suitable wavelengths for heart rate monitoring at various contact points on the body. The SFH7050 has been widely studied in clinical studies and is the de-facto standard for many FDA approved PPG sensors. In this study we use a 660 nm / 940 nm LED combination to extract the Oxygen Saturation value of the user. The tight wavelength specification and its compact size make the SFH 7050 ideal for integrated sensor systems [15]. The application of the SFH 7050 is extensively demonstrated in human subjects and is completely safe . The emitted light does not present any harm to the human tissue and the radiation is well below critical levels regarding human eye safety regulations [15]. Therefore, in this study the SFH 7050 is used as the PPG analog front end for the measurement of Photoplethysmogram based vital signals.

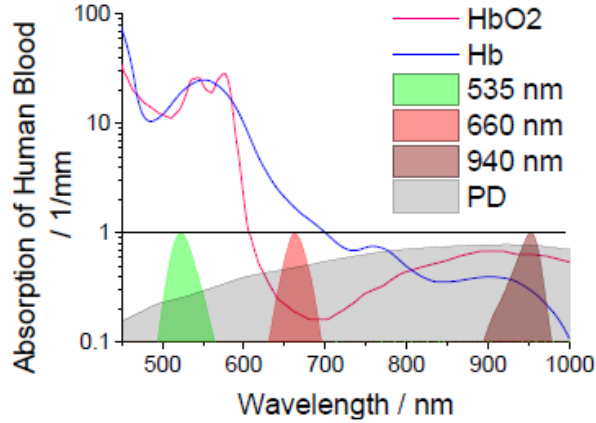


Figure 2.4.: Absorption Spectrum Of Human Blood vs Wavelength [15].

### 2.1.2 PPG Analog Front End (AFE)

The photodiode can be interfaced to an ADC for signal processing in several ways. In this study we use a transimpedance amplifier and a subsequent gain stage with filtering before sending the signal to the microcontroller for Analog to digital conversion. The gain (feedback resistor) of the transimpedance amplifier stage was selected to be very large to optimize SNR. The high feedback resistance decreases the bandwidth of the TIA as described in [15].

Our design features low input current, input current noise, and input voltage noise, as well as high-voltage operation to maximize the SNR in order to accurately measure the small currents among the large ambient currents due to the reflected LED light [15] [16]. A large feedback resistor amplifies the ambient and received current before the reflective DC component and ambient light component is removed with a high pass filter as described in [15]. The high pass filter is implemented after the sample and hold stage. The signal obtained after the filtering is amplified to maximize the dynamic range of the ADC. A programmable gain stage can compensate for different environmental factors. The dark current was minimized by operating the SFH 7050 in the absence of reverse bias voltage. The Transimpedance amplifier setup is shown in 2.5

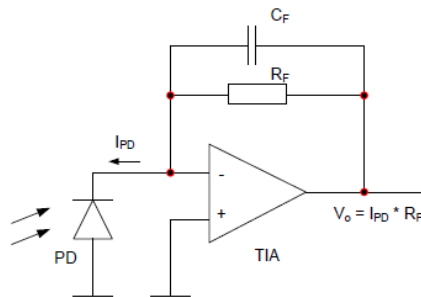


Figure 2.5.: Transimpedance Setup For PPG Analog Front End [15] [16]

The DC component of the photocurrent is omitted for heart rate monitoring designs since only the heart rate can be calculated from the frequency of the AC component of the signal. However, both the DC and the AC components are important for pulse oximetry.

## 2.2 Heart Rate Sensor

A PPG sensor can be used to measure the heart rate of the user. For the measurement of heart rate, only the AC-component of the sensor output is important. Synchronous demodulation is used to allow precise low-level measurements. The block diagram of the system is shown in 2.6. The gain stage after the TIA and the sample and hold stage consist of a band pass filter. Both these stages are essential to minimize the DC component of the photocurrent and for the amplification of the signal in order to make the acquired signal compatible with the input

range of the ADC. Electrical and optical noise is removed with a passband between 0.5 Hz to 5 Hz. Both low and high resolution ADC's can be used with synchronous modulation<sup>30</sup>

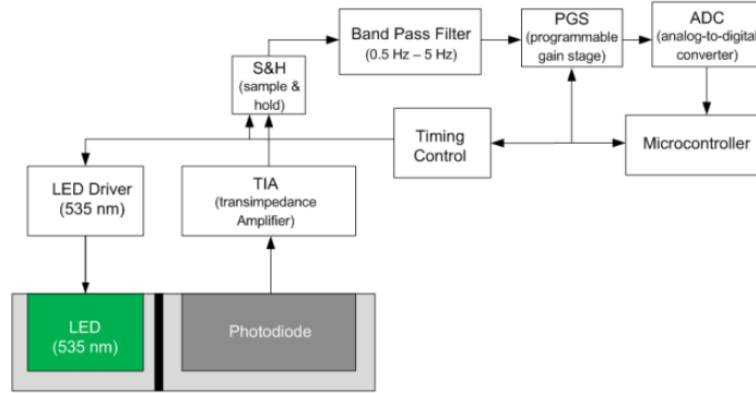


Figure 2.6.: Heart Rate Monitor [15].

The low powered PPG sensor placed on the fingertip or the wrist can be used to measure the heart rate of the user. In this study the heart rate is measured from the wrist using the green LED. The sensor measures the heart rate and the inter-beat interval. A simple IR LED based proximity sensor is used to confirm close contact between the sensor and skin since the PPG method requires close contact between skin and sensor. The beat to beat data is only recorded after a significantly high resolution of the signal can confirm the detection of a heartbeat.

### 2.3 Pulse Oximetry Sensor

The Pulse oximetry sensor is an extension of the PPG sensor [15] [16]. The two LEDs are driven with different currents to achieve an equal baseline DC level. The DC component of the photocurrent is essential for obtaining pulse oximetry measurements. The average DC value of sequential pulses can be measured by the DC tracker in the digital domain. The measured DC value are averaged in order to adjust the LED current (both red and infra red LED's) so that the DC signal can be equalized[15] [16]. It is also used to offset the second gain stage to reduce the DC component in the signal[15]. The current due to ambient light is removed by an analog filter. Another sample and Hold stage can be added to further subtract the influence of ambient light the pulse oximetry sensor. 2.7 presents the block diagram of this approach for implementing the pulse oximetry sensor. The ambient subtraction is carried out in the digital domain leading to higher system bandwidth and therefore allowing undistorted transmission of very short pulses-( $\mu$ seconds). This conventional design features one ADC, but requires larger system bandwidth and allows an individual ambient measurement[15].

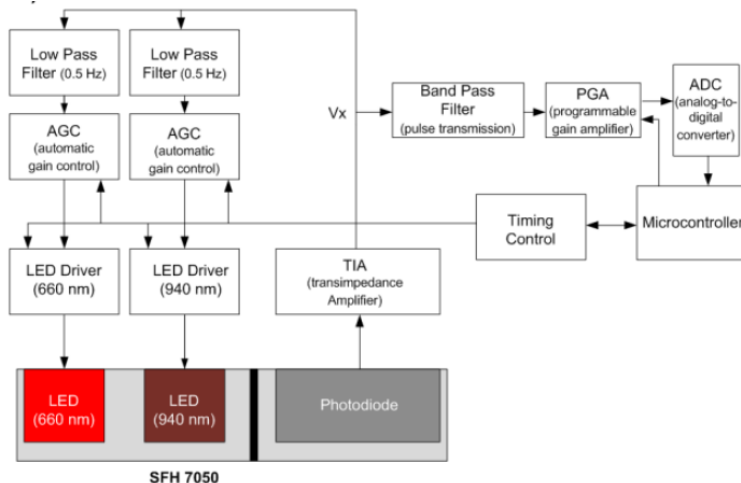


Figure 2.7.: Pulse Oximeter With Equalization Of DC levels. Ambient Subtraction Performed In The Digital Domain [15].

However, we propose a simplified pulse oximeter sensor by eliminating the process of DC level equalization. This leads to lower power consumption and a simpler architecture. A substantial DC component is subtracted from the signal following the transimpedance amplifier stage. An offset amplifier controlled by a microcontroller is programmed as a configurable subtractor to remove a substantial part of the non-pulsatile signal. A low-pass filter is used to extract the small AC signal. A programmable gain amplifier amplifies the signal to make it compatible with the input range of the ADC. The DC component is added to the filtered signal again to reconstruct the original signal [15]. The reconstructed signal contains both the correct DC and AC component. The ambient light is subtracted in the digital domain as shown in 2.8.

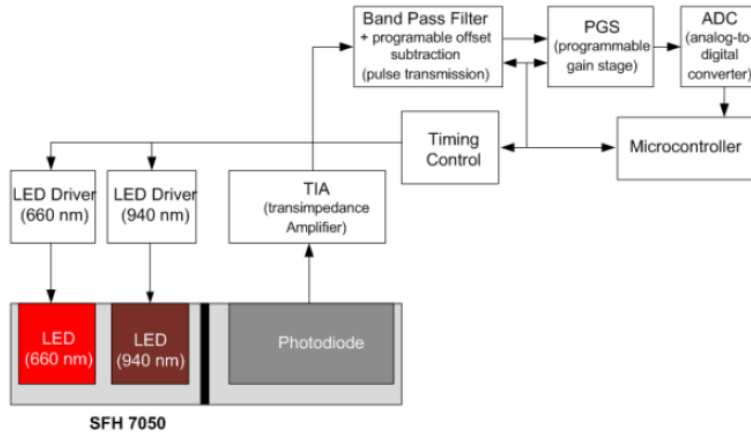


Figure 2.8.: Pulse oximeter measuring AC and DC signal level. A programmable offset via a programmable DC tracker is subtracted initially to obtain a high resolution AC component. Ambient subtraction performed in the digital domain allowing an individual ambient measurement [15].

## 2.4 Electrocardiogram (ECG)

The ECG is normally obtained for critical care patients. The ECG signal is extracted clinically with 12 electrodes. The patient must be stationary to avoid motion artifacts. Conventional ECG machines are bulky and consume a lot of power as shown in 2.9. Researchers have attempted to develop several reduced versions of the conventional ECG monitor to obtain the ECG signal accurately with 6 or 9 electrodes instead of 12. These reduced versions are advertised as portable devices yet they are still bulky, consume huge amounts of power, limit mobility and require atleast 6 elecrodes. One such a portable ECG monitor is shown in 2.10 to demonstrate the bulkiness of current portable designs. In this study we try to mediate the lack of a truly portable ECG monitor which measures the ECG signal with minimum number of contact point (electrodes), consumes less energy and is wearable.

Existing wearable system lack the ability to asses the electrical and muscular functions of the heart. An appropriate ECG sensor suitable for wearable low power application is therefore designed and implemented in the next chapter. The designed ECG sensor comprises of an ultra low power integrated signal conditioning block for biopotential measurement applications. The ECG Analog Front End AFE designed to extract, amplify, and filter small biopotential signals in the presence of noisy conditions, such as those created by motion or remote electrode placement[17]. This design allows for an ultra low power analog-to-digital converter (ADC) or an embedded microcontroller to acquire the output signal easily [17].

## 2.5 Dehydration Sensor

An ultra low power wearable water dehydration sensor was proposed and implemented in [18]. It can detect dehydration in a subject with reliable results. The PPG AFE desinged in this study can be used to measure the hydration level of the user. If a user is dehydrated the smartphone application can prompt the user to increase liquid intake.

The human body is composed of 55% to 60% water. Water is essential for critical life functions such as body temperature regulations, waste elimination and metabolic processes. If left untreated, dehydration can lead to several medical problems including stroke and kidney failure.

A photodetector was used to detect the light reflected from human tissue. the absorption spectrum of water lies in the 920 - 1000 nanometer range. The light reflected from the water molecules in the body in this range can be



Figure 2.9.: Conventional ECG Machine. Source:[careshine.en.made-in-china.com/](http://careshine.en.made-in-china.com/)



Figure 2.10.: Portable ECG Machine. Source:[handheldecgmachine.com](http://handheldecgmachine.com)

detected by a photodetector to estimate the hydration level of the body. The sensor is composed of a transmitter circuit and a receiver circuit. The sensor is implemented on a same scale and can easily be worn by a patient during daily activities. A detailed explanation is provided in [18].

A near infrared LED with a 900-980nm wavelength is used as a light source for enlightening the tissue. The water molecules present in living tissue can absorb the infrared light. A photodetector measures the intensity of the light reflected from the skin. The intensity of reflected light detected by the photodetector can be used to estimate the concentration of water molecules in the tissue. The photodetector is sealed from ambient light sources to improve accuracy and sensitivity.

## 2.6 Oxygen Saturation

Oxygen is an essential element in the blood, which plays a vital role in the metabolism and breathing processes in living organisms. Oxygen saturation  $\text{SpO}_2$  is the percentage of oxygenated hemoglobin compared to the total of hemoglobin in the blood. The  $\text{SpO}_2$  is measured by the pulse oximetry sensor using light wavelength ranging from 600 nm to 750nm. Oxygenated Hemoglobin absorbs light in this wavelength range more efficiently than other components of blood. Similarly, light range from 900 nm to 1000 nm is highly absorbed by deoxygenated Hemoglobin. The ratio

of the intensity of the absorbed light from the Red LED and the total light absorbed from both the red and Infrared LED's is calculated from :

$$x = I_{RED}/I_{IRRED}$$

The concentration of oxygen in the blood can be obtained from following equation described in [18] :

$$Oxcon = (30.667 * x^2) + (10 * x) + 102.6$$

IRED is the intensity of the absorbed light from the Red LED. IIRED is the intensity of the absorbed light from the IR LED.

## 2.7 Body Temperature

A compact precision analog temperature sensor has been used to estimate the body temperature in various studies. The sensor is composed of stacked BJT [18]. A precision amplifier buffers the analog output of the temperature sensor before it is fed to an ADC. The temperature sensor is easily integrated into a wearable device due to its small size and low power consumption. The LMT thermistor IC has been demonstrated to provide reliable body temperature measurements as described in [19] and [20].

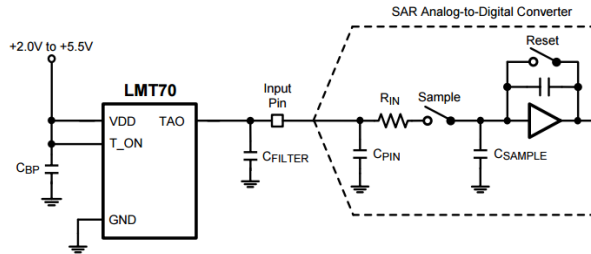


Figure 2.11.: Body Temperature Sensor and Subsequent Sampling Stage [20]

## 2.8 Ultraviolet Exposure Sensor

A UV sensor can help an individual avoid exposure to the harmful radiation of the sun. A small, ultra low power UV sensor developed in [18] is ideal for application in a wearable design. The readings from the UV sensor can be used to alert the user if the ultraviolet exposure of the user increases over a safe threshold identified in medical literature. The total exposure to UV radiation from the sun can be used to estimate the production of Vitamin D in human skin.

## 2.9 Ophthalmic Glucose Sensor

Hyperglycemia is usually conventionally diagnosed by collecting a urine or blood sample. The amount of glucose in the sample is calculated by enzymatic, amperometric or coulometric methods[21]. However, diabetic patients must draw blood through minimally invasive techniques atleast 2000 times a year to monitor blood sugar levels. Therefore, research is currently underway on developing non invasive techniques of tracking glucose such as monitoring ophthalmic glucose which has been known to track serum glucose levels since the 1980's.

An ophthalmic glucose sensor based on the enzymatic and amperometric methods is shown in 2.12. The design and fabrication process of glucose sensing lenses as described in[22] is complicated and expensive because of the small dimensions and optimized performance in the precise ocular conditions. The wearable glucose sensor is supposed to have 84mm X 3mm X 50mm laminar structure comprising of a immobilized glucose oxidase (enzyme) membrane and an oxygen film electrode. The oxygen film exlectrode is comprised of a polypropylene membrane, a 200 nm Platinum electrode, a 300 nm Silver-Silverchlorode electrode, an electrolyte and a non-permeable membrane. The enzyme membrane can be immobilized on the oxygen electrode with a photosensitive resin. The 3mm wide strip can than be attached to special contact lenses with an antenna and a chip printed on top of the lens. The antenna transmits the glucose level to a handheld device from the data stored on the printed chip. The sensor embedded in the proposed lenses can detect glucose by tracking the current produced from the following electrode reactions [22]: The current produced should be directly proportional to the amount of glucose present in the lachrymal fluid[22] [13].

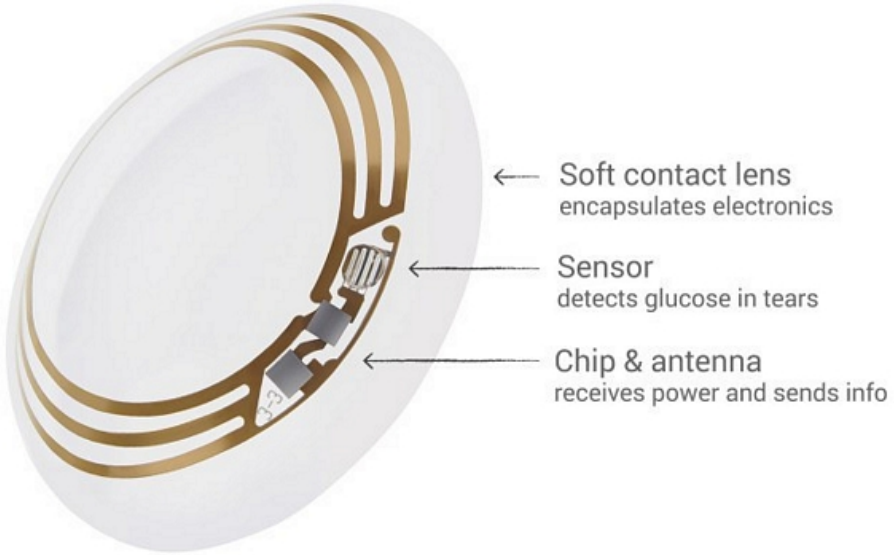
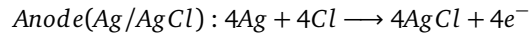
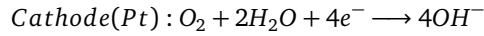


Figure 2.12.: Glucose Sensing Lenses[22] [13]. Made by Google X labs. Source:coolthings.com

The design patented by google and the ones proposed in [21] , [22] , [23] and [24] are still far from a testing a first working prototype in their development process.



Due to the limited success of prior art in monitoring ophthalmic glucose reliably we introduce a new approach to detect ophthalmic glucose by modifying over the counter lenses with a biocompatible glucose sensitive fluorescenet dye and a photospectrometer to measure the fluorescence intensity. The fluorescence intensity of the newly developed sensor is linearly related to the amount of glucose present in lachrymal fluid.

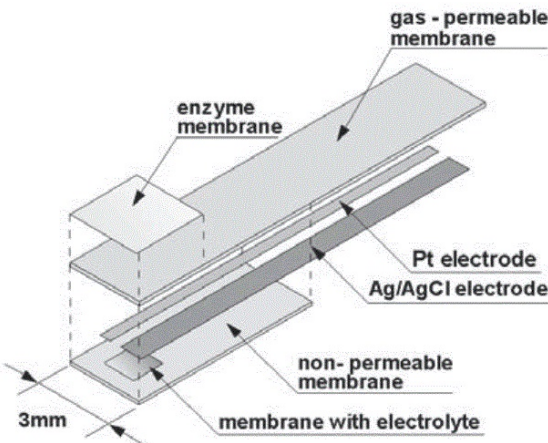


Figure 2.13.: Enzymatic Ophthalmic Glucose Monitor

In the next section we describe the architecture of the vital signal monitoring systems.

## 2.10 Architecture Of the Monitoring System

The wearable monitoring system proposed in [18] is divided into ultra portable sensors, Microcontroller, and a smart-phone application, as shown in 2.14. In this study, we adhere to this architecture to allow seamless extension of the

prior art and combat compatibility issues. The vital signs are monitored by various small sensors as voltage reading, the microcontroller converts the analog data into digital data. The digital data is transmitted to a smartphone via a small Bluetooth module suitable for wearable application. The smartphone can send the data to a remote server. This data can be accessed by medical professionals. Moreover, the huge amount of data that can be collected in this manner make it a good candidate for Big Data Analysis to identify several new pathological and diagnostic tool. For example, an artificial neural network can be trained on the data collected from a high risk population such as cancer patients or chronic heart failure patients to diagnose these conditions by noninvasive statistical analysis.

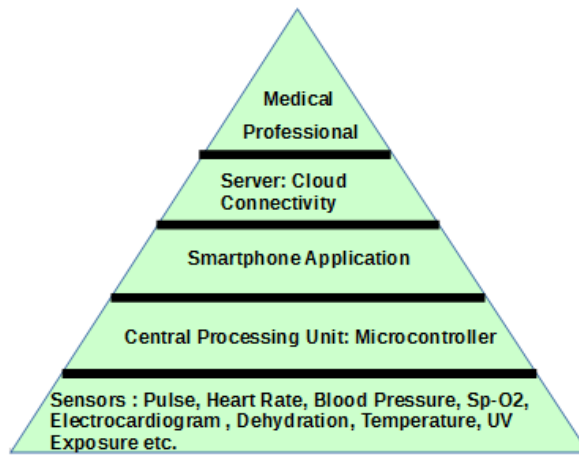


Figure 2.14.: System Architecture

In this study the vital signs data is stored and displayed on a smartphone. The microcontroller is operated in low power mode to save battery life. The sensors can be operated in a continuous operation mode or instantaneous operation mode. In the continuous operation mode, the data is continuously collected and the waveforms are plotted in realtime. In the instantaneous operation mode, the sensors are only powered on for 30 seconds. The instantaneous data is analysed to record the vital signs of the subject. A 0.92 inch LCD screen can be easily mounted on the device to display the reading. Since, the power requirements of the LCD were too high for the power limit envisioned for our wearable design, it was not incorporated into our final design. However, a 3.7V LiPo battery will last a few days even with an LCD screen and make a good addition to any commercial reiteration of our wearable design. In this study we implemented our wearble design on a standard printed circuit board(PCB), however any commercial reiteration should be assembled on a flexible PCB.

## 2.11 Cloud Connectivity

A private server provides better security and privacy but cloud connectivity enables ubiquitous and on-demand access to a shared pool of configurable computing resources [25]. The smartphone application designed in this project can be connected to a cloud service instead of a private server to make the app community driven. Cloud connectivity enables our wearable design to function as a building block of a biomedical network. Such a biomedical network can be used to develop an Internet Of Things (IOT) system of medical records. Added layers of data security and privacy must be provisioned to make sure that only authorised personnel can access patient data. The application can generate warning messages if the readings from a node are unusual. Emergency ambulance service can be notified if a node encounters critical failure as shown in 2.15. Hospitals, health care facilities and insurance companies can be interfaced to such a biomedical network. Eventually, the health of an individual can be monitored much more effectively and the overall health of the community can be improved when wearable biomedical devices become popular.

## 2.12 Limitations Of The Existing System

Portable, wrist blood pressure monitoring devices such as the H2: The First Wearable Blood Pressure Monitor, have been discarded as unreliable means of blood pressure measurement[26] and Blumio: another developer of a cuff-less blood pressure monitor has delayed product launch due to the lack of systematic data on the relationship between PTT and BP. Therefore in this study, a Non-Invasive Cuff-less Blood Pressure Monitor (NICBPM) is proposed as a solution to this problem. The device will enable researchers to investigate the potential of monitoring the PTT in daily and clinical setting.

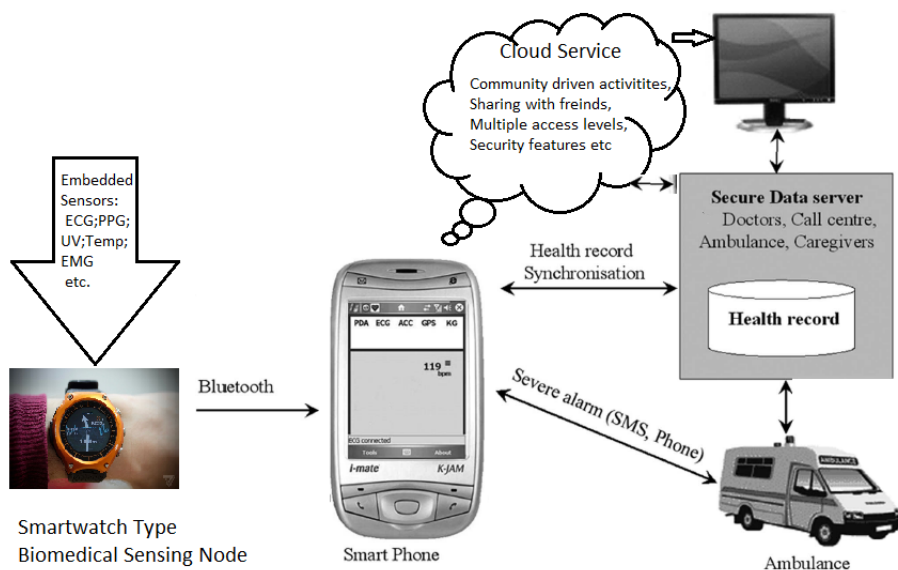


Figure 2.15.: Telemetry System

### 3 Non Invasive Cuff Less Blood Pressure Monitor (NICBPM)

Since the new breed of ultra portable wearable devices can reliably monitor vital signals such as Heart Rate, Body Temperature, Body Dehydration , Glucose level and Oxygen Saturation (SPO2) in real-time [27], we envision a design for BP sensor which is compatible with the existing body of work in wearable biomedical appliances. At the moment, there is no reliable ultra portable wearable device to monitor the Blood Pressure. The commercially available Blood pressure monitoring devices limit the mobility and comfort of the patient, since the cuff must be attached to the brachial arm[28]. Therefore we propose an approach to estimate the BP in a wearable manner.

Since the ECG AFE was added to the wearable biomedical system in this study, we can use the ECG signal and the PPG signal to calculate the Pulse Transit Time(PTT) which is assumed to be a surrogate marker of BP [29]. The next sections describes the requirements and the design of the Electrocardiogram sensor. The proposed ECG sensor along with the existing PPG sensor can be used to calculate the PTT. A propriety algorithm to calculate the PTT is proposed later in this chapter. Once the PTT is calculated the BP of the user can be estimated from the individual linear regression function obtained from a one-time calibration protocol.

#### 3.1 Electrocardiogram (ECG) Sensor

The Electrocardiogram (ECG) records the electrical activity of the heart. The most important parts of the human heart are shown in 3.1

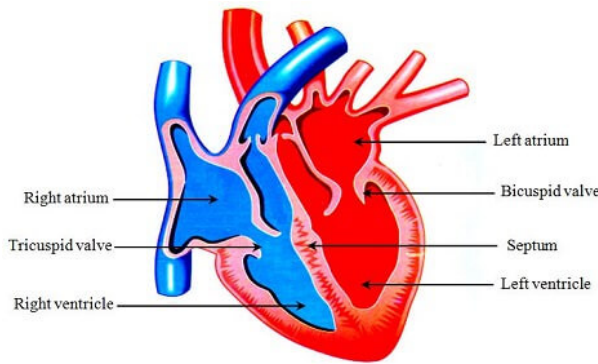


Figure 3.1.: Human Heart. Source: [cephalicvein.com](http://cephalicvein.com).

The ECG signal is conventionally now acquired with 12 disposable electrodes spread all over the body. A new approach using a 3 electrode configuration : one electrode attached to the right arm, one electrode attached on the left arm and a reference electrode on the right or left leg, was recently proposed in 2014. In this study we use a 2 electrode configuration, as shown in 3.2 to obtain a limited view of the ECG signal which is insufficient for diagnostic studies of the heart muscle but still sufficient for the estimation of BP. The ECG signal obtained from the 2-electrode configuration: one electrode on the right wrist and one electrode on the left wrist , is shown in 3.3

The electrodes can measure tiny changes in the electrical potential of the skin, which track the electrophysiologic pattern of the heart muscle as it pumps blood to other parts of the body. It is the most widely performed cardiology test in diagnostic studies of the heart. The amplitude of the ECG signal is very small and is polluted with external and internal noise. Hence the noise must be removed before the signal is amplified.

The next subsections describe the important properties of the ECG signal.

##### 3.1.1 PR Interval

The ECG signal comprises of the PR interval and the QT interval as shown in 3.4

Electrical impulses travel from the right atrium to the left atrium. The wave generated by this electrical impulse is known as the PR interval. The right and left atrium are "depolarized" during this interval . The right atrium is

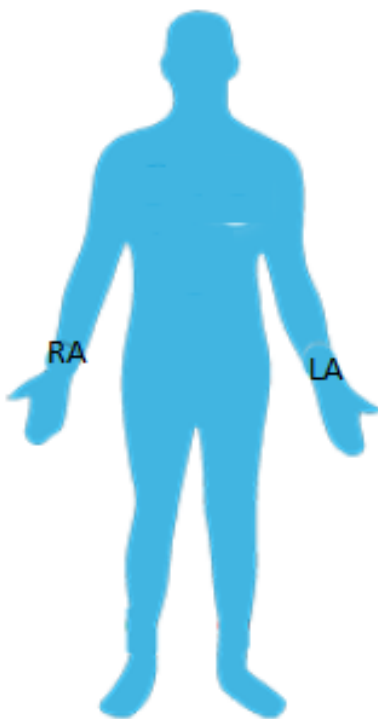


Figure 3.2.: 2-Electrode Configuration

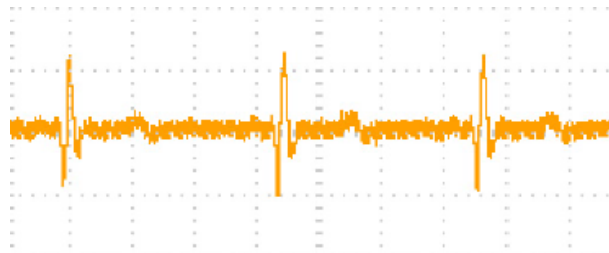


Figure 3.3.: ECG Signal Obtained From The 2-Electrode Configuration

"depolarized" first and deoxygenated blood is drained into the right ventricle from superior and inferior vena cava. As the impulse travels from right atrium to left atrium, the left atrium contracts to receive oxygenated blood from the lungs into the left ventricle through both the pulmonary veins.

### 3.1.2 QT Interval

Both ventricles begin to pump during the QRS interval. De-oxygenated blood is pumped by the right ventricle into lungs through both the pulmonary arteries. Oxygenated blood is pumped by the left ventricle into the rest of the body through the aorta. The ST interval has minimal electrical activity as the ventricles are "re-polarized" by the T-wave. The T-wave causes the both the ventricles to relax. Blood enters the ventricles through the atria during the relaxation phase.

## 3.2 Circuit Design

The circuit design for obtaining the ECG signal is limited by constraints of ultra low power and ultra portability, wearable design philosophy and small physical dimensions. The system was divided into 4 major parts : Power, Analog Front End, Communications and User Interface. The designed system could be used on a as-is basis or extended to measure other small bio potential signals.

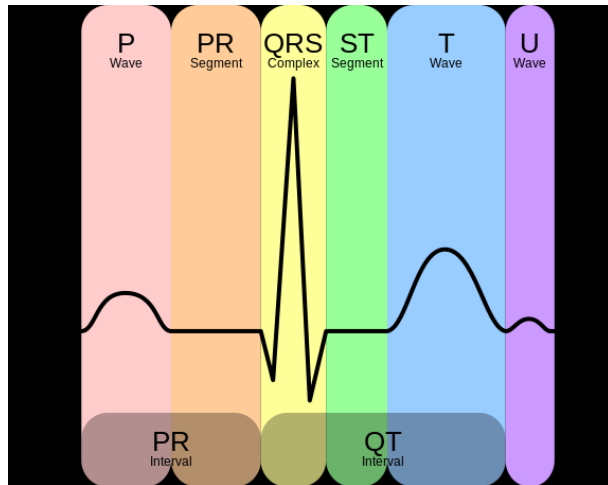


Figure 3.4.: Important Intervals In The ECG Signal. Source:Wikipedia.org

### 3.2.1 Analog Front End

The Analog Front End is the most essential part of the system. It is responsible for signal integrity and precise measurement of the ECG signal. The amplitude of the ECG signal lies in the range : 0.1mV- 1mV, and the bandwidth lies in the range from 0.2 Hz to 200 Hz. The AFE must be able to reject Common-mode noise. The most critical component of the AFE is the amplifier which is used to amplify the ECG signal without adding much noise. Other significant parts of the AFE include suitable low pass filters to remove high frequency noise and notch filter at 50-60Hz to remove power hum.

### 3.2.2 Communication

The raw ECG signal must be transmitted to a User interface for further processing to aid in patient monitoring and diagnosis. The communication block receives the raw ECG signal, carries out the Analog to Digital conversion and transmits the data to the User Interface. The amplitude of the ECG signal is rather small even after amplification and is converted from analog to digital domain using a Successive Approximation (SAR) ADC of 12 bit precision. Bluetooth was chosen as a means of transmitting the data from the communication block to the User Interface to make the system wireless and provide a hassle free and user-friendly experience. This will also allow the system to connect to a range of user platforms without any modification to the hardware. An atmel Atmega 328P- 16 Mhz surface mounted micro controller was programmed to read the analog signal, carry out the Analog to digital conversion and transmit the data over serial bluetooth line via a HC-05 Bluetooth module.

### 3.2.3 Power

The selection of the power source for the designed system was based on low power and portability restraints of the system. The power block for the ultra low power ECG monitoring system should also fulfill the requirements of basic safety, portability, maximum lifetime, minimum storage requirement and the size constraints of the system. The battery life should be sufficiently long so that the user does not have to worry about charging the device often. A simple Cr232 button cell was first investigated as a possible power source but it was quickly discarded in favor of a commercially available rechargeable GT-08 Lithium Polymer Smartwatch battery-380mAh due to the current draw requirements and insufficient life time. The smartwatch battery should last a few days in continuous operation mode and a few weeks in low power operation mode. The power profile of the designed system is investigated further in the text.

### 3.2.4 User Interface

The user interface should allow easy, real time and continuous monitoring of the ECG signal. The primary user Interface was developed for the desktop using Java Processing to display the data obtained from the hardware. The ECG and PPG signal were plotted in real time. The heart rate was calculated from both the ECG and PPG signal.

The Inter beat interval was calculated from the PPG signal and the QRS wave component in the ECG signal was also identified. After testing the hardware on the desktop platform , a cross platform mobile application was designed to plot both the ECG and the PPG signal in real-time. The data was also saved in separate csv files on the mobile phone for further processing . The data can also be transmitted to a server over WLAN or 3G internet for further processing, however this is beyond the scope of this study.

### 3.3 Analog Front End (AFE)

ECG is a very weak and noisy signal. The analog to digital converters cannot process an unamplified ECG signal due to its small amplitude. For proper signal acquisition an appropriate analog front end must be designed to amplify the small ECG signal and further condition the signal before it is fed into the system's ADC. The AFE must also compensate for noise interference and motion artifacts present in the ECG signal. This process is known as signal pre-conditioning. The signal preconditioning stages comprises of extraction, amplification and filtering stages.

#### 3.3.1 Extraction of the ECG signal

Most ECG machines have 2 or more electrodes , which monitor the voltage across one or more leads. Clinical standard uses a 12-lead ECG . It provides a detailed view of the heart's electrical activity from different points on the body. Each lead corresponds to a vector of ECG electrical potential. The electrodes are typically placed in a setup known as the Einthoven's triangle.

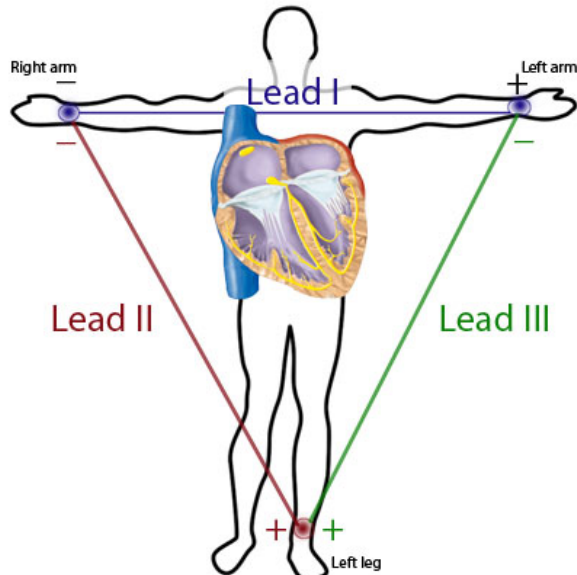


Figure 3.5.: Einthoven's Triangle [17] .

Willem Einthoven (1860-1927) explained the principles of the ECG in scientific terms. The standard connections for all three limb leads are shown in the 3.5. In Einthoven's triangle, the heart may be considered to lie at the centre of an equilateral triangle and the corners of the triangles are the effective sensing points - the right arm(RA), left arm(LA)and left leg (LL)electrodes [17]. The signal from each lead is obtained according to the following equations:

$$LeadI = (VLA - VRL) - (VRA - VRL) = VLA - VRA$$

$$LeadII = (VLL - VRL) - (VRA - VRL) = VLL - VRA$$

$$LeadIII = (VLL - VRL) - (VLA - VRL) = VLL - VLA$$

The signal received from each lead on an FDA approved standard ECG machine are shown in 3.6. Since each lead corresponds to a vector of ECG electrical potential, different ECG signals can be obtained from different lead locations. The corresponding ECG signals from different lead locations is shown in 3.7:

The most important characteristic of the ECG signal for our purpose is the positive R-wave. It can be seen that all three configurations show a pronounced R-peak which means that the QRS complex can be easily identified.

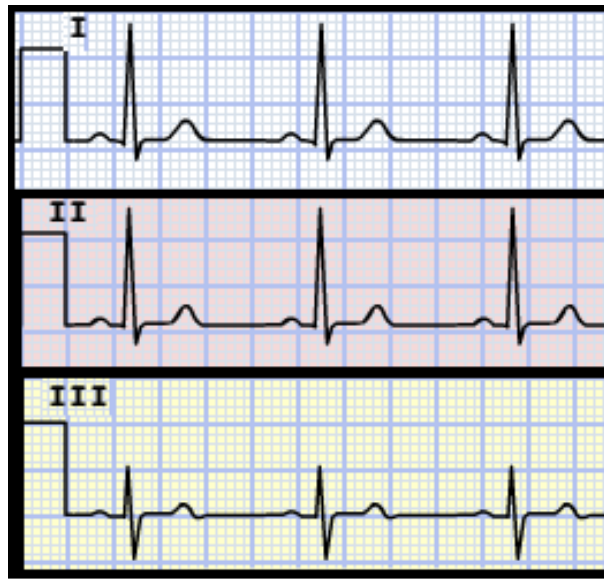


Figure 3.6.: ECG Signal From Each Lead

### 3.3.2 Three electrode Configuration

It is possible to have upto 3 unique vector for three electrodes. Two electrodes are used to form a vector and the third electrode provides a reference. This configuration allows more lead selection options and eventually less noise disturbance in the signal. The possible locations for three electrode configuration are shown in 3.8:

Configuration I is preferred in clinical studies as it offers a good view of Leads I, II and III. However, configuration II is preferred for patient comfort but it only provides a good view of lead II. A right leg drive electrode (electrode 3) is used to bias the subject to set a DC operating point determined by the operating voltage of the monitoring system. Data from lead I and lead II cannot be reliably obtained from this configuration. Important information regarding the electrical operation of the heart muscle is lost with the loss of 2-leads. However, the R-wave can still be observed with this limited view.

### 3.3.3 Two Electrode Configuration

With the two electrode configuration it is only possible to have a good view of only 1 lead. The two electrode configuration is shown in 3.9: Configuration I allows a good view of the Lead II and configuration II allows a good view of the lead I. The two electrode configuration provides a smaller amplitude of signal when compared to the lead II in 3 electrode configuration . This might lead to difficulty in identifying useful features of the ECG signal such as P and U waves but the R-wave is easily identifiable with 2 electrodes in both configurations.

Since our ECG monitor is an ultra portable smartwatch type design we use configuration II with 2 electrode to obtain a good view of lead I in order to identify the R-peak. The electrodes were placed on the right and left wrist instead of the chest. This leads to interference from various muscle groups and a noisier signal, but the R-wave can still easily be identified with visual inspection or simple signal processing with electrode placement on both wrist. The equivalence of electrode placement on wrist instead of the chest was proven with the simple ECG circuit provided in the data sheet of AD620 Instrumentation amplifier as shown in 3.10:

The reference circuit as shown in 3.10, was constructed on a breadboard and the R-wave was identified first with the electrodes placed on the chest and than on the wrist. The sample circuit served as a valuable evaluation aid, but was quickly discarded for further use due to intensive power requirements. (It requires both -5 and +5 V to operate).

## 3.4 Requirements

A detailed study of the requirements for a portable, low power ECG analog front end was carried out . It was found that the ECG monitoring szstem must be able to extract vez low voltage signals in the range 0.1mV-1mV with a frequency range from 0.2-200 Hz. The system should allow both 2-electrode and 3-electrode configurations. It was noted that skin electrode contact is a source of interefrence which produces an offset of 200-300mV. The system should

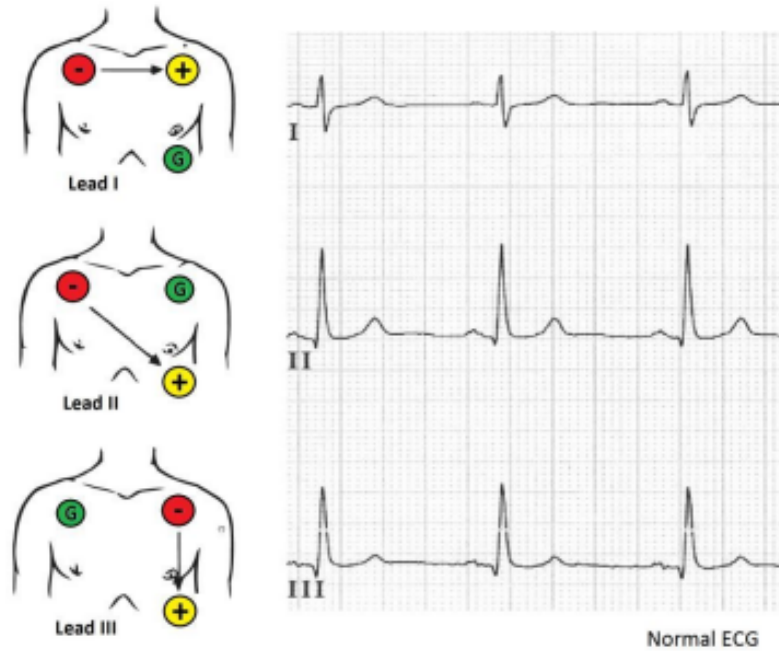


Figure 3.7.: ECG Signal From Different Electrode Placements [17].

be able to cope with this interference and other sources of noise. The AFE should be able to run on 2-4 Volts. The area of the designed PCB and the power consumed should be minimized.

The AFE should be able to take 2 types of signals at the input : Common-mode signal (same potential) and differential -mode signal (differing potential). The common-mode signal is unwanted for ECG monitoring systems. The potential between the electrodes and ground can create a Common-Mode component of up to 1.5V and the designed AFE should be able to cancel out the common-mode signal and amplify the differential-mode signal at the input. The ratio of change in output voltage to change in Common-Mode input voltage is known as the Common-Mode gain. The ratio of the differential gain to the Common-Mode gain the Common-Mode Rejection Ratio (CMRR). The CMRR of the designed system should be 80dB to 120dB over the input frequencies that need to be rejected. An instrumentation amplifier should be used to achieve sufficient gain and Common-Mode rejection. An instrumentation amplifier has a differential input and a single ended output with respect to a reference voltage. The in-amp gain is determined by external resistors that are connected between inverting input and the output. The internal structure of a classic instrumentation amplifier with 3 operational amplifiers is shown in 3.11

### 3.5 Design Choices

The data sheet for several application specific ICs and low power general instrumentation amplifiers were studied and their properties were evaluated for application in our design. A comprehensive comparison is presented in the following sections. The AD 8232 instrumentation amplifier was selected as the final choice for the AFE according to the discussion presented in the next section.

#### AD8236

AD 8236 has the lowest power consumption among the instrumentation amplifiers available commercially. A simplified version of the AD8236 is shown in 3.12. It operates on a single power supply of 1.8 V- 3V. High input impedance, a minimum gain of 5, low input bias of 1pA and a relatively high CMRR of 110dB make it suitable for our design. The rail-to-rail input and output provides a wide dynamic range, which means that the maximum input or output swing is equal to the power supply voltage [3]. The output can be easily shifted according to individual application by applying a reference voltage to the REF pin. The shifted output can be easily integrated with the ADC. The default gain value of 5 can be reconfigured by placing a resistor across the RG pin. The additional gain can be set with respect to the resistor value. The resistor value for the desired gain can be calculated according to Equation below:

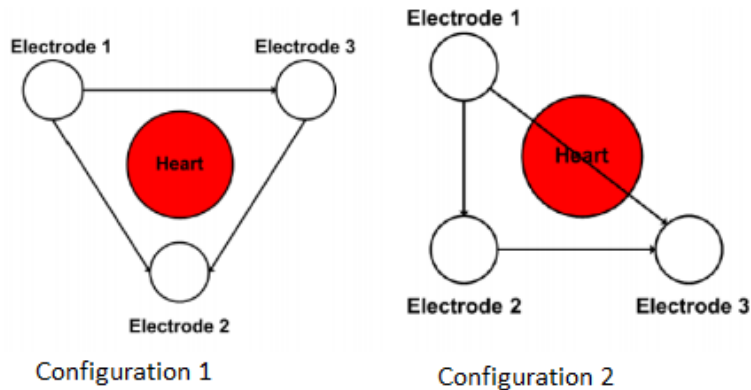


Figure 3.8.: Possible 3 Electrode Configurations [17]

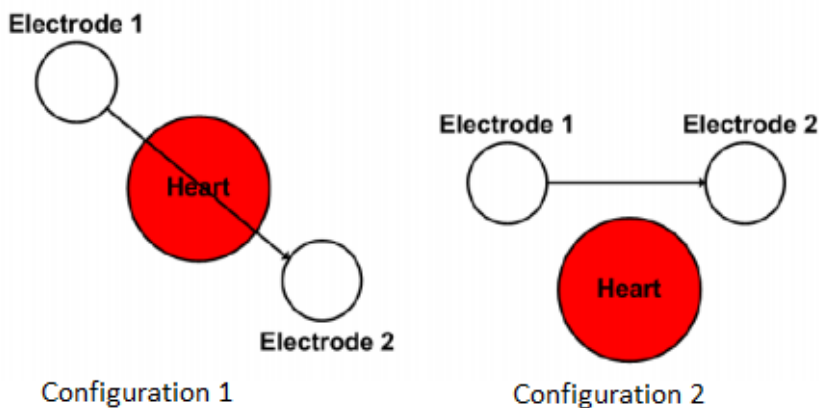


Figure 3.9.: Possible 2 Electrode Configurations [17].

$$R = 420k/G - 5$$

The AD8236 has DC overload protection, which allows a diode drop (approximately 0.7V) above the positive supply and a diode drop below the negative supply. It can handle a continuous current of 6mA. The relatively high CMRR (110dB) and the capability to remove any differential DC offsets (electrode half-cell potential) make AD8236 a good candidate for ECG monitoring system. A sample low power heart rate monitor provided in the data sheet is shown in 3.13 which demonstrate the common application of this IC in ECG monitoring systems[33].

---

#### ADAS1000

The ADAS1000 is a high-performance, low power analog front end (AFE) IC. It is widely used in monitoring ECG signal. It was designed according to the various clinical and electrical standards for electrocardiograph apparatuses. It can also measure thoracic impedance and pacing artifacts [34]. This makes it suitable for monitoring patients with surgically implanted pace makers and its electrical effects. The ADAS1000 has five acquisition channels and a Right Leg Drive (RLD). The right leg drive serves as a reference voltage. The channels are equipped with a differential preamplifier with configurable gain, a fixed gain 2-pole anti-aliasing filter, a 14 bit 2MHz ADC, and buffers. An anti-aliasing filter can detect pace artifacts. The Leads can be configured as either digital and analog [34]. The functional block diagram of the ADAS1000 is shown in 3.14 [34].

---

#### Power Consumption

The ADAS1000 requires an operating voltage of 3.3V to 5V. The power consumption is shown for various electrode configurations are shown in the table below:

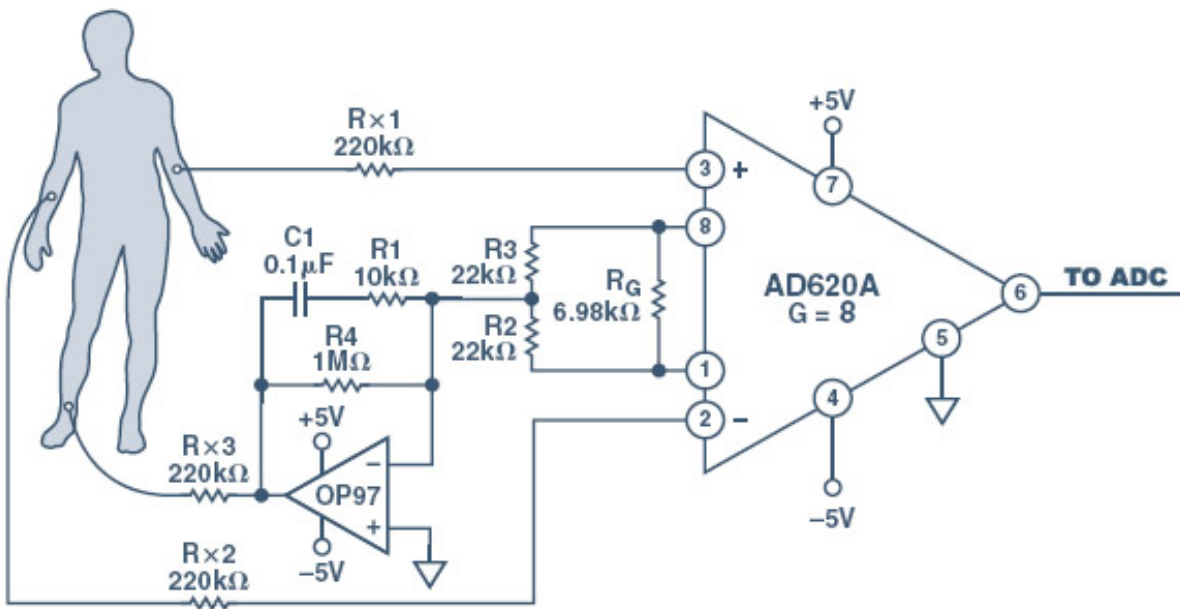


Figure 3.10.: ECG AFE based on the AD620 Instrumentation Amplifier [30] [31]

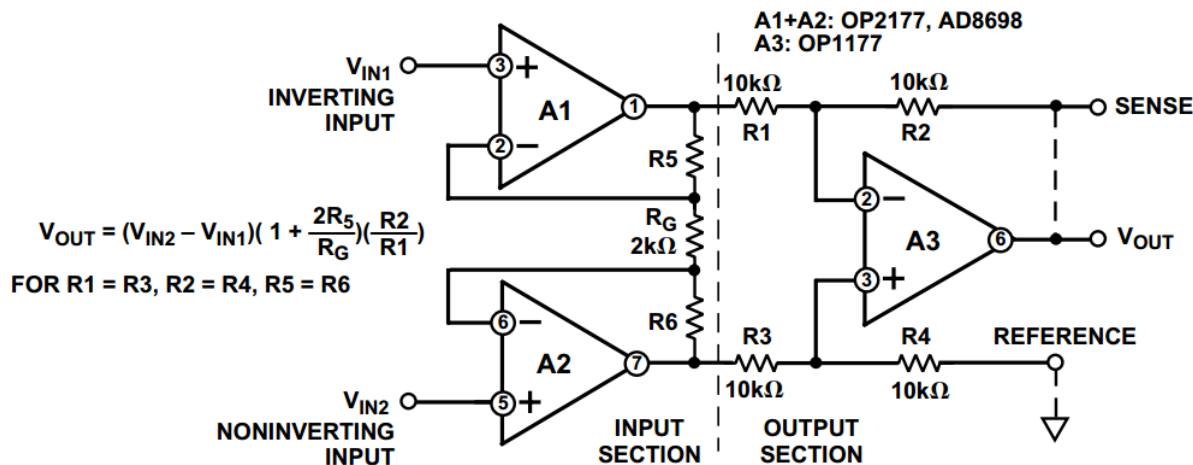


Figure 3.11.: Internal Structure Of An Instrumentation Amplifier [32]

The noise power can be reduced by increasing the power consumption. The power consumption can be reduced by enabling the power-down mode. In the power-down mode, the signal acquisition channels are switched off and the data rate is reduced [34]. The ADAS1000 also offers the capability of AC and DC lead off detection. A 8.192MHz crystal can be connected externally and the internal regulators can be used to drive the IC with a raw input. A power on self-test performs various critical operations such as : reading registers, Cyclic Redundancy Check (CRC) and calibration of the Digital to Analog Converter (DAC). The aquired data can be sent to a DSP or microcontroller through Serial interface SPI or QSPI at configurable data rates.

Electrode Configuraton	Power Consumption
1-Lead	11mW
2-Lead	15mW
3-Lead	21mW

## AD8232

The AD8232 is another ultra low power instrumentation amplifier capable of acquiring and amplifying small bio signals. It can also remove motion artifacts and interference from electrode half cell potential . A leads off detection

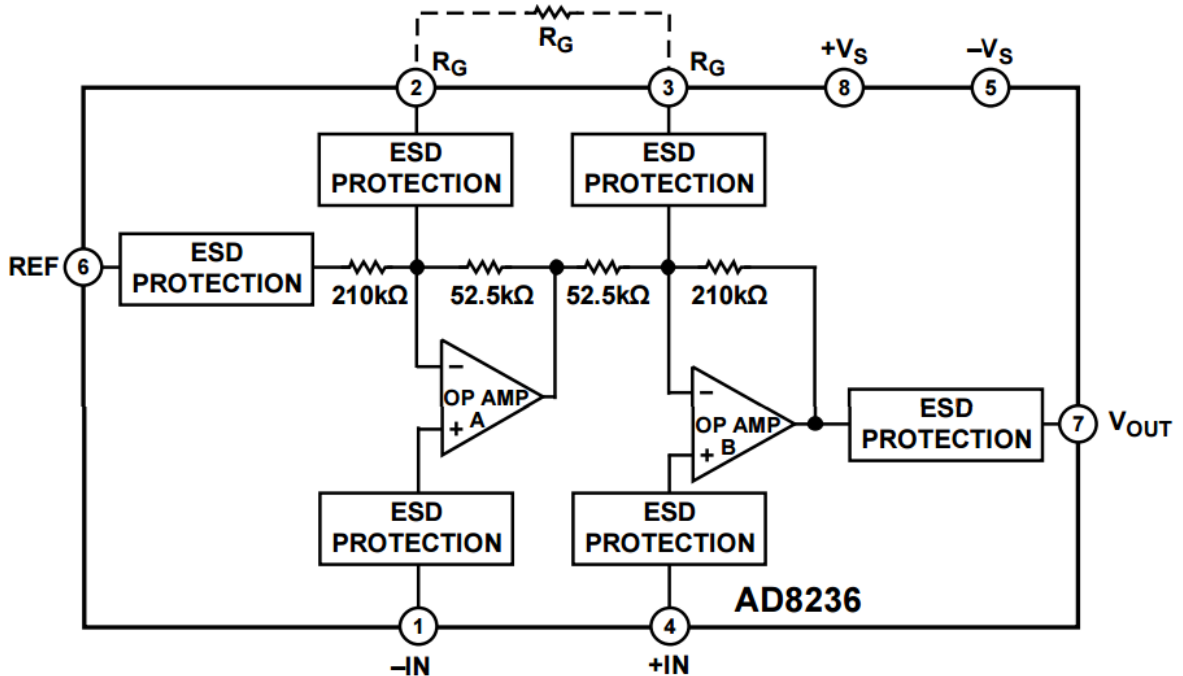


Figure 3.12.: Internal Structure Of The AD8236[33] .

circuitry and fast restore capability is implemented in the AD8232 to reduce the recovery time if one of the leads is disconnected. The AD8232 comprises of four amplifier : an instrumentation amplifier, an operational amplifier (A1), a Right Leg Drive (RLD) A2, and a buffer amplifier A3.

The AD8232 can be operated with both 2-electrode and 3-electrode configurations. The Right Leg Drive (RLD) serves as the reference lead in a 3-electrode configuration. The Right Leg Drive amplifier rejects the Common-Mode voltage at the input of the instrumentation amplifier. The AD8232 has a CMRR of 86dB. All terminals of the AD8232 are shielded against electrostatic discharge (ESD). External resistors can be utilized to avoid overload conditions at the input [35]. The functional block diagram of the AD8232 is shown in 3.15 [35]

The instrumentation amplifier in the AD8232 has a fixed gain of 100. An operational amplifier is available for selectively low pass filtering the noise components in the signal. A low pass filter with a cutoff frequency of 1.1 Mhz is implemented at each input pin of the AD8232 to avoid RF interference[6]. This prevents a DC offset in the acquired signal.

A reference buffer is used to create a virtual ground (reference voltage) between the actual ground and the power supply. A voltage divider and an external power supply can be used to drive the reference voltage from REFIN pin. The virtual ground is available at REFOUT. The AD8232 provides AC and DC leads off detection. The connection at each input is checked using DC lead off detection in the three electrode configuration. If the IN+ electrode is disconnected the LOD+ pin is set and if the IN- is disconnected the LOD- pin is set.

For the 2-electrode configuration AC lead off detection is used. A high impedance AC signal is injected into the input terminals every few seconds. If the lead is connected the AC signal will be heavily attenuated, if it is not attenuated the lead has been disconnected.

The AD8232 requires an operating voltage of 2-3.5V. It can be operated with CR2032 cell batteries or rechargeable lithium ion batteries. A power save mode with a current draw of less than 200nA can be enabled to minimize power consumption.

### 3.6 Final Design

The complexity, adaptability and portability of the three AFE blocks were compared. The features available in each AFE were evaluated according to design requirements. The ADAS1000 offers a lot of features but it requires more power. Additional features are packaged with greater complexity and a higher price. The AD8236 is a general purpose instrumentation amplifier with a verz attractive power consumption profile. But it would require atleast four other operational amplifiers to design the desired AFE. The additional amplifiers will increase the PCB footprint . An AFE designed with the AD8236 might be the most power efficient but it cannot be the smallest design in terms of physical

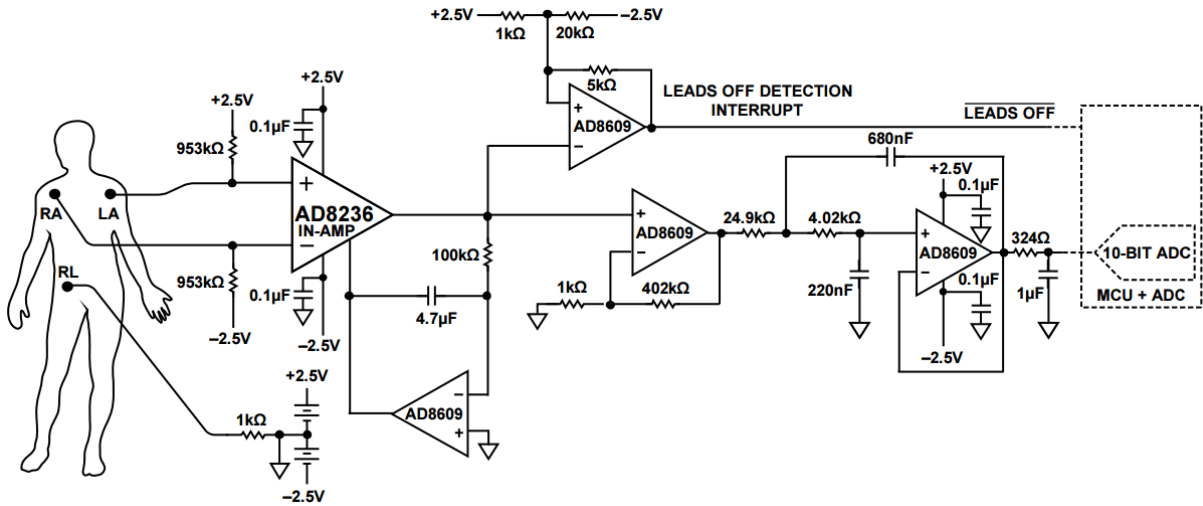


Figure 3.13.: Heart Rate Monitor Based On AD8236 [33]

dimensions. The AD8232 emerges as a clear winner, as it consumes less power than the ADAS1000. The AD8232 offer fewer features in comparison to the ADAS1000. However, this leads to reduced complexity. On the other hand, it offers more features than the AD8236. The AD8232 was therefore selected for the purpose of this project. The table below shows the most important features for comparison.

IC	Operating Voltage	Operating Current ( $\mu\text{A}$ )	No. of Electrodes	CMRR (dB) for gain value of 100
AD8232	2-3.5V	170	3	86
AD8236	1.8-5V	33	-	110
ADAS	3.15-5.5V	785	5	110

### 3.6.1 Hardware

ECG AFE consists of AD8232, since it can accommodate both the two-electrode and three-electrode configurations. The two electrode configuration use LA and RA pins as an input, whereas the three-electrode configuration uses right leg drive (RLD) pin in addition to RL and LA. Fast restore (FR) pin is set to high to enable Fast Restore functionality and improve signal quality. The detailed schematic is shown in Appendix A

Since we use a 2 electrode configuration the default leads off detection is set to AC. This can also be set to DC for 3 electrode configuration. The LO+ and LO- are connected to the microcontroller to warn the user of improper electrode contact with the skin. The input bias resistors R7, R8 are chosen to be  $10M\Omega$ . Resistors R9 and R10 are chosen as  $182k$ . The input resistances of the in-amp are biased for the 2 electrode configuration. For the two-electrode configuration, the resistors are biased with RLD voltage value while SJ2 uses the REFOUT voltage for biasing.

The signal obtained from the AFE is fed to the microcontroller where the ADC converts the analog voltages to digital domain. Power consumption is optimized by regulating the SDN pin digitally. This enables us to reduce the current drawn. R11 and R12 form a voltage divider connected to the supply voltage  $+VS$ . A mid supply voltage is supplied at the REFIN using this voltage divider setup. A buffer amplifier is used to supply the same voltage level at the REFOUT. Capacitor C17 removes the power line hum, (noise) from the signal. C12 and C13 act as DC coupling capacitors. A two-pole Sallen Key low-pass filter comprising of R17, R18, C21 and C25 filters and amplifies the output signal. The cut-off frequency and gain of the two-pole Sallen Key low-pass filter are calculated according to the equations below.

$$f_c = \frac{1}{2\pi(R_{17}.R_{18}.C_{21}.C_{25})^{\frac{1}{2}}} = \frac{1}{2\pi(200K\Omega.1M\Omega.10nF.22nF)^{\frac{1}{2}}} = 24\text{Hz}$$

$$\text{Gain} = 1 + \frac{R_{20}}{R_{23}} = 1 + \frac{1M\Omega}{100K\Omega} = 11$$

A high-pass filter with a gain of 100 comprises of C13, R15 and the internal in-amp remove low frequency noise. The cutoff frequency of the high-pass filter is given by Equation given below.

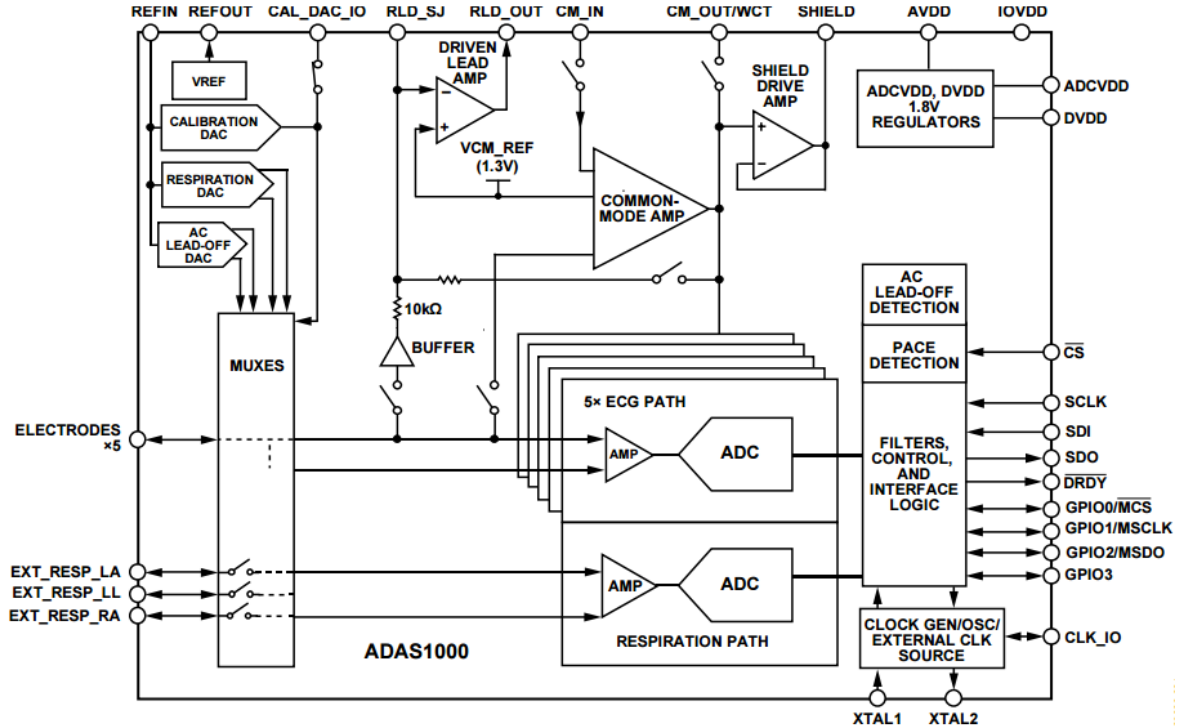


Figure 3.14.: Internal Structure Of The ADAS1000 [34]

$$f_c = \frac{100}{2\pi R5 C13} = \frac{100}{2\pi \cdot 10M\Omega \cdot 0.22\mu F} = 7.23\text{Hz}$$

The 7.23Hz cutoff frequency allows for the in-amp to reject the DC components of the inputs. C22 and R22 are used to make an AC coupling network between the output of the in-amp output (IAOUT) and the REfout pin to allow negative signal swing.

A 1nF capacitor C20, between the RLD and RLDFB pins improves the CMRR at the input of the in-amp, if a 3 electrode configuration is used. The C20 and 150k resistor form an integrator on the Right Leg Drive Amplifier with a gain of 20 between 50Hz and 60Hz. The Right Leg Drive current opposes the variations in Common-Mode voltage. The current to the RLD pin of the AD8232 is limited to a maximum of 5µA by a resistor R16 as a safety measure.

The PCB designed for the ECG Analog Front End is extremely small at 2.2cm X 2.5cm , and therefore ideal for application in wearable biomedical devices. The board layout is shown in A

The R-peak was easily identified by visual inspection using this hardware setup and a 2 electrode configuration. The next section describes signal analysis to obtain Pulse Transit Time (PTT) and the calibration process of the NICBPM to estimate BP.

### 3.6.2 Wearable Design

The physical form factor of the NICBPM draws its inspiration from the smartwatch. A 3D printable watch housing was designed for the NICBPM to contain the printed circuit boards in a silicon molded prototype, as shown in 3.16 and 3.17 . The metallic underbelly of the watch and the metallic bezel on top of the watch serve as the left wrist electrode and the right wrist electrode respectively, as shown in 3.18. The PPG sensor is embedded in the strap of the NICBPM. The Silicon molded prototype containing the PCB with embedded sensors is shown in 3.19. The ultra portable, wearable design of the NICBPM improves patient comfort and offers greater mobility when compared to conventional BP monitoring devices.

The NICBPM obtains the electrocardiogram (ECG) signal of the subject from a 2 electrode configuration to measure the lead I configuration ECG signal. The lead I configuration is selected as it shows a pronounced R peak. The detection of the R-peak is of particular interest to the estimation of PTT. An integrated signal conditioning block for biopotential signal measurement is used to extract the ECG signal. The ECG signal is filtered and amplified by a two-pole Sallen Key low-pass filter (LPF) and a high-pass filter (HPF) with a combined gain of 1100, and a cutt-off frequency of 24Hz and 7.23 Hz, respectively. A reflective optoelectronic sensor with an embedded green, red and

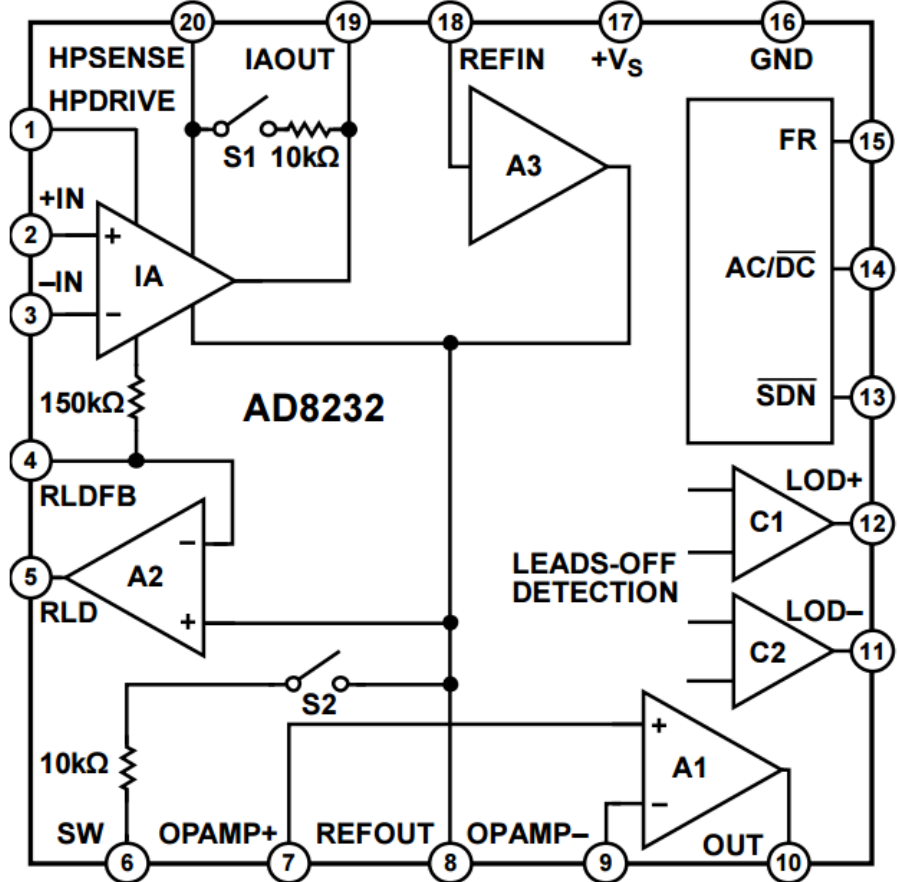


Figure 3.15.: Functional Block Diagram of AD8232 [35]

infrared light emitter and a phototransistor is used to obtain the PPG signal at the wrist. The PPG signal is filtered with a passive HPF and an active LPF with a cut-off frequency of 0.5 Hz and 3.4 Hz respectively. The active LPF is configured with a gain of 48.

### 3.6.3 Power Consumption

Additionally, we focus on reducing the power consumption. The existing device with the Bluetooth module consumes 30mA. The microcontroller in active mode consumes 10mA , the temperature sensor consumes 120uA, the sun intensity sensor consumes 300uA and the Spo2 and PPG sensors consumes 15mA [18]. The proposed BP sensor consumes an additional 4.85mA. The battery of the existing design is upgraded from a 3.3V Lithium ion coin battery to a 3.7V Lithium polymer smartwatch battery.

### 3.7 Pulse Transit Time (PTT)

Pulse Transit Time (PTT) is defined as the time required for the arterial pulse pressure wave to travel from the aortic valve to periphery [36] (Smith et al. 1999). It can be estimated as the delay between the peak of the R wave in the ECG signal and the arrival of the corresponding pulse wave at a peripheral extremity such as the finger or the wrist. Since our design draws its inspiration from a smartwatch, the arrival of the corresponding pulse wave at the periphery is approximated by the steepest slope of the PPG signal obtained at the wrist. PTT was calculated from the peak of each R-wave in the ECG to the point of the steepest slope of the corresponding upstroke in the plethysmogram [29] in MATLAB, as shown in 3.20.

PTT, the time interval between ventricular electrical activity and peripheral pulse wave, is assumed to be a surrogate marker for blood pressure[29] [38]. Recent research has suggested that BP is inversely related to the PTT. With a rise in BP - increasing distending pressure, the arterial compliance decreases, the pulse wave velocity increases and as result the pulse transit time decreases [39][29]. PTT has also been demonstrated as a useful research and diagnostic tool in recent studies on sleep disorders, anesthesia, dialysis and psycho-physiological stress [40][41] [42][43]. However,

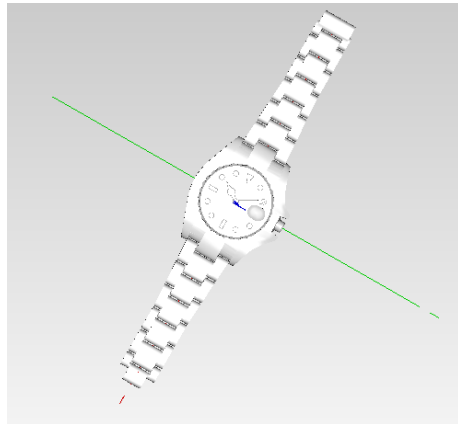


Figure 3.16.: Top view of 3D Printable Watch Housing.

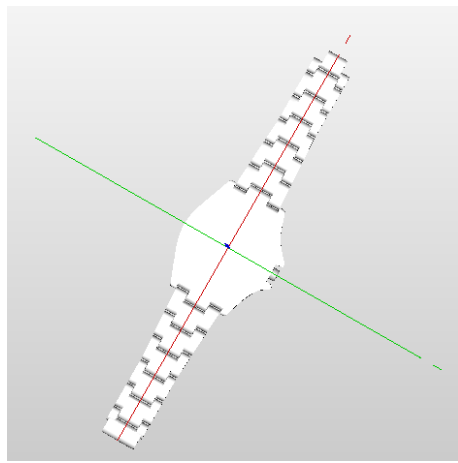


Figure 3.17.: Bottom view of 3D Printable Watch Housing.

the popularity of this method in clinical settings is limited due to the lack of systematic data in human subjects and an incomplete understanding of the relationship between PTT and BP.

PTT is a promising, potentially useful index of arterial stiffness and cardiac output and has been proposed to be a substitute for continuous blood pressure measurement [44] [45]. However, various researchers have presented conflicting data on the effectiveness of PTT as a biomarker for BP [46] [47] [48] hence it is absolutely essential to present systematic data on the effectiveness of PTT as a biomarker for BP make sense of these studies. Therefore, the relationship between PTT and BP during routine cardiac exercise stress test is investigated in this study by means of the ultra portable, ultra low-power smartwatch type design: the NICBPM, and an FDA approved electronic blood pressure monitor. The next subsection describes the algorithm for the detection of the R-peak.

---

### 3.7.1 Algorithm For PTT Calculation

---

PTT is obtained from simultaneous recording of the ECG and the PPG signal. PTT was calculated for each R-wave in the ECG and the steepest slope of the corresponding upstroke in the PPG signal [29] in Matlab according to the equation given below. The beat to beat PTT values were filtered with a moving average filter of 30 second window length.

$$PTT = T_{PPG} - T_{ECG}$$

$T_{PPG}$  = time at steepest slope of the PPG signal and  $T_{ECG}$  = time at R-peak in the ECG signal

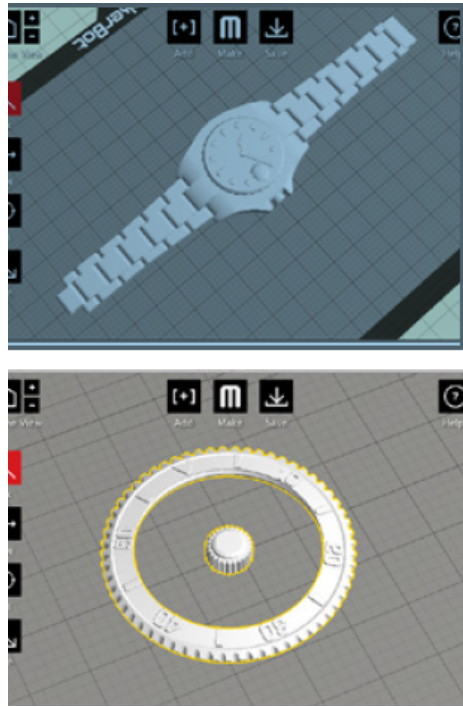


Figure 3.18.: Metallic Bezel on Top.



Figure 3.19.: Silicone Molded Prototype

---

### Signal Analysis

Wavelet decomposition was used to decompose the ECG signal into time-varying frequency components. The signal components were separated into various frequency bands to generate a reduced representation of the signal. This enables us to reproduce a sparser representation of the signal. The sym4 wavelet was selected to detect the QRS complex because it resembles the ECG signal, as shown in 3.21.

The R-peak was identified with 99.9% accuracy using a peak finding algorithm (findpeak in MATLAB) on the squared absolute values of the signal approximation constructed from the wavelet coefficients to obtain the  $T_{ECG}$  array, as shown in 3.22.

A similar peak detection algorithm was used to detect the peaks in the differentiated PPG signal to obtain the  $T_{PPG}$ , as shown in 3.24. The PPG signal and the first derivative of the PPG signal is shown in 3.23. The beat to beat PTT values were calculated by obtaining the time between the identified R-peak and the next peak in the differentiated PPG signal. The beat to beat PTT values was averaged over a 30 second interval (moving average filter) to make sense of the data.

---

#### 3.7.2 Pseudocode

Input ECG signal.

Apply 60 second window to ECG signal.

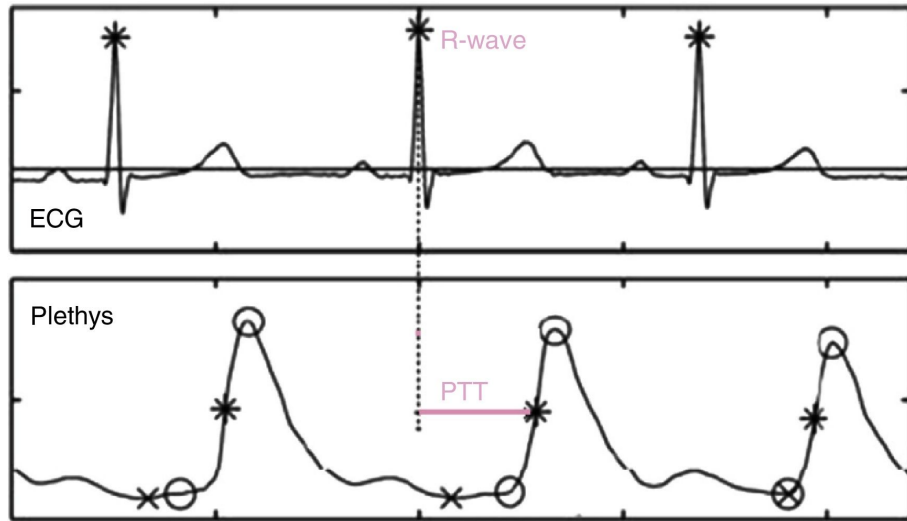


Figure 3.20.: Pulse Transit Time [37]

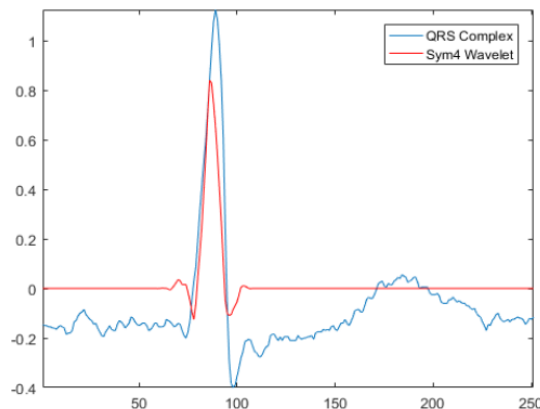


Figure 3.21.: QRS complex vs sym4 wavelet[49]

Apply wavelet transform to ECG signal to separate signal components into different frequency bands.  
 Decompose ECG signal to level 5 using sym4 wavelet.  
 Reconstruct a frequency-localized version of the ECG waveform using only the wavelet coefficients at scales 4 and 5.  
 (Scale 4 – [11.25, 22.5] Hz, Scale 5 – [5.625, 11.25] Hz)  
 Square absolute values of the signal approximation built from the wavelet coefficients.  
 Employ a peak finding algorithm on square absolute values to identify the R peaks.  
 Output array  $T_{ECG}$ .  
 Input PPG signal.  
 Apply 60 second window to PPG signal.  
 Plot 1st order derivative of PPG signal.  
 Employ a peak finding algorithm on the differentiated PPG signal to find the steepest point of PPG signal.  
 Output array  $T_{PPG}$   
 Calculate beat to beat PTT values in ms  
 Apply 30 seconds moving average filter to PTT curves.  
 Output PTT values averaged over 30 seconds

### 3.8 Calibration of BP sensor

A total of 30 subjects, participated in the study. Patient characteristics are shown in Table 3.1. The subjects were asked to fill out a medical history form to exclude any subjects with chronic heart failure. Simultaneous reading of

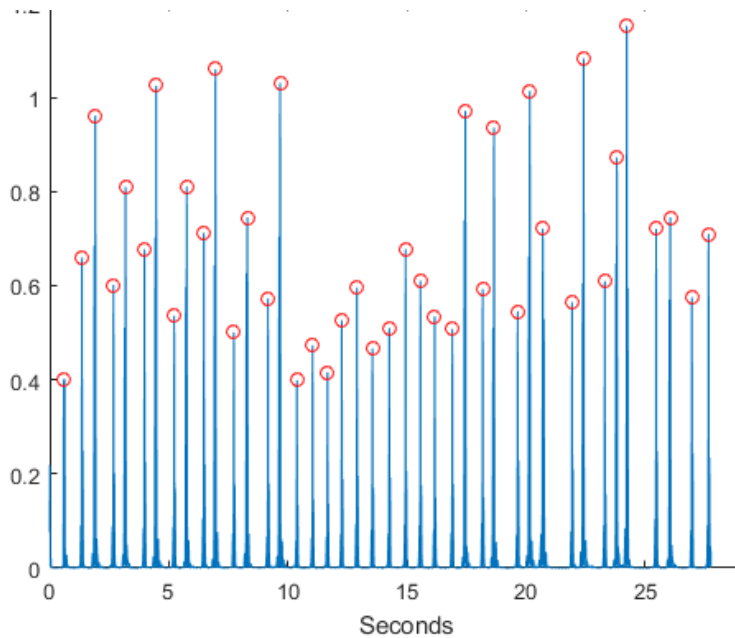


Figure 3.22.: Detection of R-peak using the sym4 wavelet vs visual inspection

sBP and dBp and the ECG and PPG signal are obtained from the automated oscillometric system (model BP101A, cuff-based apparatus as shown in 3.25) and the NICBPM before, during and after an exercise test.

Characteristic	N=30
Age	44.1+- 20.2
Male,n %	19(63.3%)
Body Height,cm	170+- 15.9

Table 3.1.: Patient Charcateristics

The exercise test comprised of riding a stationary bike with incremental load until exhaustion. Three data points (T1,T2,T3) are obtained during the 10 min reference period before the start of the exercise, five data points (T4,T5, T6,T7,T8) during exercise and 2 data points (T9,T10) during the recovery period, as shown in 3.2.

Data Pair	Description
T1,T2,T3	Recorded at Rest
T4,T5	Recorded during Exercise
T6	Recorded at Peak Exercise
T7,T8	Recorded after Peak Exercise
T9,T10	Recorded during Recovery

Table 3.2.: Description of Data Pairs

### 3.8.1 Data Analysis

The time synchronized ECG and PPG signal values were saved in a CSV file on the smartphone and uploaded to a PC for statistical analysis. The corresponding blood pressure reading were stored on the internal memory of the automated cuff-based blood pressure monitor. The PTT for each R-wave in the ECG signal and the steepest slope of the PPG signal was calculated [29] in Matlab. The beat to beat PTT values were filtered with a moving average filter, window length of 30 sec. 10 data pairs were selected for each subject.

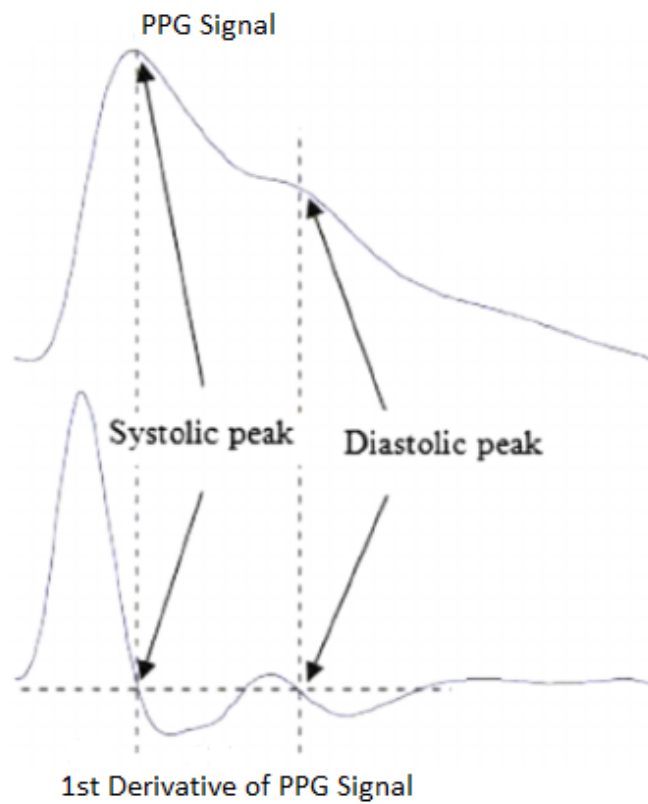


Figure 3.23.: PPG signal vs first derivative of PPG signal

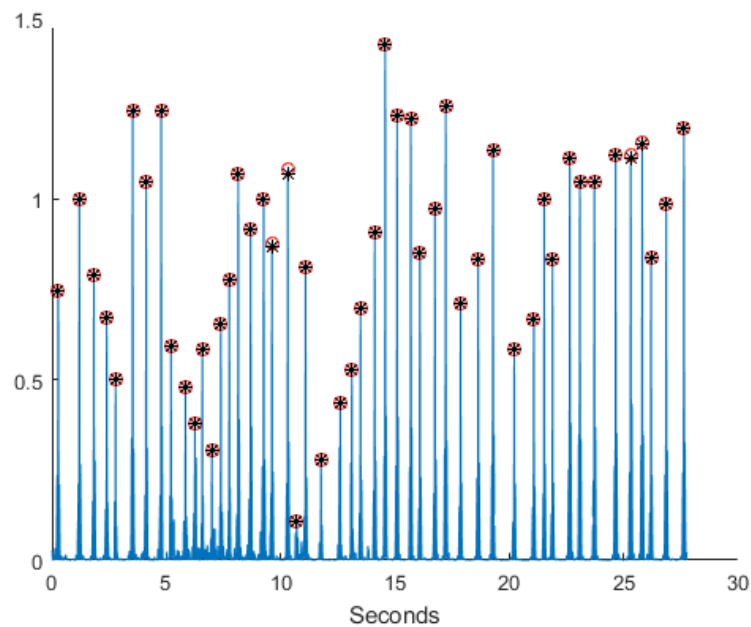


Figure 3.24.: Detection of steepest point in the PPG signal



Figure 3.25.: Cuff based apparatus

### 3.8.2 Statistical Analysis

Linear and non-linear regression models are used to analyze the relationship between PTT and BP on the acquired data. The standard linear regression model, as shown below was used to fit a linear function to the set of 10 data pairs obtained for each subject.

$$BP = m.PTT + C$$

An exponential non-linear regression model was used to fit a non-linear function, as shown in (2), to the same set of 10 data pairs obtained for each subject. A and B are constants unique to each subject.

$$BP = A \cdot exp^{B \cdot PTT}$$

The linear and non-linear best-fit curves obtained for each patient were used to calibrate the device to estimate BP respectively. The estimated BP was compared with the reading from the cuff-based apparatus for accuracy, and sensitivity.

## 4 Noninvasive Ophthalmic Glucose Monitor

Diabetes causes weight loss, frequent urination, excessive thirst and can eventually lead to death if left untreated. Around 150 million people suffer from diabetes worldwide. Researchers have been interested in the management of diabetes as a medical condition for more than 3000 years.

The first written record of diabetes can be found in Ebers Papyrus which was excavated from an ancient grave in Thebes, Egypt[8]. However, the first crude test for diabetes was reported by Indian doctors around 1500 BC when they observed that ants and flies were attracted to urine from people with diabetes. In 1815 Eugene Chevreul conclusively demonstrated that urine samples did in fact contain glucose. This lead to the development of the first quantitative test for glucose in urine by Von Fehling in 1848[8].

Since the development of the first quantitative test for glucose in blood, researchers have continuously tried to develop better ways to monitor blood glucose because strict regulation of blood glucose level is essential for the management of diabetes. This information helps the patient to monitor food intake. Strict regulation of blood glucose levels is achieved through timely food intake, regular blood glucose monitoring through finger-picking and carefully calculated insulin dosage delivered through an injection.

Unfortunately, it is necessary to collect blood to determine the serum concentration of glucose. Therefore, diabetics have no choice but to draw blood using a needle. Millions of diabetics draw blood invasively many times a day to monitor glucose levels. Researchers have developed several technologies to mediate the obvious discomfort of the conventional invasive approach. The GlucoWatch, as shown in 4.1 was awarded conditional FDA approval in 2001 as a noninvasive and continuous means of monitoring physiological glucose. Since the Glucowatch does not completely fulfill the reliability and accuracy criteria defined by FDA, it is strictly recommended that sugar levels must be monitored simultaneously and intermittently using conventional invasive blood sampling techniques to ensure reliable results.



Figure 4.1.: The Glucowatch- A noninvasive wearable Physiological Glucose Monitor. [50]

The Glucowatch is shown in, as shown in 4.1. The Glucowatch uses reverse iontophoresis to extract skin glucose as shown in 4.2. However, 15 years of research and development in the area of reverse iontophoresis based glucose sensors since the launch of the Glucowatch have failed to yield a reliable noninvasive glucose monitoring sensor according to FDA standards. Other emerging technologies such as glucose sensitive skin patches and implantable glucose sensors coupled insulin pumps have shown promising results but are still far from commercial production and FDA approval due to unreliability, high cost of manufacture and the relatively slow pace of advancement in applied technology required to catch up with theoretical models and proof of concept prototypes [8]. Even with all these emerging technologies, the demand for new noninvasive and continuous monitoring technology remains urgent and pressing both in the professional medical community and diabetic patients.

In this study we propose a glucose sensing contact lens which can potentially monitor tear glucose level. It has been reported by several researchers that tear glucose directly tracks blood glucose level [8][52], therefore it is a good choice to monitor tear glucose level. The contact lens was chosen as a preferred sensor since a majority of diabetics have weak eyesight and require glasses or contact lenses to improve their vision. The glucose sensing lense can be worn continuously by the user during daily activities. An optoelectronic sensor embedded within the wearable smartwatch type design or even directly in the users smartphone can analyse the glucose sensitive-optical properties of the lense

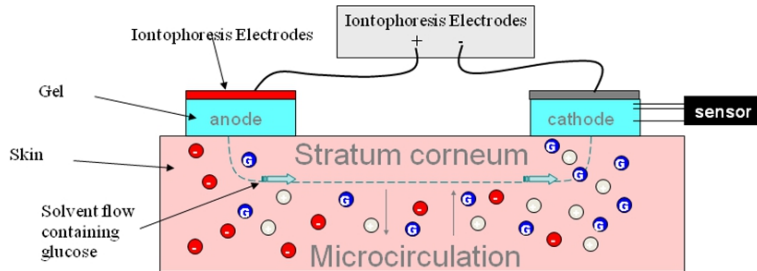


Figure 4.2.: Non Invasive Glucose Measurement Through Reverse Iontophoresis [51]

to calculate the concentration of tear glucose, which can be directly translated to blood sugar levels, while it is still in the eye. In this manner the user can track his blood sugar level simply by looking at the optoelectronic sensor as shown in 4.3. The whole process is as simple as taking a selfie of your eye.

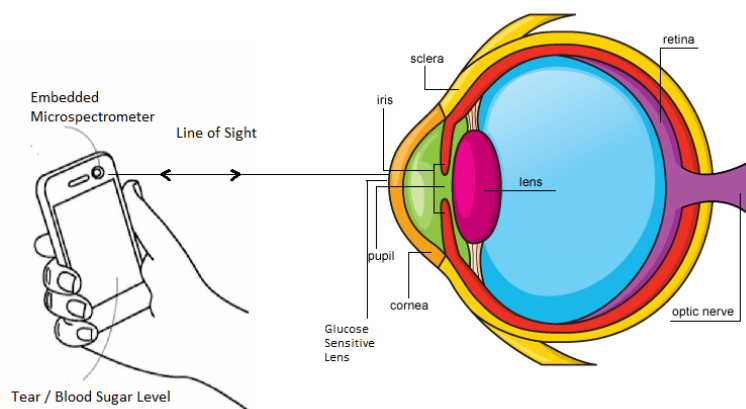


Figure 4.3.: Noninvasive Ophthalmic Glucose Monitor

In the next section the challenges of noninvasive ophthalmic glucose monitoring are discussed.

#### 4.1 Challenges

In this study we propose a new wearable noninvasive ophthalmic glucose sensor to monitor tear glucose level, which can directly track blood sugar levels. The new sensor should be affordable, easy to use and realizable within the realm of current technology.

The contact lens is to be doped with a glucose sensing fluorescent probe. The greatest challenge was to identify a suitable signalling probe which can produce a measurable signal in the presence of glucose. Several transduction elements were studied to identify a probe which had a measurable response to glucose and was considered safe for application in human eye by the FDA. Due to these limitations boronic acids which have been shown to display high affinity for diol compounds such as carbohydrates [53] [8], were selected as the primary candidates for developing a signalling probe. [54], [55] and several other researchers have used a variety of boronic acid derivatives to develop chemosensors for fructose and other monosaccharides.

The second challenge was the design of a mold which could incorporate this signalling probe and provide noninvasive access to human tears. Hence a disposable contact lens which is widely available over the counter was selected as a matrix to contain the signalling probe. We chose an OTC lens as the mold which holds the glucose sensing probe since its compatibility and safety in the human eye has been widely studied. Last but not least, the sensitivity, accuracy, reversibility, response time and the shelf life of the sensor needs to be optimized [8].

#### 4.2 Principles of Non Invasive Ophthalmic Glucose

Fluorescence is a form of luminescence caused by the emission of light by a substance that has absorbed light or other electromagnetic radiation [56]. Fluorophores are fluorescent chemical compound that re-emit light upon excitation

through light. Fluorophores typically contain several aromatic, planar or cyclic molecules with several pi bonds. Generally, the emitted light has a longer wavelength, and therefore lower energy, than the absorbed radiation. The fluorescence response of a glucose sensitive fluorophore can be analysed by a spectrophotometer to estimate the concentration of glucose.

#### 4.2.1 Spectrophotometer

A spectrophotometer measures the spectrum of light. It shows the intensity of light as a function of wavelength or frequency, as shown in 4.5.

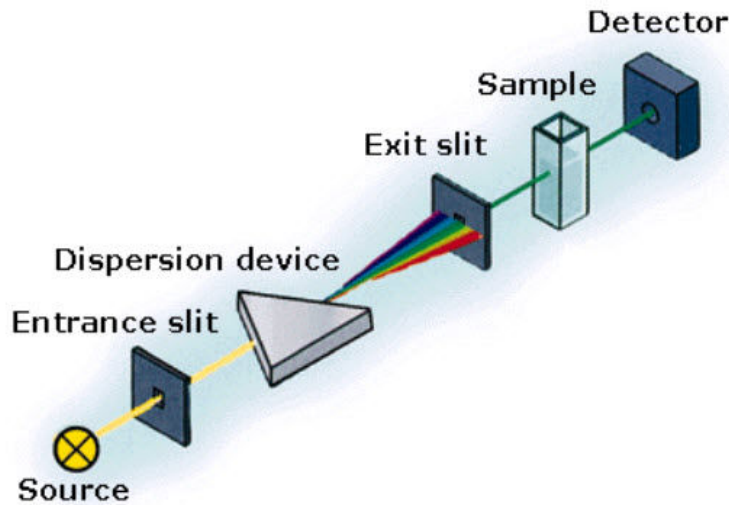


Figure 4.4.: Basic Concept of an Absorbance Optical Spectrometer [57]

A spectrophotometer works by splitting the incident light into its component frequencies As shown in 4.5. The intensity of these component frequencies are measured to evaluate the composition of the incident light. A lamp or an LED serves as the light source. The light beam strikes the dispersion device, usually a diffraction grating or a prism. The dispersion device separates the light into its component wavelengths. The diffraction grating is mechanically rotated to ensure that only a specific wavelength of light passes through the exit slit. The light interacts with the sample by reflectance and transmittance. The detector at the end can measure the transmittance, absorbance and reflectance of the sample.

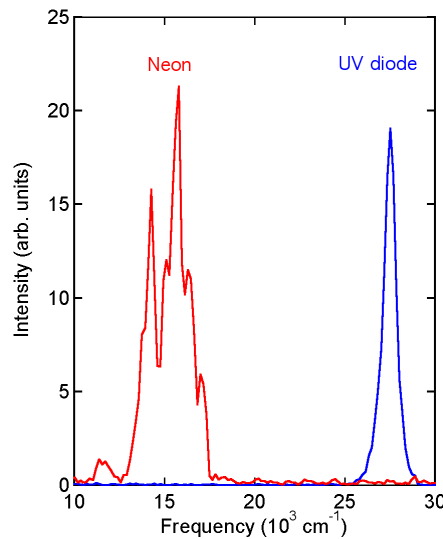


Figure 4.5.: Spectrum of Neon lamp vs UV diode as measured by a spectrophotometer [58]

In this study a Varian Cary UV/VIS 50 spectrophotometer as shown in 4.7 and 4.6 was used to evaluate the feasability of the approach described in the next sections. The Varian Cary 50 UV-Vis Spectrophotometer is a dual

beam, Czerny-Turner monochromator with a 190-1100 nm wavelength range and 1.5 nm fixed spectral bandwidth. It contains full spectrum Xe pulse lamp, dual Si diode detectors, quartz coated optics and a scan rates of up to 24000 nm/min and room light immunity.



Figure 4.6.: Varian UV/VIS 50 spectrophotometer

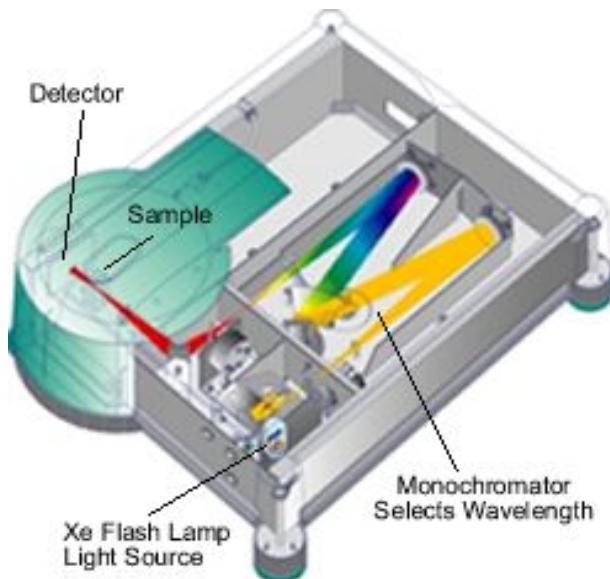


Figure 4.7.: Internal structure of the Varian UV/VIS 50 spectrophotometer

The conventional spectrophotometer is bulky and requires a lot of power. The spectrometer has been limited to laboratory environment due to a lack of availability of small, compact and low power spectrometers on the market. However, Hamamatsu Photonics K.K (Japan) launched the C12666MA microspectrometer in February 2015, which can perform the same functions as a conventional spectrometer and form the basis of any wearable ultra low-power design for spectroscopic application outside the lab. The next section discusses the selection of C12666MA Microspectrometer for our design.

#### 4.2.2 The C12666MA Microspectrometer

The C12666MA is an ultra-compact spectrometer head based on Micro-Electro-Mechanical Systems (MEMS) and image sensor technology as shown in 4.8 and the Data Sheet of the component [59]. The sensor is covered in a hermetic packaging against humidity resistance. The small spectrometer head was developed for integration into printers and hand-held color monitoring devices. However, the small size and its power profile make it suitable for applications in portable devices, such as smartphones, tablets and wearable devices[59] .

The fingertip sized dimensions: 20.1 X 12.5 X 10.1 mm are achieved by combining an input slit-integrated CMOS image sensor and a grating formed through nanoimprint on a convex lens[59]. The optical slit is achieved through

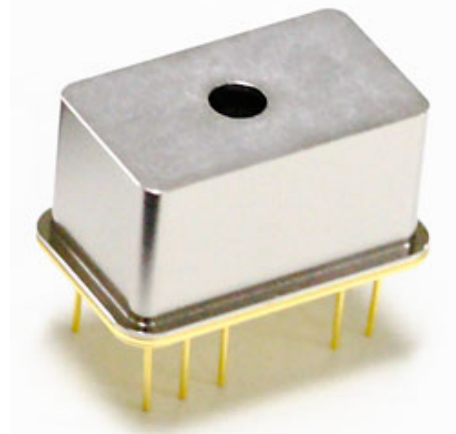


Figure 4.8.: The C12666MA Microspectrometer[59]

etching. The nanoprinted grating is a brazed concave reflective surface as shown in 4.9. It has a spectral resolution of 15 nm and a spectral response range from 340 to 780 nm. The sensor typically consumes 30mW and an output impedance of  $150 \Omega$  when the current flow is minimized by a CMOS buffer amplifier connected to the video output terminal [59]. The C12666MA can be easily integrated with an Atmel Atmega 328P microcontroller, as shown in 4.10. The output from the C12666MA can also be fed to a high resolution ADC for greater accuracy. The detailed schematic for the C12666MA Analog Front End (AFE) can be found in Appendix A

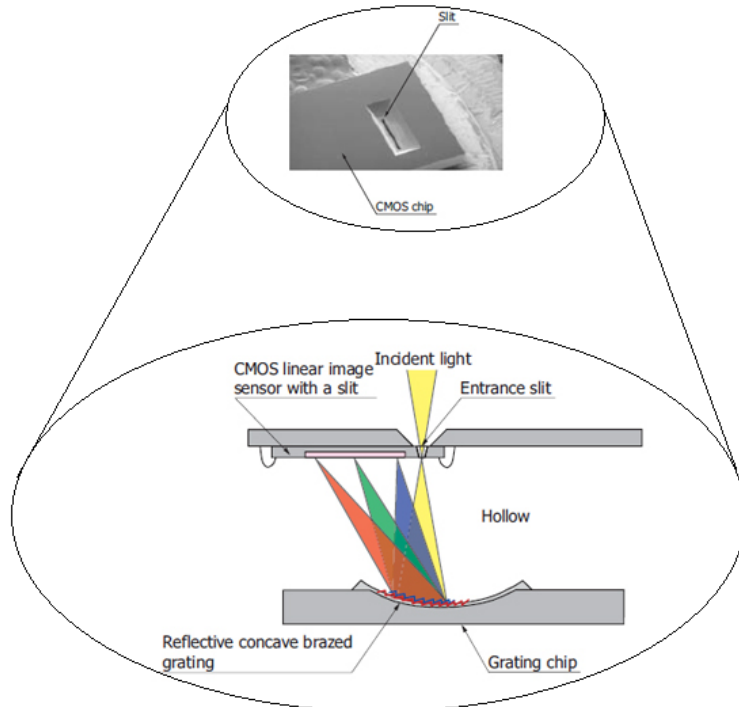


Figure 4.9.: Internal Structure of the C12666MA Microspectrometer [59]

#### 4.2.3 Molecular Absorbance Spectroscopy

A beam of ultraviolet or visible light is directed through a sample. A portion of that light is transmitted through the sample while the rest is absorbed. Transmittance is defined as the amount of light that passes completely through the sample and strikes the detector i.e ratio of  $P/P_o$ , as shown in 4.12. Absorbance is defined as the amount of light

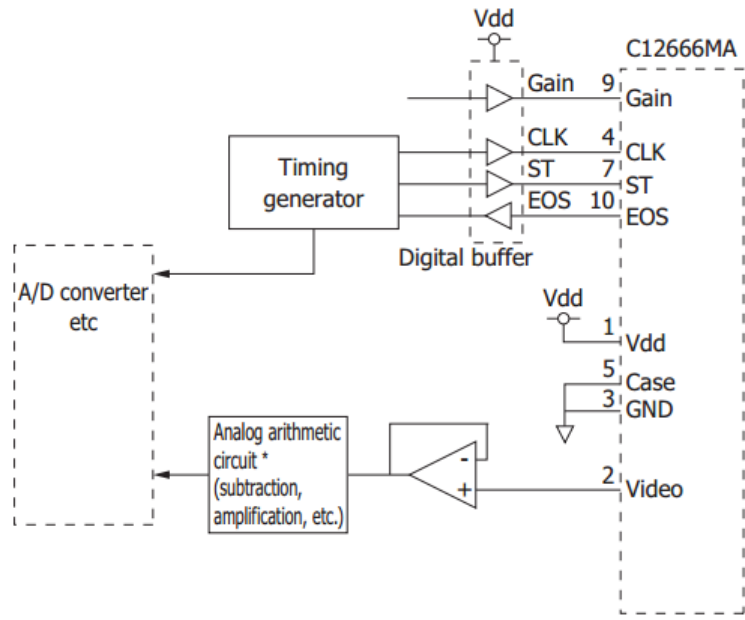


Figure 4.10.: C12666MA Analog Front End [59]

that is absorbed by the sample i.e ratio of  $-\log(P/P_o)$ , as shown in 4.12. Reflectance is defined as the amount of light reflected by the sample. The reflectance can be measured by changing the location of the detector.

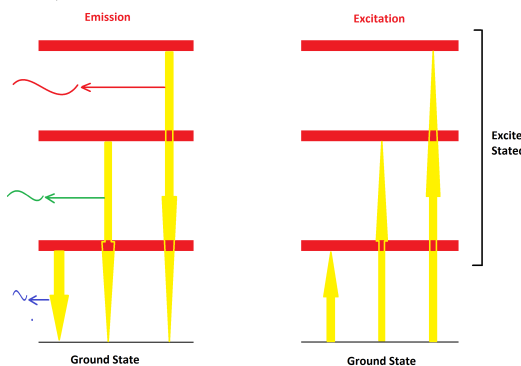


Figure 4.11.: Absorbance of Light

A molecule absorbs some of the light if it can accommodate the additional energy by elevating an electron to higher energy level as shown in 4.11. The energy of the light being absorbed must perfectly match the energy required to elevate the electron. Therefore, all wavelengths are not equally absorbed by a sample. The absorbance spectrum shows what wavelengths are absorbed by a sample as shown as 4.5. It can be easily seen which wavelengths are absorbed (peaks) and which wavelengths are transmitted (troughs). The concentration of the absorbing molecule is determined according to Beer's law:  $C = \frac{A}{m \cdot l}$  by measuring its absorbance, where  $A$  is the absorbance,  $m$  is the ability of a molecule to absorb radiation at a particular wavelength,  $l$  is the length of sample through which the light beam passes and  $c$  is the concentration of the absorbing molecule.

#### 4.3 Boronic Acid Fluorophores

Boronic acids are weak Lewis Acids containing an electron deficient boron atom and two hydroxyl groups, as shown in 4.13 [8]. Boronic acids react with strong bases to form anionic borate as shown in 4.14-top reaction, with a high pKa around 9 [60]. Boronic acids react with diols to form boronic acid diester as shown in 4.14- bottom reaction. The diol

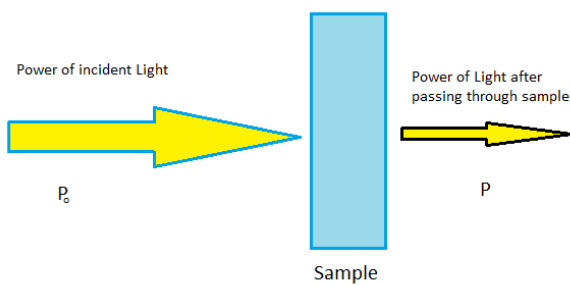


Figure 4.12.: Fluorescence: Excitation and Emission

establishes a reversible covalent bond making the reaction quick and completely reversible [60]. The diester shows higher acidity, pKa around 6, due to an electrophilic boron atom [61] [8]. The monophenylboronic acid group shows higher affinity for D-fructose with a smaller affinity for D-glucose, with a binding constants of 0.5 Molar and 10 milli molar respectively [60] [8]. The wide range of affinities of boronic acid groups for sensing monosaccharides makes it suitable for designing transduction elements with sensitivities ranging from millimolar concentration of glucose in blood to micromolar concentration in tear[61]. Since, we want to detect tear glucose we must identify a boronic acid with the appropriate molecular geometry and aromatic complex to achieve glucose sensitivity in the micro molar range.

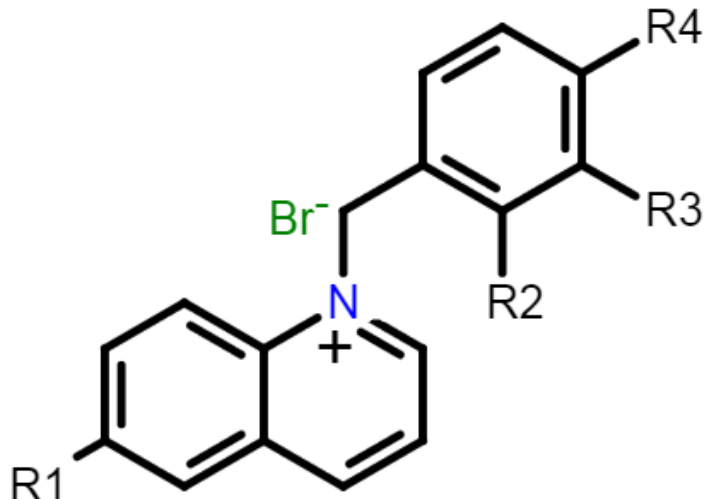


Figure 4.13.: Molecular Structure of Boronic Acid Glucose Sensing Probe

Isomer	R1	R2	R3	R4
Ortho-BMQBA	$OCH_3$	$B(OH)_2$	H	H
Meta-BMQBA	$OCH_3$	H	$B(OH)_2$	H
Para-BMQBA	$OCH_3$	H	R3	$B(OH)_2$
Ortho-BMQBA	$CH_3$	$B(OH)_2$	H	H
Para-BMQBA	$CH_3$	H	$B(OH)_2$	H
Isomer	$CH_3$	H	H	$B(OH)_2$

Table 4.1.: Molecular Structure of BMOQBA and BMQBA Isomers [8] [9] .

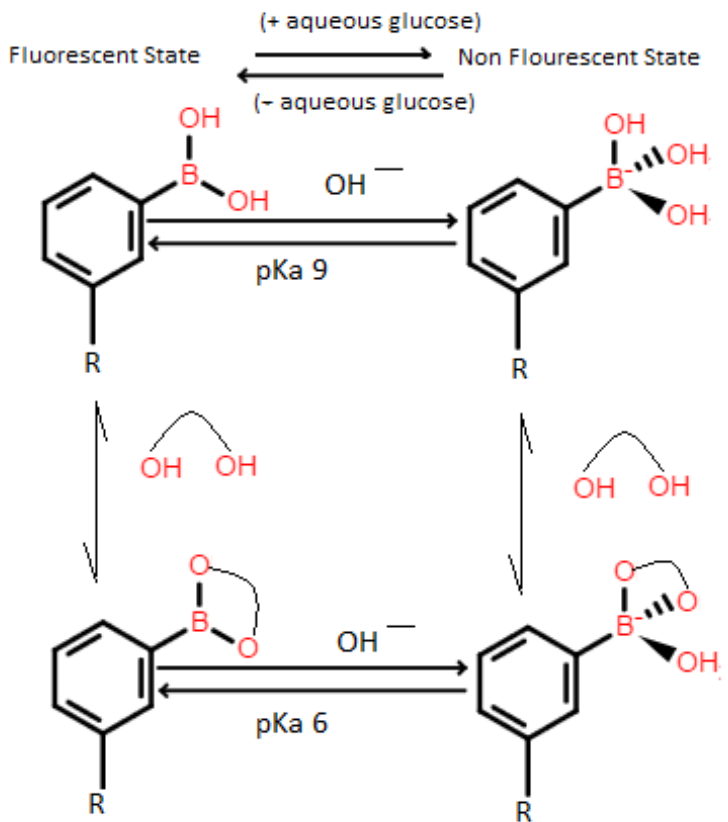


Figure 4.14.: Formation of anionic borate in basic medium.(Top);Formation of Diester in acidic medium ,(bottom)

#### 4.3.1 Design of New Glucose Sensing Probes

Since, OTC contact lenses display methanol like polarity and the internal environment is slightly acidic, we must identify a boronic acid fluorophore with significant glucose response in the mildly acidic environment within the contact lens polymer i.e a sugar-bound pKa of 6 [8]. The probe should be sensitive to extremely low concentrations of glucose present in tears (approx. 500  $\mu$ M) of healthy subject right upto 5 to 10 milli molar concentrations present in tear solution of diabetics. Since the pKa of phenyl boronic acid is tunable with appropriate additives [62] [8], the chemical and optical properties of 2 classes of isomeric boronic acid containing probes with pKa around 6 :BMOQBA: N-(boronobenzyl)-6-methoxyquinolinium bromide and BMQBA: N-(boronobenzyl)-6-methylquinolinium bromide, were studied to select an isomer with appropriate glucose affinity in ophthalmic conditions, as discussed in [9] [8] [9] [23] [55] and [62]. The molecular structure of BMOQBA and BMQBA are shown in table 4.1. Both molecules are based on the 6-methoxy quinoline compound. Badugu et al 2004 have demonstrated that the ortho isomer of both the boronic acid fluorophores has the greatest response towards glucose due to through-bond and through-space interaction [8] whereas the para isomer shows the weakest response due to the prevalence of through-bond mechanism[8]. The spectral response of the ortho isomers was therefore studied to assess the feasibility of the proposed approach.

#### 4.4 Materials and Methods

The disposable daily contact lenses were ordered online from Bausch and Lomb as shown in 4.15. This lens was chosen as a polyvinyl alcohol wetting agent containing both lipophilic and hydrophilic groups was used to condition the surface of the lenses during the manufacturing process. The lipophilic groups attach to the surface of the lense and the hydrophilic groups improve diffusion of aqueous compounds. The ortho isomer of BMOQBA and BMQBA were investigated as possible glucose sensitive probes since the maximum excitation dependent emission band of the ortho isomers lies in the range 427- 450nm [8] which is suitable for high resolution detection by the C12666MA spectrometer head.

The lenses were doped by incubating the lenses in a saturated solution of boronic acid containing signalling probe for 48 hours. The lenses were than rinsed with deionised water. For the simulation of lacrimal fluid which forms the

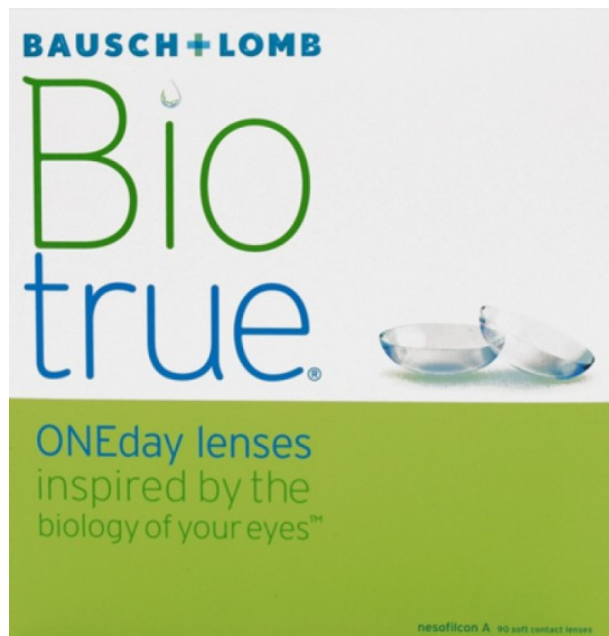


Figure 4.15.: Bausch and Lomb Daily Contact Lenses

precorneal film of the eye Tear Naturale from Novartis was used as the solvent for aqueous glucose solution to prepare various molar concentrations, ranging from 100 micromolar to 10 millimolar. The doped lens was placed in a transparent quartz lens holder with a raised surface and 0.05 ml of glucose solution was added to the lens holder with a dropper. The lens holder was then placed in a standard fluorometric cuvette and the fluorescence intensity of the lens was measured with a Varian Cary UV/VIS 50 spectrophotometer. The convex edge of the lens was excited with a vertically polarized LED source at 10 MHz with an excitation wavelength of approx. 370nm. The emission spectrum was captured at the magic angle of 54.7 degrees. The excitation wavelength was filtered optically. The fluorescence intensity of the emission spectrum was analyzed as a surrogate marker for ophthalmic glucose concentration. The experimental setup is shown in 4.16. The relationship between fluorescence intensity and glucose concentration was investigated in the ophthalmic glucose range observed in healthy individuals and diabetic i.e 0.5mM to 5 mM.

Saturated solution of signalling probes was prepared at room temperature and similarly all reading were taken at room temperature.

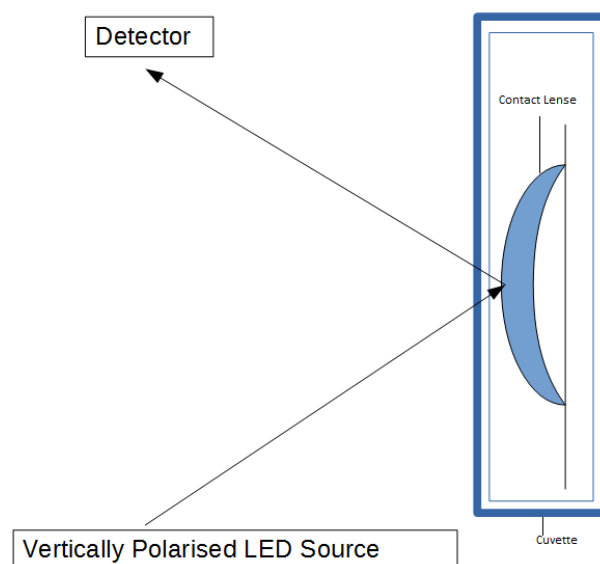


Figure 4.16.: Experimental Setup for Non Invasive Ophthalmic Glucose Monitoring Lenses



## 5 Results

### 5.1 NICBPM

An Atmel Atmega328P, 8Mhz microcontroller serves as the central processing unit of the device. The AD8232 serves as the analog front end for the measurement of ECG signal. The SFH7050 serves as the AFE for the measurement of PPG signal. The signals from the ECG AFE and PPG AFE are converted from analog to digital domain using a Successive Approximation (SAR) ADC of 12 bit precision. The time-stamped, digital data is finally transmitted by HC-05 Bluetooth communication module to a smart phone, as shown in 5.1.

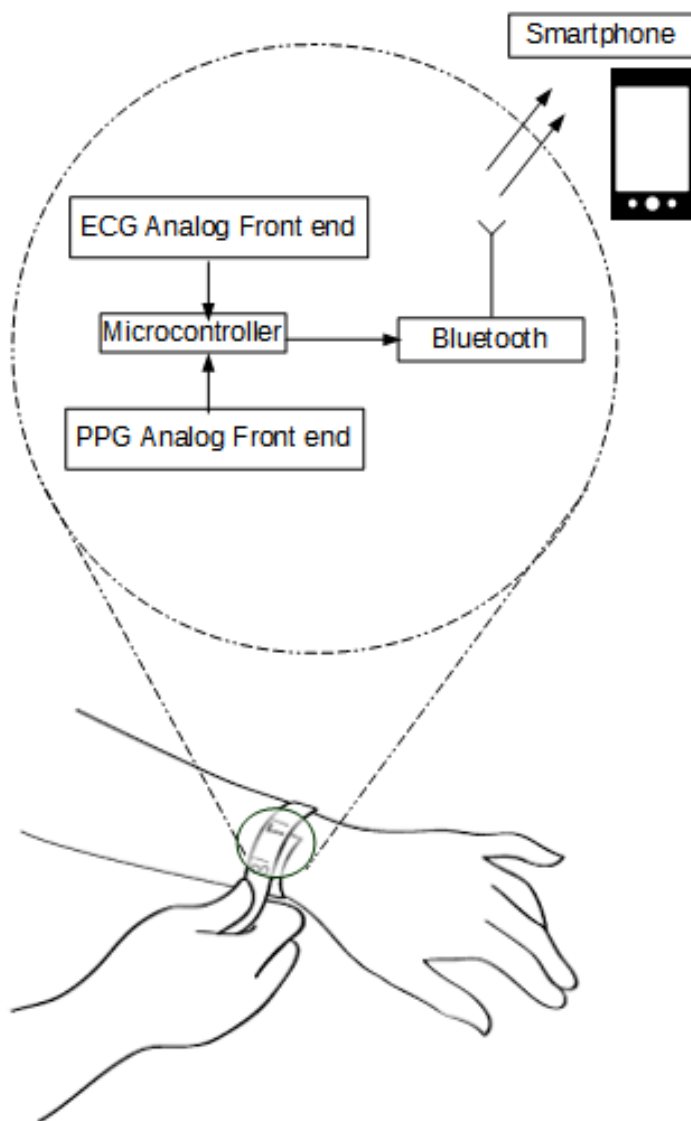


Figure 5.1.: Building Blocks of the Non Invasive Cuff Less Blood Pressure Monitor (NICBPM)

A commercially available 3.7V, 370mAh LiPo smartwatch battery is used to power the device. The maximum current draw of NICBPM in continuous operation mode is 4.85 mA.

### 5.1.1 Statistical Results

The majority of patients had no history of pulmonary disease. Mean sBP, dBP and PTT at rest were  $118 \pm 12$  mmHg,  $79 \pm 14$  mmHg and  $371 \pm 31$  ms respectively,  $190 \pm 35$  mmHg,  $89 \pm 14$  mmHg and  $276 \pm 25$  ms under maximum exercise, and  $128 \pm 10$  mmHg,  $83 \pm 13$  mmHg and  $354 \pm 38$  ms during recovery.

The correlation coefficients between PTT and sBP and dBP are calculated for each subject with linear regression model and non-linear regression model, resulting in a unique best fit curve for each subject. The coefficients of determination estimated for each subject are shown in 5.1. The estimated best-fit curves for subject 24 is shown in 5.4. Similar curves were obtained for each subject with  $0.92 < R_2 < 0.99$  and  $0.92 < r_2 < 0.99$  for sBP. In all subjects a strong negative correlation ( $r$ ) between PTT values and systolic Blood Pressure (sBP) was revealed by linear regression. The correlation between PTT and distolic Blood Pressure (dBP) was rather weak.

		$r^2$ Linear Regression	$r^2$ Linear Regression	$R^2$ Non Linear Regression	$R^2$ Non Linear Regression
Subject	Data Pairs (n)	sBP	dBP	sBP	dBP
1	10	0.95	0.28	0.97	0.27
2	10	0.95	0.29	0.96	0.28
3	10	0.98	0.28	0.95	0.28
4	10	0.94	0.28	0.99	0.27
5	10	0.93	0.29	0.93	0.27
6	10	0.92	0.28	0.93	0.28
7	10	0.98	0.51	0.98	0.49
8	10	0.96	0.28	0.95	0.27
9	10	0.97	0.51	0.92	0.51
10	10	0.98	0.28	0.94	0.29
11	10	0.95	0.28	0.98	0.28
12	10	0.95	0.53	0.98	0.57
13	10	0.97	0.27	0.97	0.27
14	10	0.98	0.6	0.92	0.61
15	10	0.95	0.27	0.98	0.28
16	10	0.96	0.27	0.92	0.28
17	10	0.98	0.29	0.93	0.28
18	10	0.97	0.28	0.93	0.28
19	10	0.92	0.29	0.96	0.29
20	10	0.92	0.28	0.94	0.28
21	10	0.96	0.29	0.94	0.29
22	10	0.96	0.27	0.98	0.28
23	10	0.92	0.71	0.92	0.64
24	10	0.99	0.11	0.99	0.27
25	10	0.99	0.28	0.96	0.28
26	10	0.97	0.52	0.96	0.52
27	10	0.96	0.06	0.95	0.07
28	10	0.95	0.29	0.94	0.28
29	10	0.95	0.27	0.94	0.27
30	10	0.93	0.27	0.93	0.27

Table 5.1.: Description of Data Pairs

Our results demonstrate that NICBPM must be calibrated atleast once, with intermittent readings from the gold standard method during an exercise test to obtain the individual best-fit curve for each subject.

5.2 shows the box plot of beat to beat PTT values for each patient. The box represents full range of values. The variance in beat to beat PTT makes it unreliable and impractical from a diagnostic point of view. In this study, a 30 second moving average filter was applied to make sense of the beat to beat PTT data. The effect of the length and type of the filter remains a subject of further investigation.

A comparison of the mean PTT curve and the mean sBP and dBP is shown in 5.3. The strong correlation between the PTT and sBP can be translated to accurate estimate of sBP but the mean dBP curve is only weakly correlated with the PTT.

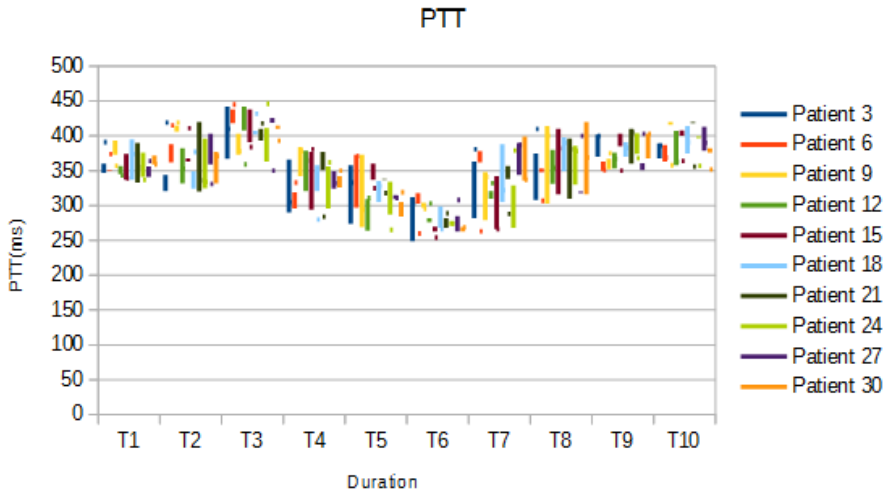


Figure 5.2.: Box plot of PTT at measuring points T1 to T10.

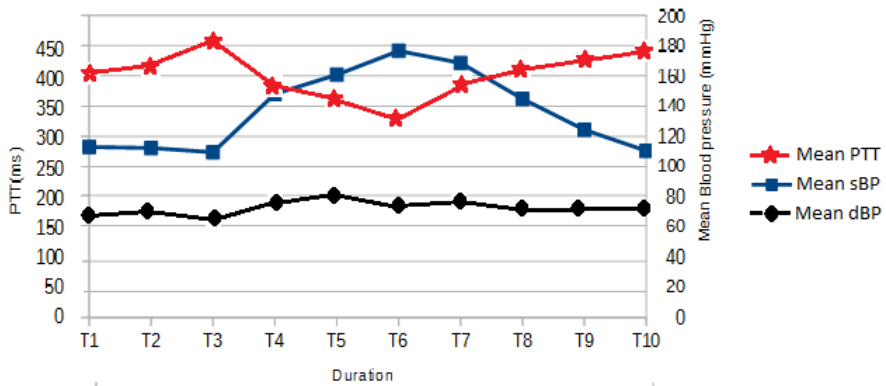


Figure 5.3.: Mean PTT, Mean sBP and Mean dBP for subject 24.

It is suspected that dBP is not strongly correlated with PTT because it is strongly related to vascular stiffness, vascular thickness and the clinical characteristics[63]. The dBP should be further studied for bivariate dependence with symmetric regression instead of standard regression. Some researchers have assumed linear relationship between dBP and sBP and presented various mathematical approaches to calculate the dBP from the sBP. However, our results indicate that any such approach is unreliable. It can be clearly seen that single dBP values correspond to multiple sBP values.

5.4 shows that the linear model assumes negative values of PTT for high BP values and vice versa. The non linear model provides a more realistic model for the asymptotic nature of the relationship. Hence, the non-linear model should be the primary choice for any future endeavour.

Unique best-fit curves similar to 5.4 characterize the relationship between PTT and sBP for each individual. However, this means that the NICBPM cannot be considered a universal BP monitoring device, yet it can accurately estimate the sBP from the PTT once it is calibrated for a particular individual during an exercise test.

Bland Altman Plot (BAP) [64] shows the difference and the limits of agreement between the measurement of BP from both instruments; the cuff-based apparatus and NICBPM. BAP revealed better limits of agreements ( $\pm 1.96$  Standard Deviation) for nonlinear model;  $\pm 8.5$ mmHg for sBP and  $\pm 6.6$  6.6mmHg for dBP, when compared to  $\pm 10.6$ mmHg for sBP and  $\pm 10.5$ mmHg for dBP for linear model, as shown in Fig. 9. Gesche et al reported agreement limits of  $\pm 19.8$ mmHg [65], and MasÁl et al reported  $\pm 12.9$  mmHg [66] for sBP, using different approaches. Hence, the NICBPM improves performance over previous work. Table 5.2 provides a simple comparison between our results and those reported previously.

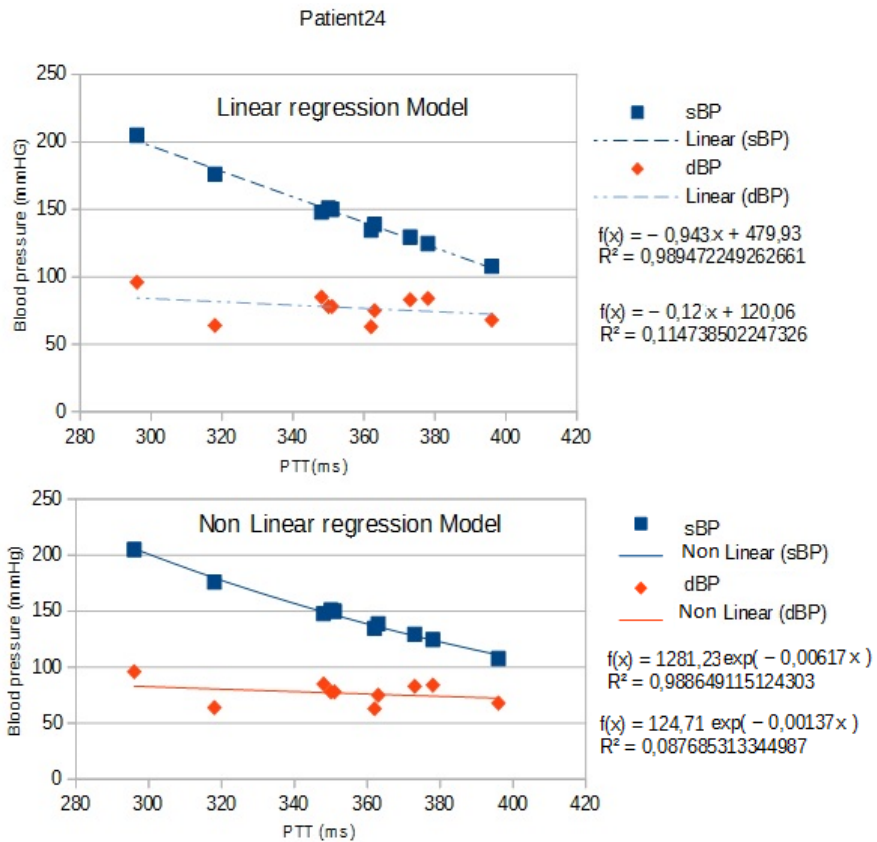


Figure 5.4.: Unique Best-fit Curves for patient 24 using Linear regression model (top) and non-linear regression model (bottom)

Limits of agreement (sBP)	$\pm 10.6$ mmHg	$\pm 8.5$ mmHg	$\pm 19.8$ mmHg	$\pm 13$ mmHg	$+18/-15$ mmHg
Limits of agreement (dBp)	$\pm 10.5$ mmHg	$\pm 6.5$ mmHg	-	$\pm 11.9$ mmHg	$+14 -13$ mmHg
	Linear Model	Non Linear Model	Gesche et al [65]	Mase et al [66]	Haber et al[67]

Table 5.2.: A Comparison with Prior Art

### 5.1.2 Discussion and Future Work

In the present study, linear and non-linear regression was performed to evaluate the relationship between Pulse Transit Time (PTT) and blood pressure. Previous studies have reported either only linear relationships between PTT and blood pressure or non-linear relations. A number of approaches are proposed to provided a suitable model for this relationship in our work. Callaghan et al. 1986; Gesche et al. 2012; Lass et al. 2004; Muehlsteff et al. 2006; Payne et al. 2006; Porta et al. 2006; Schmalgemeier et al. 2011; Yamashina et al. 2003 present conflicting results with varying approaches. Our work mediates the lack of availability of systematic data to make sense of previous and future studies on the relationship between PTT and BP. For the first time we have compared the linear and the non-linear model on the same set of data in human subjects with a wearable design.

The linear model assumes negative PTT values when blood pressure increases as well as negative blood pressure at higher PTT values. Therfore, the linear model is obviously limited in its scope and can lead to erroneous estimates of BP at higher PTT values. We proposed a simple new exponential non-linear model by assuming asymptotic behavior at higher PTT and BP values. Data analysis revealed that the exponential non-linear model was indeed more realistic. However, both models fitted the majority of observed data sets well.

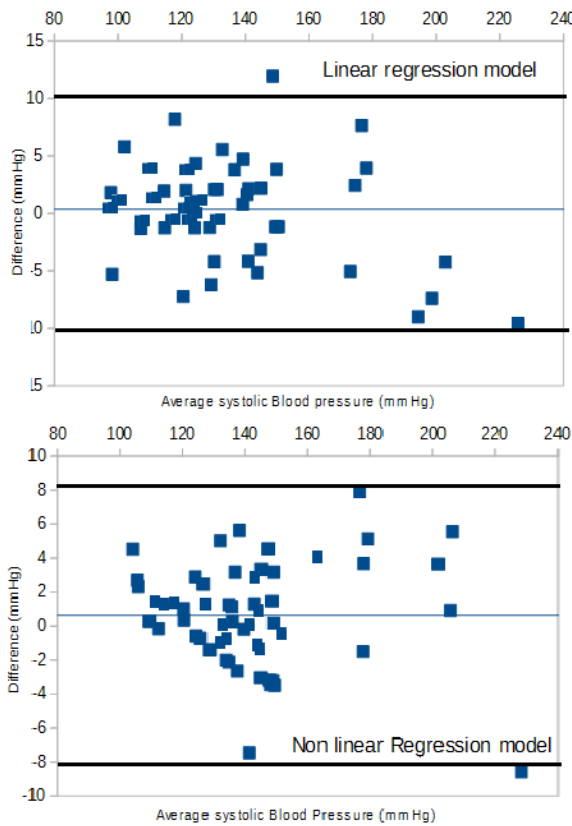


Figure 5.5.: Bland-Altman plots of sBP illustrates the disagreement between cuff-based apparatus and NICBPM from Linear (top) and non linear model (bottom) for 300 data pairs.

Since both models show strong correlation between PTT and sBP, we focus on the ability to predict sBP values from PTT using an ultra portable wearable design. Bland-Altman plots of the calculated BP values using both the linear and the non-linear approach show the limits of agreements between BP values estimated from our wearable design and the BP measured by the cuff method. The limits of agreements between the two methods obtained from the non-linear model were marginally better than those revealed from the linear model. Hence , we have demonstrated that any future scientific work should be based on a non-linear model. However, the linear model presents an alternative option in the absence of non-linear model. The overall limits of agreement between the two methods make our wearable design a good candidate for FDA approval. Our work paves the way for commercially available non-invasive cuff-less blood pressure monitoring devices.

It is noteworthy that continuous estimation of BP from the beat to beat PTT values is not possible using the method presented in our work. The variances in beat to beat PTT and BP clearly show that the beat to beat PTT values must be averaged. However, it must be stressed that estimation of continuous systolic blood pressure is not the only application of PTT. Wagner et al. 2010 have shown that the PTT-BP relationship at rest is altered in patients with chronic heart failure [38]. The relationship between PTT and BP during an exercise test can be characterized for the individual subjects using the methods presented here. This can provide information about the individual cardiovascular and autonomic response to exercise testing. Future work should be conducted to study the parameters of the non-linear model in chronic heart failure patients and other high risk patient groups to isolate the potential diagnostic application of PTT measurement.

We used an automated, intermittent, noninvasive, oscillometric system for blood pressure measurement. Continuous blood pressure measurement, including non-invasive methods as the volume clamp technique would have provided a large sample of beat-to-beat PTT-BP data, which could have allowed us to estimate the strength of the relationship and the goodness of fit more precisely. However, all methods of blood pressure measurements have known limitations and could have caused bias [68]. Interference from movement during exercise could have affected BP values from cuff based apparatus and PTT values from the PPG AFE. The error seemed tolerable but it should be studied systematically in future work. The role of room temperature, contact force of the PPG sensor and other such factors should also be systematically evaluated in future work. Bias and limits of agreement obtained during exercise test,

may not be compared to those for the validation of blood pressure measuring devices, since the relationship between PTT and BP may be altered by exercise. However, the overall results look very promising. If similar results can be obtained under the ANSI/AAMI SP10-2002 protocol or the protocol presented by O'Brien et al. 2010, the NICBPM can easily replace conventional blood pressure monitoring devices as a reliable alternative.

Measurement of PTT during exercise test is an easy method for monitoring systolic Blood Pressure when calibrated once with a simultaneous intermittent cuff -based BP readings. The algorithm for PTT calculation presented in our work, should be implemented in the commonly used cardiopulmonary ergometers. This can make PTT a widely available research tool in clinical setting.

### 5.1.3 Conclusion

In this study we present systematic data on the comparison of linear and non linear regression model on same data set to assess the relationship between PTT and BP. Based on this data, we concluded that the non-linear model provides a more accurate estimate of sBP. The NICBPM can estimate sBP with 99% accuracy and 99% sensitivity, after calibration. The dBP estimates were poorly correlated and therefore unreliable. The agreement between NICBPM and cuff-based method was within 10 mmHg for 99% of sBP readings. BP values above 160mmHg showed higher scatter and were the main source of error. We demonstrated that sBP can be reliably monitored with an ultra low-power, wearable, smartwatch type design. An effective calibration routine for such devices was presented.

## 5.2 Noninvasive Ophthalmic Glucose Monitor

A small, ultra-low power wearable photofluorometer based on the ultra portable spectrometer head was designed to be integrated into the smartwatch design . The Analog Front End for the integration of C12666MA spectrometer with an Atmel Atmega328P, 8Mhz microcontroller was designed and tested. The output from the sensor is fed to an external high resolution ADC (14-bit 100kSPS) instead of the one available in the microcontroller to overcome reduced sensitivity due to the limited resolution of the microcontroller ADC. A low power, precision operational amplifier, TI OPA344 is proposed as a buffer to reduce the current flow to the sensor, which may heat the sensor or raise the dark current. A low pass Pi filter with a cutoff frequency of 150 KHz removes high frequency components of the signal. An addressable Neopixel LED covers the range of light source required for excitation of the doped lenses. A TSL2560 ambient light sensor was used to detect the levels ambient light which was subtracted digitally from the signal obtained. The time-stamped, digital data can be transmitted by the HC-05 Bluetooth communication module to a smart phone as discussed in Chapter 4. The detailed schematic of the c12666MA can be seen in A

### 5.2.1 Wearable Design

The small dimensions of the spectrometer AFE allows it to be readily integrated into the smartwatch designed proposed earlier in this work. The user can check his sugar by activating the spectrometry sensor embedded in the watch and staring directly into it. The c12666MA Analog Front End (AFE) can also be integrated with a smartphone besides a regular camera which can allow the user to check his sugar level by taking a picture of his eye.

### 5.2.2 Ortho-BMOQBA

Ortho-BMOQBA was easily soluble in water in moderate quantities. The exact solubility of the probe was not investigated since the preparation of saturated solution required undissolved solvent. The emission spectrum of the Ortho-BMOQBA doped lens shows a pronounced maximum peak at 450 nm. The maximum absorption band was observed at 318 nm. The maximum emission band was independent of the excitation wavelength. However, a second absorbance band at 345 nm was observed. The 90% response time without subsequent excitation was 651 seconds. Figure 5.6 shows the changes in the emission spectrum of the BMOQBA doped lens in varying concentrations of glucose solution. It can be clearly seen that the fluorescence intensity of the Ortho-BMOQBA doped lens was inversely related to the concentration of glucose solution. A 70% decrease in fluorescence intensity was observed by increasing glucose concentration from 0.01 mM to 100 mM. A 23.8% decrease in fluorescence intensity was observed in the 0.01 mM to 5 mM range. The decrease in fluorescence intensity was significantly reduced at higher concentrations.

The maximum fluorescence intensity  $I^0$  at 450 nm was recorded in the absence of glucose and the fluorescence intensity  $I$  in glucose solution was used to plot the ratiometric fluorescence intensity  $I^0/I$  and the glucose concentration as shown in 5.8 and 5.9. Linear regression model revealed strong correlation  $r^2 = 0.99$  between the ratiometric fluorescence intensity in the ophthalmic glucose range. Changes of upto 0.1mM produced detectable changes in the

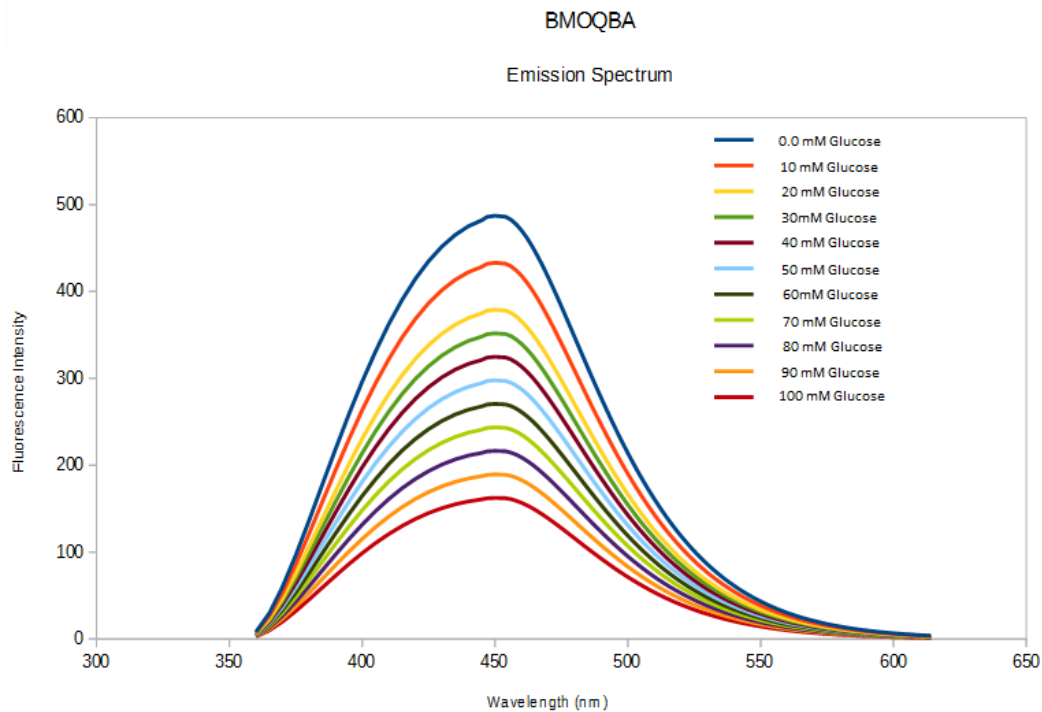


Figure 5.6.: Emission Spectrum of Ortho-BMOQBA Doped Contact Lenses In Increasing Concentrations of Ophthalmic Glucose Solution

fluorescence intensity. The linear response of the probe in the ophthalmic glucose range (0.5mM to 5mM) is shown in 5.9. However, the decrease in fluorescence intensity was not linearly related to the increase in glucose concentration over the entire range from 0.5mM to 100mM with minimal but detectable changes in fluorescence response at glucose concentrations above 12mM as shown in 5.8.

### 5.2.3 Ortho-BMQBA

Ortho-BMQBA also demonstrated similar characteristics. It was also easily soluble in water in moderate quantities. The emission spectrum of the Ortho-BMQBA doped lens shows a pronounced maximum peak at 427 nm. The maximum absorption band was observed at 320 nm. The maximum emission band was independent of the excitation wavelength. The second absorption band at 345 nm observed in the BMOQBA doped lense was missing in the absorbance spectrum of the BMQBA doped lense. Figure 5.7 shows the changes in the emission spectrum of the BMOQBA doped lens in varying concentrations of glucose solution. The fluorescence intensity of the Ortho-BMOQBA doped lens was also inversely related to the concentration of glucose solution. A 78% decrease in fluorescence intensity was observed by increasing glucose concentration from 0.01 mM to 100 mM and a 15.2% decrease in fluorescence intensity was observed in the 0.5 mM to 5mM range.

The maximum fluorescence intensity  $I^0$  for the Ortho-BMQBA probe was recorded at 427 nm in the absence of glucose. The fluorescence intensity  $I$  in varying concentrations of glucose solution was used to plot the ratiometric fluorescence intensity  $I^0/I$  versus the glucose concentration as shown in 5.8 and 5.9. Linear regression model revealed strong correlation  $r^2 = 0.99$  between the ratiometric fluorescence intensity in the ophthalmic glucose range. The linear response of the newly developed sensor in the ophthalmic glucose range (0.5mM to 5mM) is shown in 5.9. Figure 5.8 shows the fluorescence response of the probe over the entire range. The decrease in fluorescence intensity was significantly reduced at glucose concentration higher than 10mM. Changes of upto 0.12mM could be reliably detected with this probe. The 90% response time without subsequent excitation was 728 seconds.

### 5.2.4 Discussion and Future Work

The emission band of both the probes was independent of the excitation wavelength suggesting a simple binary (on-off) transition in terms of fluorescence. However, the second absorbance band observed for the Ortho-BMOQBA probes suggest an additional electronic transition for the oxygen atom. It is speculated that this transition is a n to pi star

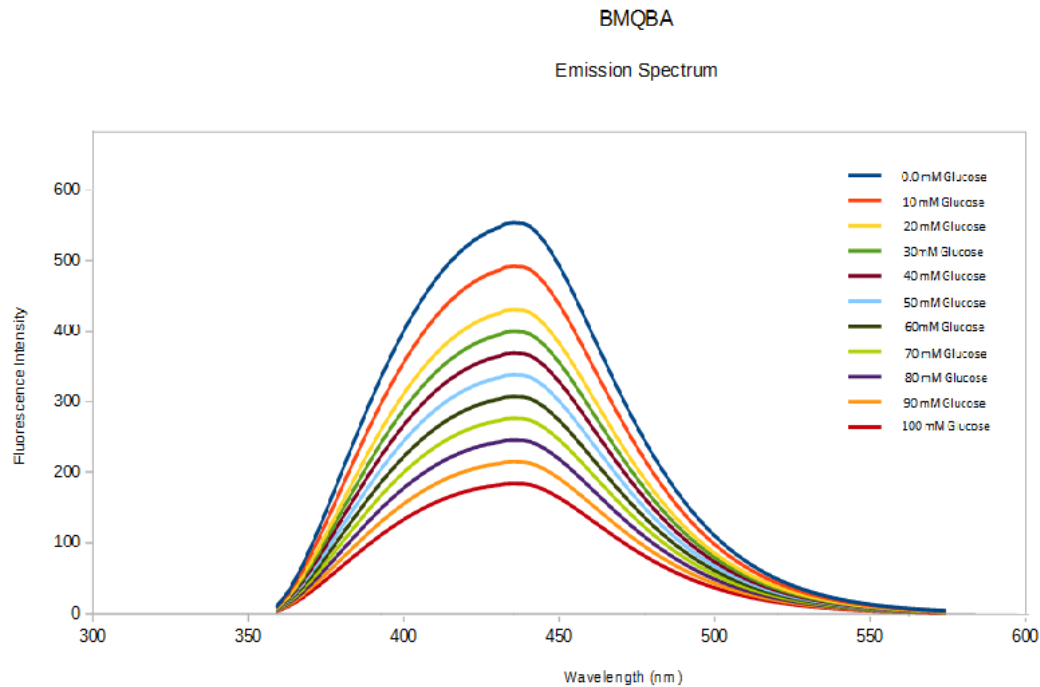


Figure 5.7.: Emission Spectrum of Ortho-BMQBA Doped Contact Lenses In Increasing Concentrations of Ophthalmic Glucose Solution

transition because it lies in the 190-380nm range. Any future work on the Ortho-BMOQBA probe should strive to understand the mechanism of this transition. The Ortho-BMOQBA probe exhibits a larger Stokes shift of 132nm making it easier to remove the excitation wavelength from the emission spectrum.

This study was restricted to simple fluorescence intensity measurements of the probes. In that regard both probes demonstrated similar qualitative results. The Ortho-BMOQBA probe was slightly more sensitive to glucose in the tear glucose concentration range as shown in 5.9. The Ortho-BMQBA probe could detect changes of upto 0.12 micromolar in contrast with 0.1 micromolar for Ortho-BMQBA in ophthalmic glucose concentration range, which is atleast a 10 fold improvement over the most sensitive conventional amperometric or enzymatic glucose sensor. This means that the Ortho-BMQBA probe has the ability of detecting a change of as little as  $7.2 \times 10^{11}$  molecules of glucose in 1 microlitre tear solution. A simple comparison of the glucose sensitivity and linear response range of the sensors as reported by other researchers is presented in Table 5.3. The detection sensitivity of the probes is inversely related to the concentration of glucose which suggests that the minimum detection threshold of our optoelectronic approach should lie in the molecular fingerprinting range. Any future work in this area should investigate the minimum detection threshold of our approach.

Sensitivity	0.1 $\mu$ M	0.12 $\mu$ M	0.1mM	1 $\mu$ M	2 $\mu$ M	53 $\mu$ M
Range	0.5 $\mu$ M to 10mM	0.5 $\mu$ M to 10mM	0.5 to 5 mM	4 $\mu$ M to 6 mM	5 $\mu$ M to 0.62 mM	0.55 to 4.4 mM
	Ortho-BMOQBA	Ortho-BMQBA	Badugu et al [8]	Peng et el [21]	Chowdary et el [69]	Farid et el[70]

Table 5.3.: A Comparison Of Sensitivity

It is noteworthy that qualitative similarity in the observed optical behaviour cannot easily be translated to other optical properties of probes with similar molecular structure. The quantum yield, mean life time and the exponential fluorescence lifetimes of similar probes reported by Badugu et el had no correlation with the glucose sensing ability of the probe, but they affected the overall effectiveness of the probe. These properties along with chemical interactions and safety standards for application in human subjects must be considered to design feasible signalling probes. In this study we investigated only the Orhto isomer of both probes since the monoexponential fluorescence lifetime of the ortho isomer is greater than the para or the meta isomer. However, the ortho isomers had the lowest quantum yield which means that probability of deactivating the excited state through fluorescence was not very high. The trade-off between monoexponential fluorescence lifetime and the quantum yield needs to be optimized for continuous monitoring. A

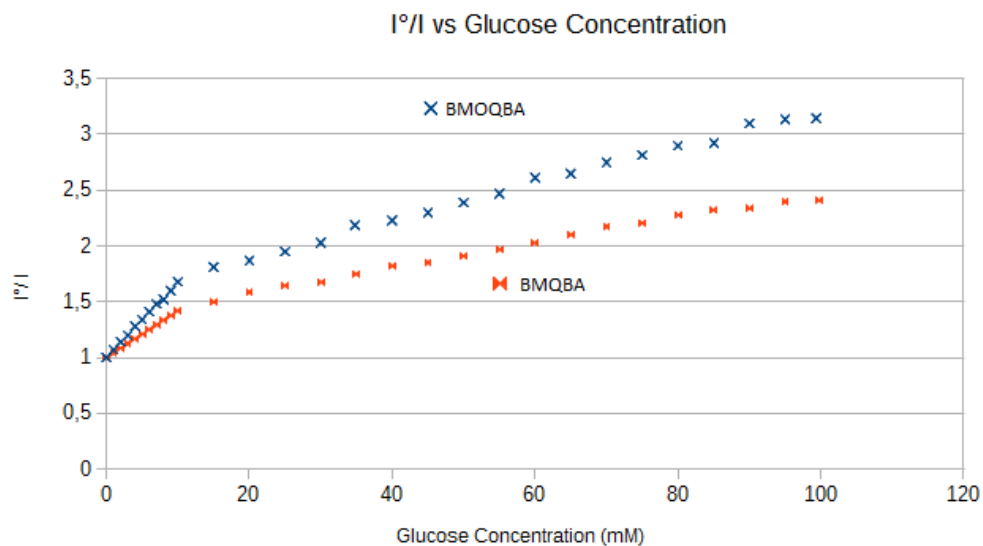


Figure 5.8.: Intensity ratio  $I^o/I$  of ortho-BMOQBA and ortho-BMQBA in increasing concentration of Glucose Solution.

higher quantum yield is desirable for ease of detection and increasing sensitivity and a longer fluorescence lifetime is desirable for continuous monitoring.

The absorption spectrum of the doped lenses does not lie in the visible spectrum range. Hence, the doped lenses are colourless which make them ideal for daily use. However, it is also possible to design glucose signalling probes with a visible absorption spectrum. A possible avenue for future development would be the design of coloured signalling probes which can change colour according to the concentration of glucose in tears, thus eliminating the need for a handheld photofluorometer to analyze the spectrum of the lenses. The user can simply stand in front of a mirror and compare the colour of the glucose sensitive lenses in his eye with a precalibrated colour card. In this study our focus lies on simple glucose sensing fluorescence probes and a wearable photofluorometer but this approach can be reproduced with colorimetric methods using a regular smartphone camera and a colour changing lense. The colorimetric approach may not be as accurate as our approach but the results might still be better than the current enzymatic or amperometric methods. Future work in this area should be concentrated on the polarization characteristics and fluorescence lifetime of the probes. Our approach should be tweaked with suitable fluorescent agents to detect chemical biomarkers for other diseases such as Glaucoma and corneal ulceration. Glaucoma can be diagnosed by designing the lense to detect catecholamines and corneal ulceration can be detected by designing a lens to detect collagenase. A major hurdle in the design of such sensors might be the identification of probes which are biocompatible, safe for application in the human eye, compatible with the chemistry of the current lenses manufacturing technology and an optical spectrum responsive to photochemical changes in ocular condition. The sensor should exhibit a biomarker dependent optical spectrum in the physiological pH range. The boronic acid fluorophores have been identified as a viable probe for glucose detection in this study. Future effort in this regard should be directed at identifying isomers in the same family (methylquinolone derivatives like BMQBA and BMOQBA) which can be chemically engineered to detect any molecule in an extremely small volume (5-10 microlitre) of the solution. Vitamin A and its derivatives and FRET pair-labeled concanavalin A along with fluorescent labelled proteins should be explored in future work as a potential probe for the detection of halides and electrolyte concentration of tear. The lenses could even be doped with a temperature sensitive probe to track body temperature. Indeed, our ophthalmic sensing approach could be modified to track all vital parameters of an individual through the eye.

Hamamatsu is a market leader in introducing the microspectrometer head to the market. The lack of competition from other manufacturers allows them to demand unreasonably high prices currently. With the development of microspectrometer heads from other manufacturers, the price will fall exponentially and it can be foreseen that a microspectrometer similar to the C126666MA would be available under 10 \$ within the next 10 years. The reduction in price will enable widespread integration in biomedical devices or labs-on-chip systems which can analyze the molecular composition of samples outside the conventional laboratory environment. However, the microspectrometer head is a relatively new addition to the market and it may be difficult to introduce this component as a biomedical sensor before its effectiveness and application in the optical communication domain is demonstrated extensively.

### I<sup>o</sup>/I vs Glucose Concentration

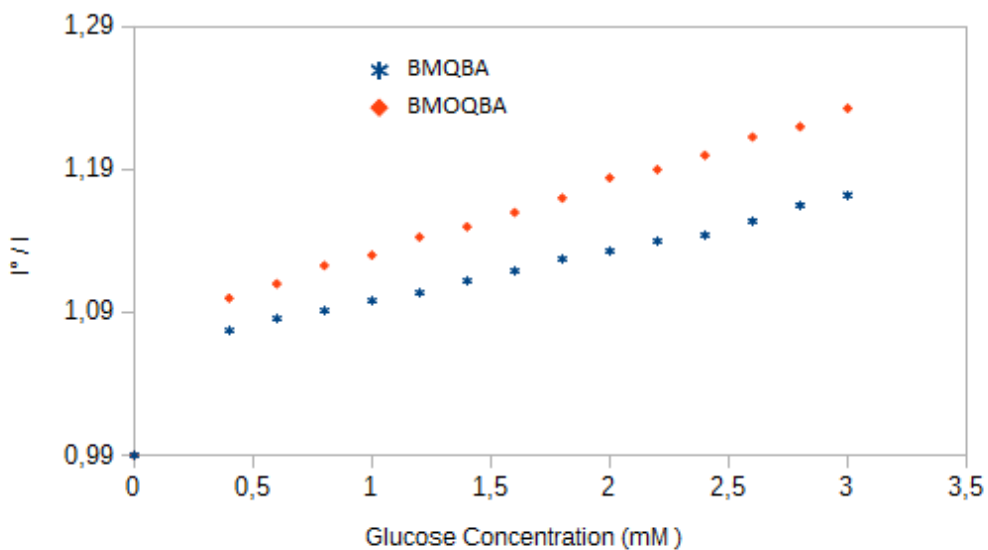


Figure 5.9.: Intensity ratio  $I^o/I$  of ortho-BMOQBA and ortho-BMQBA in Ophthalmic Glucose Range.

#### 5.2.5 Conclusion

In this study the feasibility of using fluorophore doped over the counter lenses to monitor tear glucose non invasively is clearly demonstrated. For the first time, a wearable photofluorometer based on the C12666MA micro-spectrometer head to monitor the glucose dependent fluorescence intensity of the doped lense is proposed.

2 new types of glucose sensitive contact lenses are developed in this study. A new breed of fluorescent glucose signalling probes is identified and the fluorescence response of the ortho isomer in the range of ophthalmic glucose concentrations is evaluated. Commercially available over the counter lenses were doped with these fluorescent agents. The chemistry of the lenses was consistent with the fluorescent signalling probes. Our results show that the doped fluorescent lenses can be used in tandem with a handheld photofluorometer to detect changes of upto 0.1mM in tear glucose noninvasively. Moreover, the response of the fluorescent lenses for both probes was linear in the tear glucose range for healthy individuals as well as diabetics, i.e 0.5mM to 5mM. Our approach offers significant improvements in range, accuracy, sensitivity, ease of use and linearity over conventional methods such as enzymatic, amperometric and coulometric approaches of monitoring glucose which require blood sampling through invasive means. We believe that the fluorophore doped lense and a wearable photofluorometer is a promising approach for monitoring physiological glucose noninvasively and accurately.

## 6 Summary

The real time portable low power wearable vital signs monitoring system proposed in [18] was extended with an Electrocardiogram Analog Front End and a Blood Pressure sensor. The proposed system can now monitor the heart rate, inter beat interval, blood oxygen saturation and dehydration level, Photoplethysmogram, Electrocardiogram, Pulse Transit Time, body temperature and exposure to ultraviolet radiation with similar core architecture as described in [18]. The physical form factor of the proposed system was designed as a 3D-printable smartwatch housing. The electrical design was based on minimalism to reduce power consumption. The finished prototype was calibrated to estimate the Blood Pressure of an individual non-invasively. The system could estimate sBP with 99% accuracy and is a good candidate for FDA approval. The wearable cuff less blood pressure monitor has the potential of replacing the auscultatory method as the gold standard. Due to our minimalist approach the ECG signal of the subject was obtained with only 2 electrodes instead of 3. Hence the effectiveness of the ECG signal as a potential diagnostic tool for heart conditions should be studied in further research alongwith the implementation of our propriety algorithm for PTT calculation on conventional ergonometers to popularize the use of PTT as a diagnostic tool. An innovative new approach for noninvasive glucose sensor was introduced in this study. The new sensor was based on a boronic acid fluorophore doped contact lenses and a wearable photospectrometer. The linearity of these sensors in the tear glucose concentrations was demonstrated. An Analog Front End for the integration of the microspectrometer in the existing smartwatch design is presented. The safety and the efficiency of the proposed glucose sensor needs to be evaluated in clinical settings to determine the correlation of glucose concentration dependent fluorescence intensity and blood sugar levels. A logical next step in the development of this technology would be the calibration of the sensor presented here against an invasive technique such as blood sampling by fingerpicking using the statistical methods presented for the calibration of the BP sensor.



# List of Figures

1.1 Popular Wearable Devices. Credit:elekslabs.com . . . . .	7
1.2 E-Textile Monitoring Systems Credit:SmartX, Italy . . . . .	8
1.3 Trends in unobtrusive sensing . . . . .	9
1.4 SmartBand Talk SWR30, Credit: Sonymobile.com . . . . .	9
1.5 Wearable Devices During Daily Activities . . . . .	10
2.1 Conventional reflectance Photoplethysmogram sensing from the Fingertip . . . . .	11
2.2 Photoplethysmogram signal obtained from the wrist [14]. . . . .	11
2.3 SFH 7050 Sensor with integrated LEDs and photodiode [15]. . . . .	12
2.4 Absorption Spectrum Of Human Blood vs Wavelength [15]. . . . .	13
2.5 Transimpedance Setup For PPG Analog Front End [15] [16] . . . . .	13
2.6 Heart Rate Monitor [15]. . . . .	14
2.7 Pulse Oximeter With Equalization Of DC levels. Ambient Subtraction Performed In The Digital Domain [15]. . . . .	14
2.8 Pulse oximeter measuring AC and DC signal level. A programmable offset via a programmable DC tracker is subtracted initially to obtain a high resolution AC component. Ambient subtraction performed in the digital domain allowing an individual ambient measurement [15]. . . . .	15
2.9 Conventional ECG Machine. Source:careshine.en.made-in-china.com/ . . . . .	16
2.10 Portable ECG Machine. Source:handheldecmachine.com . . . . .	16
2.11 Body Temperature Sensor and Subsequent Sampling Stage [20] . . . . .	17
2.12 Glucose Sensing Lenses[22] [13]. Made by Google X labs. Source:coolthings.com . . . . .	18
2.13 Enzymatic Ophthalmic Glucose Monitor . . . . .	18
2.14 System Architecture . . . . .	19
2.15 Telemetry System . . . . .	20
3.1 Human Heart. Source: cephalicvein.com. . . . .	21
3.2 2-Electrode Configuration . . . . .	22
3.3 ECG Signal Obtained From The 2-Electrode Configuration . . . . .	22
3.4 Important Intervals In The ECG Signal. Source:Wikipedia.org . . . . .	23
3.5 Einthoven's Triangle [17] . . . . .	24
3.6 ECG Signal From Each Lead . . . . .	25
3.7 ECG Signal From Different Electrode Placements [17]. . . . .	26
3.8 Possible 3 Electrode Configurations [17] . . . . .	27
3.9 Possible 2 Electrode Configurations [17]. . . . .	27
3.10 ECG AFE based on the AD620 Instrumentation Amplifier [30] [31] . . . . .	28
3.11 Internal Structure Of An Instrumentation Amplifier [32] . . . . .	28
3.12 Internal Structure Of The AD8236[33] . . . . .	29
3.13 Heart Rate Monitor Based On AD8236 [33] . . . . .	30
3.14 Internal Structure Of The ADAS1000 [34] . . . . .	31
3.15 Functional Block Diagram of AD8232 [35] . . . . .	32
3.16 Top view of 3D Printable Watch Housing. . . . .	33
3.17 Bottom view of 3D Printable Watch Housing. . . . .	33
3.18 Metallic Bezel on Top. . . . .	34
3.19 Silicone Molded Prototype . . . . .	34
3.20 Pulse Transit Time [37] . . . . .	35
3.21 QRS complex vs sym4 wavelet[49] . . . . .	35
3.22 Detection of R-peak using the sym4 wavelet vs visual inspection . . . . .	36
3.23 PPG signal vs first derivative of PPG signal . . . . .	37
3.24 Detection of steepest point in the PPG signal . . . . .	37
3.25 Cuff based apparatus . . . . .	38
4.1 The Glucowatch- A noninvasive wearable Physiological Glucose Monitor. [50] . . . . .	39

4.2	Non Invasive Glucose Measurement Through Reverse Iontophoresis [51]	40
4.3	Noninvasive Ophthalmic Glucose Monitor	40
4.4	Basic Concept of an Absorbance Optical Spectrometer [57]	41
4.5	Spectrum of Neon lamp vs UV diode as measured by a spectrophotometer [58]	41
4.6	Varian UV/VIS 50 spectrophotometer	42
4.7	Internal structure of the Varian UV/VIS 50 spectrophotometer	42
4.8	The C12666MA Microspectrometer[59]	43
4.9	Internal Structure of the C12666MA Microspectrometer [59]	43
4.10	C12666MA Analog Front End [59]	44
4.11	Absorbance of Light	44
4.12	Fluorescence: Excitation and Emission	45
4.13	Molecular Structure of Boronic Acid Glucose Sensing Probe	45
4.14	Formation of anionic borate in basic medium.(Top);Formation of Diester in acidic medium ,(bottom)	46
4.15	Bausch and Lomb Daily Contact Lenses	47
4.16	Experimental Setup for Non Invasive Ophthalmic Glucose Monitoring Lenses	47
5.1	Building Blocks of the Non Invasive Cuff Less Blood Pressure Monitor (NICBPM)	49
5.2	Box plot of PTT at measuring points T1 to T10.	51
5.3	Mean PTT, Mean sBP and Mean dBp for subject 24.	51
5.4	Unique Best-fit Curves for patient 24 using Linear regression model (top) and non-linear regression model (bottom)	52
5.5	Bland-Altman plots of sBP illustrates the disagreement between cuff-based apparatus and NICBPM from Linear (top) and non linear model (bottom) for 300 data pairs.	53
5.6	Emission Spectrum of Ortho-BMQBA Doped Contact Lenses In Increasing Concentrations of Ophthalmic Glucose Solution	55
5.7	Emission Spectrum of Ortho-BMQBA Doped Contact Lenses In Increasing Concentrations of Ophthalmic Glucose Solution	56
5.8	Intensity ratio $I^o/I$ of ortho-BMQBA and ortho-BMQBA in increasing concentration of Glucose Solution.	57
5.9	Intensity ratio $I^o/I$ of ortho-BMQBA and ortho-BMQBA in Ophthalmic Glucose Range.	58
A.1	Schematic of Control Unit	65
A.2	Schematic of Electrocardiogram (ECG) Analog Front End (AFE)	66
A.3	Schematic of C12666MA Analog Front End (AFE)	67
A.4	Schematic of Photoplethysmogram (PPG) Analog Front End (AFE)	68

## Acronyms

ADC Analog to Digital Converter. 48

AFE Analog Front End. 14, 18, 25, 48, 55, 66–68

BAP Bland Altman Plot. 41

BJT Bipolar Junction Transistor. 17

BP Blood Pressure. 3, 7, 21

dBp distolic Blood Pressure. 40

ECG Electrocardiogram. 3, 17, 18, 22, 23, 66

HPF High Pass Filter. 22

HR Heart Rate. 7

IOT Internet Of Things. 11

MEMS Micro-Electro-Mechanical Systems. 47

NICBPM Non Invasive Cuff Less Blood Pressure Monitor. 3, 21, 22, 24, 26, 28, 30, 32–34, 36, 38, 39

OTC Over The Counter. 46

PPG Photoplethysmogram. 3, 12–14, 68

PTT Pulse Transit Time. 3, 33–35, 41, 42

sBP systolic Blood Pressure. 40

SPO<sub>2</sub> Oxygen Saturation. 7, 13

T Body Temperature. 7



# A Schematics

## A.1 Schematic of Control Unit

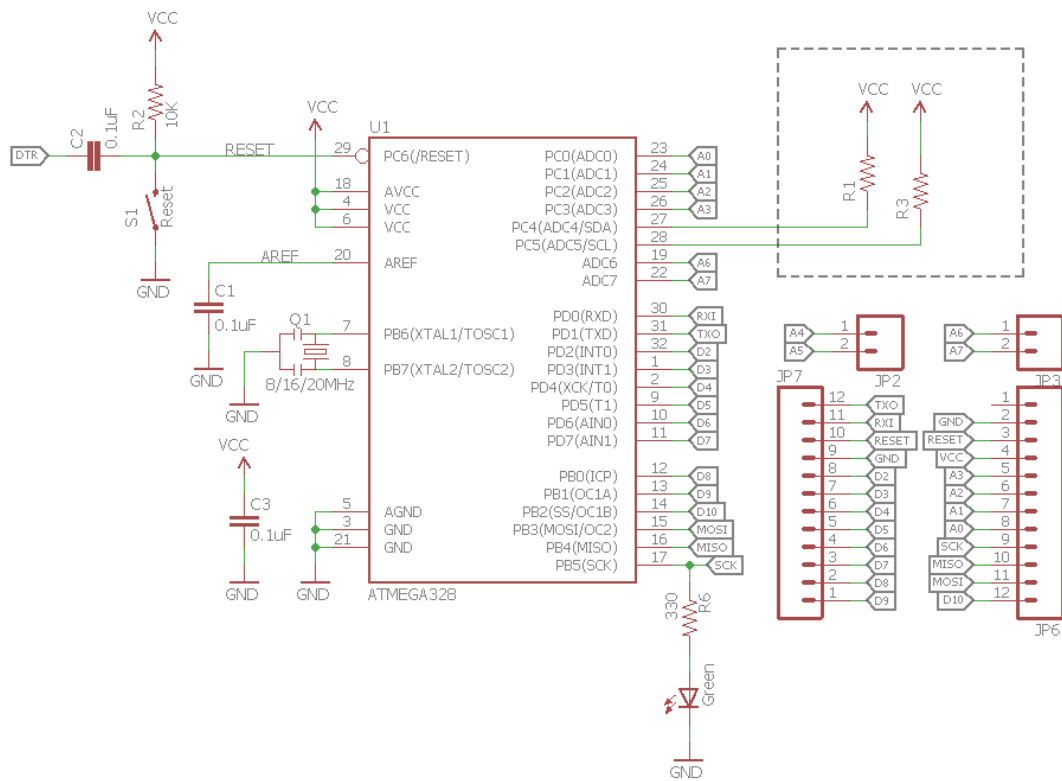


Figure A.1.: Schematic of Control Unit

## A.2 Schematic of ECG Analog Front End

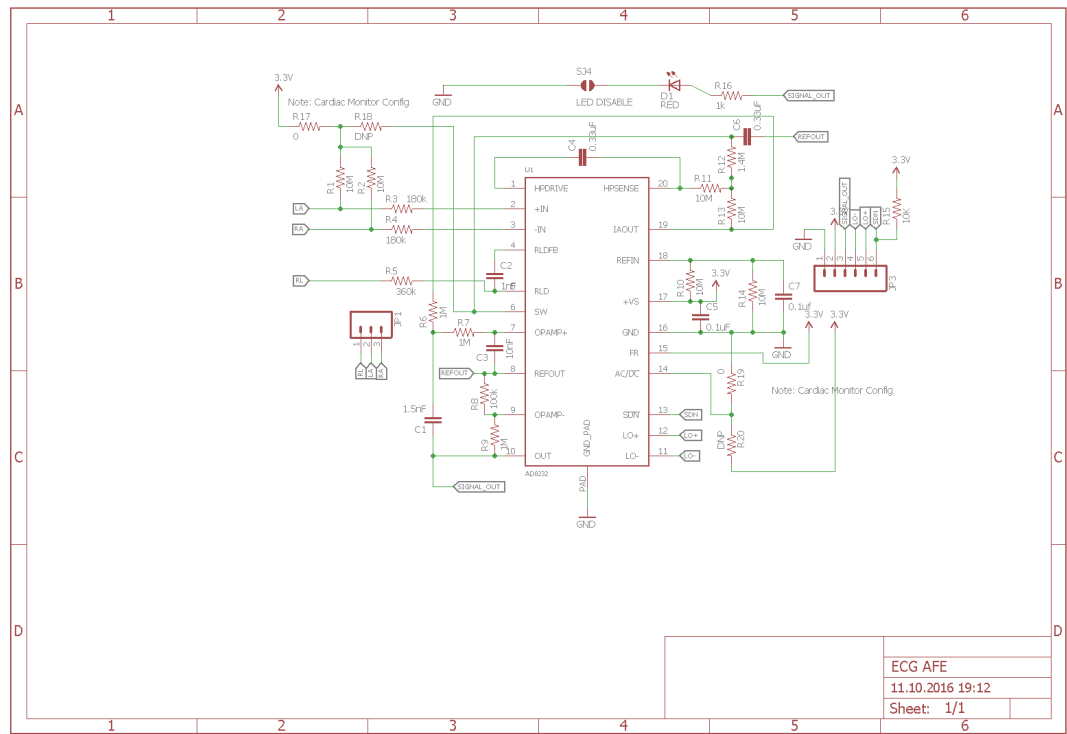


Figure A.2.: Schematic of Electrocardiogram (ECG) Analog Front End (AFE)

### A.3 Schematic of C12666MA Analog Front End

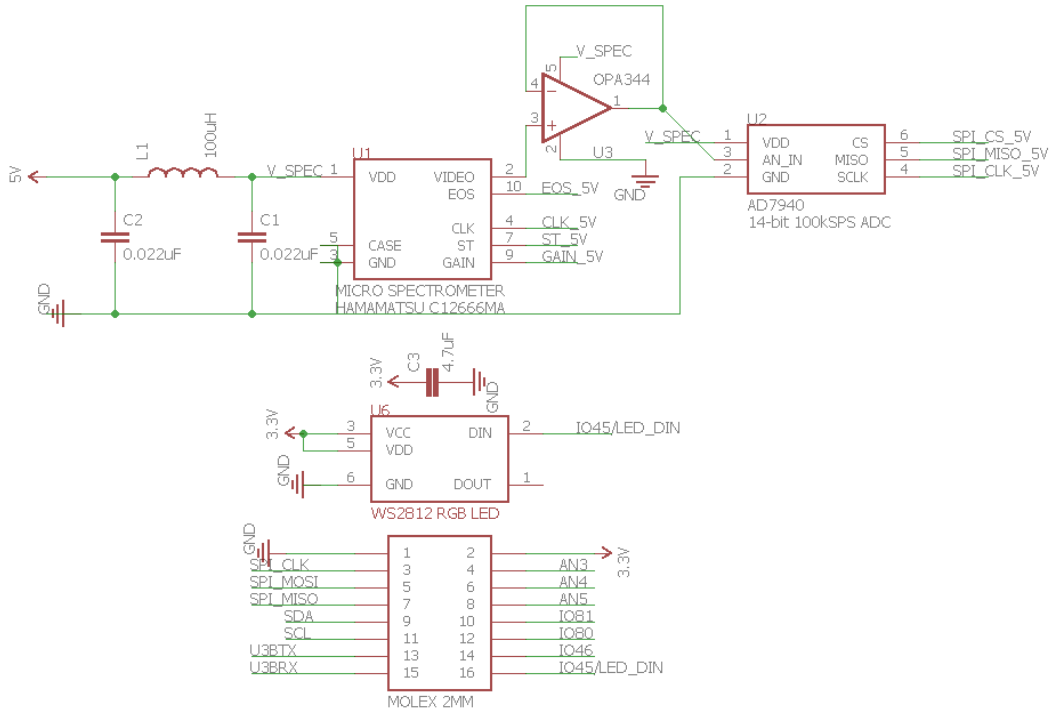


Figure A.3.: Schematic of C12666MA Analog Front End (AFE)

---

#### A.4 Schematic of PPG Analog Front End

---

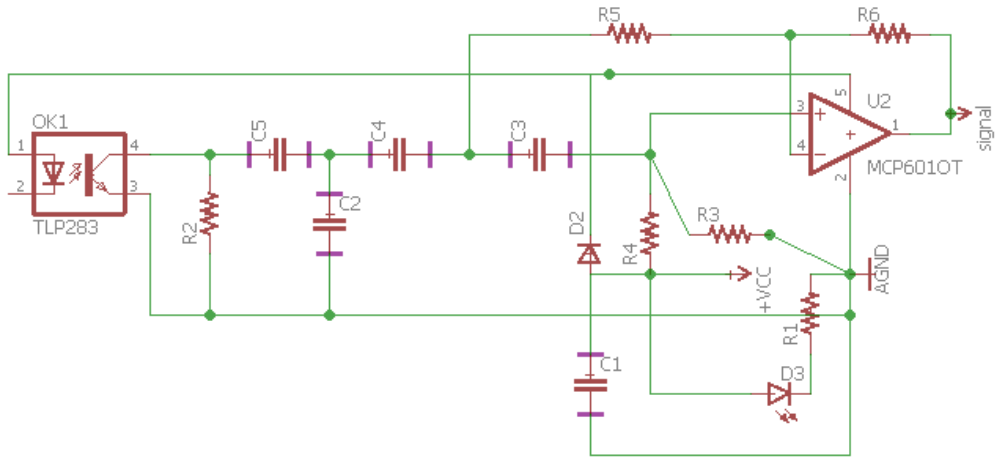


Figure A.4.: Schematic of Photoplethysmogram (PPG) Analog Front End (AFE)

# Bibliography

- [1] J. S. Alpert, R. Smith, C. J. Carlson, I. S. Ockene, L. Dexter, and J. E. Dalen, “Mortality in patients treated for pulmonary embolism”, *Jama*, vol. 236, no. 13, pp. 1477–1480, 1976.
- [2] U. E. Bauer, P. A. Briss, R. A. Goodman, and B. A. Bowman, “Prevention of chronic disease in the 21st century: Elimination of the leading preventable causes of premature death and disability in the usa”, *The Lancet*, vol. 384, no. 9937, pp. 45–52, 2014.
- [3] B. P. McGrath, “Is white-coat hypertension innocent?”, *The Lancet*, vol. 348, no. 9028, p. 630, 1996.
- [4] K. Hung, Y. Zhang, and B. Tai, “Wearable medical devices for tele-home healthcare”, in *Engineering in Medicine and Biology Society, 2004. IEMBS'04. 26th Annual International Conference of the IEEE, IEEE*, vol. 2, 2004, pp. 5384–5387.
- [5] Y.-L. Zheng, X.-R. Ding, C. C. Y. Poon, B. P. L. Lo, H. Zhang, X.-L. Zhou, G.-Z. Yang, N. Zhao, and Y.-T. Zhang, “Unobtrusive sensing and wearable devices for health informatics”, *IEEE Transactions on Biomedical Engineering*, vol. 61, no. 5, pp. 1538–1554, 2014.
- [6] K. Ma, J. C. Khoo, and T. I. Brown, “Development of an ambulatory multi-parameter monitoring system for physiological stress related parameters”, in *Bioinformatics and Biomedical Technology (ICBBT), 2010 International Conference on, IEEE, 2010*, pp. 324–328.
- [7] D. Da He, E. S. Winokur, T. Heldt, and C. G. Sodini, “The ear as a location for wearable vital signs monitoring”, in *2010 Annual International Conference of the IEEE Engineering in Medicine and Biology, IEEE, 2010*, pp. 6389–6392.
- [8] R. Badugu, J. R. Lakowicz, and C. D. Geddes, “Noninvasive continuous monitoring of physiological glucose using a monosaccharide-sensing contact lens”, *Analytical chemistry*, vol. 76, no. 3, pp. 610–618, 2004.
- [9] Badugu, Ramachandram and Lakowicz, Joseph R and Geddes, Chris D, “Ophthalmic glucose monitoring using disposable contact lenses-a review”, *Journal of fluorescence*, vol. 14, no. 5, pp. 617–633, 2004.
- [10] M. Ahmad, A. Kamboh, and A. Khan, Non-invasive blood glucose monitoring using near infrared spectroscopy, 2013.
- [11] M. J. Tierney, J. A. Tamada, R. O. Potts, L. Jovanovic, S. Garg, C. R. Team, et al., “Clinical evaluation of the glucowatch biographer: A continual, non-invasive glucose monitor for patients with diabetes”, *Biosensors and Bioelectronics*, vol. 16, no. 9, pp. 621–629, 2001.
- [12] A. Giardini and J. Roberts, “Concentration of glucose and total chloride in tears”, *The British journal of ophthalmology*, vol. 34, no. 12, p. 737, 1950.
- [13] F. Honore, B. Otis, and A. Nelson, Reader communication with contact lens sensors and display device, US Patent App. 14/536,856, Nov. 2014.
- [14] S. Chakraborty, Why is the ppg signal acquired by the afe 44x0 gui software on the led ir seems like a mirror image of what it should be, 436227, <https://e2e.ti.com/support/applications/medical/f/30/t/436227>, Jul. 2005.
- [15] S. S. Hubert Halbritter Rolf Weber, Sfh 7050 - photoplethysmography sensor, SFH7050, Available online: [http://www.osram-os.com/Graphics/XPic9/00194555\\_0.pdf](http://www.osram-os.com/Graphics/XPic9/00194555_0.pdf)/*BioMon20Sensor20SFH207050.pdf*, OSRAM OPTO SEMICONDUCTORS, Jun. 2014.
- [16] J. G. Webster, Design of pulse oximeters. CRC Press, 1997.
- [17] L. N. et al Neda Seyedmahmoud, Analog integrated circuit applications, Thesis, Available online: [https://web.wpi.edu/Pubs/E-project/Available/E-project-043015-041512/unrestricted/mqp\\_report\\_combined\\_4\\_28\\_15.pdf](https://web.wpi.edu/Pubs/E-project/Available/E-project-043015-041512/unrestricted/mqp_report_combined_4_28_15.pdf), Worcester Polytechnic Institute, Apr. 2015.
- [18] A. A. A. Mohamed A. Abd El Ghany, “Unobtrusive wearable health monitoring system”, 2016.
- [19] T. Instruments, Wearable temperature sensing layout considerations optimized for thermal response.
- [20] Instruments, Texas, Lmt70 data sheet, 2015.
- [21] B. Peng, “Studies of miniature tear glucose sensors and electromodulated nitric oxide delivery devices”, PhD thesis, The University of Michigan, 2013.

- [22] Z. Jin, R. Chen, and L. A. Colon, “Determination of glucose in submicroliter samples by ce-lif using precolumn or on-column enzymatic reactions”, *Analytical chemistry*, vol. 69, no. 7, pp. 1326–1331, 1997.
- [23] R. Badugu, J. R. Lakowicz, and C. D. Geddes, “A glucose sensing contact lens: A non-invasive technique for continuous physiological glucose monitoring”, *Journal of Fluorescence*, vol. 13, no. 5, pp. 371–374, 2003.
- [24] A. Tura, A. Maran, and G. Pacini, “Non-invasive glucose monitoring: Assessment of technologies and devices according to quantitative criteria”, *Diabetes research and clinical practice*, vol. 77, no. 1, pp. 16–40, 2007.
- [25] P. Mell and T. Grance, “The nist definition of cloud computing”, 2011.
- [26] L. Ashall-Payne, “Health apps, the good, the bad, and the ugly: The importance of information”, in *International Technology Enabled Care Conference*, 2016.
- [27] B. Fernandes, J. A. Afonso, and R. Simoes, “Vital signs monitoring and management using mobile devices”, in *6th Iberian Conference on Information Systems and Technologies (CISTI 2011)*, IEEE, 2011, pp. 1–6.
- [28] T. G. Pickering, J. E. Hall, L. J. Appel, B. E. Falkner, J. W. Graves, M. N. Hill, D. W. Jones, T. Kurtz, S. G. Sheps, and E. J. Roccella, “Recommendations for blood pressure measurement in humans: An aha scientific statement from the council on high blood pressure research professional and public education subcommittee”, *The Journal of Clinical Hypertension*, vol. 7, no. 2, pp. 102–109, 2005.
- [29] T. Wibmer, K. Doering, C. Kropf-Sanchen, S. Rüdiger, I. Blanta, K. Stoiber, W. Rottbauer, and C. Schumann, “Pulse transit time and blood pressure during cardiopulmonary exercise tests”, *Physiological Research*, vol. 63, no. 3, p. 287, 2014.
- [30] A. Devices, “Ad620 data sheet”, [Http://www.analog.com.](http://www.analog.com), vol. 10, pp. 08–09, 2008.
- [31] R. Hadzialic, Diy heart monitoring device (simple ecg), LTC1044, Available online: <http://www.radiolocman.com/shem/schematics.html?di=47010>, Apr. 2008.
- [32] C. Kitchin and L. Counts, *A designer’s guide to instrumentation amplifiers*. Analog Devices, 2004.
- [33] A. Devices, “Ad8236 data sheet”, [Http://www.analog.com.](http://www.analog.com), p. 15, 2009.
- [34] Devices, Analog, “Adas1000 data sheet”, [Http://www.analog.com.](http://www.analog.com), p. 10, 2012.
- [35] A. Devices, Ad8232 data sheet, 2012.
- [36] D. Pitson, A. Sandell, R. Van den Hout, et al., “Use of pulse transit time as a measure of inspiratory effort in patients with obstructive sleep apnoea”, *European Respiratory Journal*, vol. 8, no. 10, pp. 1669–1674, 1995.
- [37] M. Gómez García, M. Troncoso Acevedo, M. Rodriguez Guzmán, R. Alegre de Montaner, B. Fernandez Fernandez, G. Del Rio Camacho, and N. Gonzalez-Mangado, “?“ puede ser el tiempo de tránsito de pulso útil para detectar hipertensión arterial en pacientes remitidos a la unidad de sueño?”, *Archivos de Bronconeumología*, vol. 50, no. 7, pp. 278–284, 2014.
- [38] D. R. Wagner, N. Roesch, P. Harpes, H. Kortke, P. Plumer, A. Saberin, V. Chakoutio, D. Oundjede, C. Delagardelle, J. Beissel, et al., “Relationship between pulse transit time and blood pressure is impaired in patients with chronic heart failure”, *Clinical research in cardiology*, vol. 99, no. 10, pp. 657–664, 2010.
- [39] R. P. Smith, J. Argod, J.-L. Pepin, and P. A. Levy, “Pulse transit time: An appraisal of potential clinical applications”, *Thorax*, vol. 54, no. 5, pp. 452–457, 1999.
- [40] R. Ochiai, J. Takeda, H. Hosaka, Y. Sugo, R. Tanaka, and T. Soma, “The relationship between modified pulse wave transit time and cardiovascular changes in isoflurane anesthetized dogs”, *Journal of clinical monitoring and computing*, vol. 15, no. 7-8, pp. 493–501, 1999.
- [41] M. Kortekaas, S. P. Niehof, M. VELZEN, E. Galvin, F. Huygen, and R. Stolker, “Pulse transit time as a quick predictor of a successful axillary brachial plexus block”, *Acta Anaesthesiologica Scandinavica*, vol. 56, no. 10, pp. 1228–1233, 2012.
- [42] A. Hennig and A. Patzak, “Continuous blood pressure measurement using pulse transit time”, *Somnologie-Schlaforschung und Schlafmedizin*, vol. 17, no. 2, pp. 104–110, 2013.
- [43] B. Chakrabarti, S. Emegbo, S. Craig, N. Duffy, and J. O'Reilly, “Pulse transit time changes in subjects exhibiting sleep disordered breathing”, *Respiratory Medicine*, 2016.
- [44] M. E. Sanchez-Hechavarria, R. Carrazana-Escalona, B. Ricardo-Ferro, M. Drinnan, and A. Ciampi, “The interrelation between time-frequency heart rate variability and pulse transit time during psychophysiological stress”, *International Journal of Psychophysiology*, no. 108, p. 166, 2016.
- [45] S. N. Kounalakis and N. D. Geladas, “The role of pulse transit time as an index of arterial stiffness during exercise”, *Cardiovascular Engineering*, vol. 9, no. 3, pp. 92–97, 2009.

- [46] X.-R. Ding, Y.-T. Zhang, J. Liu, W.-X. Dai, and H. K. Tsang, “Continuous cuffless blood pressure estimation using pulse transit time and photoplethysmogram intensity ratio”, *IEEE Transactions on Biomedical Engineering*, vol. 63, no. 5, pp. 964–972, 2016.
- [47] M. Gao, N. B. Olivier, and R. Mukkamala, “Comparison of noninvasive pulse transit time estimates as markers of blood pressure using invasive pulse transit time measurements as a reference”, *Physiological reports*, vol. 4, no. 10, e12768, 2016.
- [48] O. Contal, C. Carnevale, J.-C. Borel, A. Sabil, R. Tamisier, P. Levy, J.-P. Janssens, and J.-L. Pepin, “Pulse transit time as a measure of respiratory effort under noninvasive ventilation”, *European Respiratory Journal*, vol. 41, no. 2, pp. 346–353, 2013.
- [49] B. Mathworks, *Wavelet Toolbox: For Use with MATLAB;[Examples]*. MathWorks, 2012.
- [50] A. Schorr, Continuous glucose monitoring systems, Diapedia 81040851560 rev. no. 11, Available online: <http://dx.doi.org/10.14496/dia.81040851560.11> (accessed on 07 December 2016), Mar. 2015.
- [51] C. M. Patricia Connolly David Heath, Biosensors - emerging materials and applications, 10.5772/19340, <http://www.intechopen.com/books/export/citation/BibTex/biosensors-emerging-materials-and-applications/minimally-invasive-sensing>, Mar. 2011.
- [52] C. Geddes, R. Badugu, and J. Lakowicz, “Contact lenses may provide window to blood glucose”, *BIOPHOTONICS INTERNATIONAL*, vol. 11, no. 2, pp. 50–53, 2004.
- [53] G. Springsteen and B. Wang, “A detailed examination of boronic acid–diol complexation”, *Tetrahedron*, vol. 58, no. 26, pp. 5291–5300, 2002.
- [54] W. Yang, H. He, and D. G. Drueckhamer, “Computer-guided design in molecular recognition: Design and synthesis of a glucopyranose receptor”, *Angewandte Chemie International Edition*, vol. 40, no. 9, pp. 1714–1718, 2001.
- [55] W. Wang, S. Gao, and B. Wang, “Building fluorescent sensors by template polymerization: The preparation of a fluorescent sensor for d-fructose”, *Organic letters*, vol. 1, no. 8, pp. 1209–1212, 1999.
- [56] Z. Yang, M. Xu, Y. Liu, F. He, F. Gao, Y. Su, H. Wei, and Y. Zhang, “Nitrogen-doped, carbon-rich, highly photoluminescent carbon dots from ammonium citrate”, *Nanoscale*, vol. 6, no. 3, pp. 1890–1895, 2014.
- [57] T. Owen, *Fundamentals of modern UV-Visible spectroscopy: A Primer*. Hewlett-Packard, 1996.
- [58] N. I. Agladze and A. J. Sievers, “Miniaturization of holographic fourier-transform spectrometers”, *Applied optics*, vol. 43, no. 36, pp. 6568–6579, 2004.
- [59] Micro-spectrometer, C12666MA, Available online: [https://www.hamamatsu.com/resources/pdf/ssd/c12666ma\\_kacc1216e.pdf](https://www.hamamatsu.com/resources/pdf/ssd/c12666ma_kacc1216e.pdf) (accessed on 07 November 2015), Hamamatsu, Feb. 2016.
- [60] N. DiCesare and J. R. Lakowicz, “Charge transfer fluorescent probes using boronic acids for monosaccharide signaling”, *Journal of biomedical optics*, vol. 7, no. 4, pp. 538–545, 2002.
- [61] R. Badugu, J. R. Lakowicz, and C. D. Geddes, “Boronic acid fluorescent sensors for monosaccharide signaling based on the 6-methoxyquinolinium heterocyclic nucleus: Progress toward noninvasive and continuous glucose monitoring”, *Bioorganic & medicinal chemistry*, vol. 13, no. 1, pp. 113–119, 2005.
- [62] N. DiCesare and J. R. Lakowicz, “Spectral properties of fluorophores combining the boronic acid group with electron donor or withdrawing groups. implication in the development of fluorescence probes for saccharides”, *The Journal of Physical Chemistry A*, vol. 105, no. 28, pp. 6834–6840, 2001.
- [63] B. Gavish, I. Z. Ben-Dov, and M. Bursztyn, “Linear relationship between systolic and diastolic blood pressure monitored over 24 h: Assessment and correlates”, *Journal of hypertension*, vol. 26, no. 2, pp. 199–209, 2008.
- [64] J. M. Bland and D. Altman, “Statistical methods for assessing agreement between two methods of clinical measurement”, *The lancet*, vol. 327, no. 8476, pp. 307–310, 1986.
- [65] H. Gesche, D. Grosskurth, G. Kuchler, and A. Patzak, “Continuous blood pressure measurement by using the pulse transit time: Comparison to a cuff-based method”, *European journal of applied physiology*, vol. 112, no. 1, pp. 309–315, 2012.
- [66] M. Mase, W. Mattei, R. Cucino, L. Faes, and G. Nollo, “Feasibility of cuff-free measurement of systolic and diastolic arterial blood pressure”, *Journal of electrocardiology*, vol. 44, no. 2, pp. 201–207, 2011.
- [67] R. Haberl, M. Wesely, K. Thimel, J. Gehring, and G. Kuchler, “[pp. 27.05] continuous and non-invasive blood pressure measurement based on pulse transit time compared to ambulatory blood pressure measurement.”, *Journal of Hypertension*, vol. 34, e287, 2016.

- 
- [68] M. Ward and J. A. Langton, "Blood pressure measurement", *Continuing Education in Anaesthesia, Critical Care & Pain*, vol. 7, no. 4, pp. 122–126, 2007.
- [69] M. Chowdhury, F. Cummings, M. Kebede, and V. Fester, "Binderless solution processed zn doped co<sub>3</sub>o<sub>4</sub> film on fto for rapid and selective non-enzymatic glucose detection", *Electroanalysis*, 2016.
- [70] M. M. Farid, L. Goudini, F. Piri, A. Zamani, and F. Saadati, "Molecular imprinting method for fabricating novel glucose sensor: Polyvinyl acetate electrode reinforced by mno<sub>2</sub>/cuo loaded on graphene oxide nanoparticles", *Food chemistry*, vol. 194, pp. 61–67, 2016.